University of Alberta

MODELLING THE RHEOLOGY OF COMPLEX FLUIDS : Cases of Bitumen and Heavy Oils at low temperatures.

by

Moïse DION

A thesis submitted to the Faculty of Graduate Studies and Research
in partial fulfillment of the requirements for the degree of

Master of Science
in
Chemical Engineering

Chemical and Materials Engineering Department

©Moïse DION
Fall 2011
Edmonton, Alberta

Permission is hereby granted to the University of Alberta Libraries to reproduce single copies of this thesis and to lend or sell such copies for private, scholarly or scientific research purposes only. Where the thesis is converted to, or otherwise made available in digital form, the University of Alberta will advise potential users of the thesis of these terms.

The author reserves all other publication and other rights in association with the copyright in the thesis and, except as herein before provided, neither the thesis nor any substantial portion thereof may be printed or otherwise reproduced in any material form whatsoever without the author's prior written permission.

Examining Committee

Dr. Carlos Lange, Mechanical Engineering

Dr. Jos Derksen, Chemical and Materials Engineering

Dr. Sean Sanders Chemical and Materials Engineering

ABSTRACT

As complex fluids such as heavy oil or bitumen pass from the field to process units, structural and compositional changes occur that are intimately linked with pressure (P), temperature (T), and shear histories. In this exploratory work, a modified Structural Kinetics Model is used to calculate the apparent shear viscosity of three complex fluids: Maya Crude Oil (MCO), Athabasca Bitumen (AB) and Safaniya Heavy Oil (SP) and their related nano-filtered fractions (permeates and retentates) at low temperatures. The proposed model involves a structural parameter $\boldsymbol{\lambda}$ that tracks the mechanical history of these fluids and a temperature shift factor $\mathbf{a_{TP}}$ that integrates the thermal history, through the usage of the concept of fictive temperature $\mathbf{T_{eff}}$ inside a modified Williams Landel Ferry (WLF) equation. Rheological data for the feedstocks were divided into a training data set, used to fit model parameters, and an extrapolation data set, used to test the asymptotic behaviour of the model with respect to temperature and shear history. Rheological data for the nano-filtered permeates and retentates, with varying mass fractions of structured phase, comprised a prediction data set. Average absolute deviations (**AAD)** less than 15% and $\mathbf{R^2}$ values approaching unity were obtained for the prediction data set. AAD values were less than 4 % for the training and less than 10 % for the extrapolation data sets. The modified Structure-Kinetics Model offers insights, as well as flexibility and accuracy for simulating heavy oil and bitumen rheological properties under conditions where these fluids are structured.

ACKNOWLEDGMENT

As I'm writing this thesis, my deepest thoughts go to all those "innocent people" afflicted around the world. The victims of the tsunami in Japan, the fatalities in the on-going civilian war in Ivory Coast and the fallen in the Arabic Uprising, may not be forgotten.

My gratitude goes to my family (parents and siblings) for being supportive and continuously ensuring me with their love. I want to thank Dorcas, my fiancé, for her undefeated care and encouragement in my life. God bless them all.

I am thankful to my supervisor, Dr. John SHAW, for accepting me onto his team to complete this M.Sc. from an M. Eng. program. Your attention, help, suggestions, patience, kindness and your extraordinary comprehension shaped this thesis. Thank you for the Experience and the Knowledge.

I would also like to thank Dr Jos DERKSEN (Department of Chemical and Material Engineering, University of Alberta) for his orientation, his critical analysis, his advice, his methodology during the theoretical and modeling part of this work. Your advices on numerical methods and your explanations about rheological concepts was determining in tackling this work.

It was a great human experience to work with Brady MASIK, Collins OBIOSA-MAIFE, Dmytro STRATIYCHUK-DEAR, Jesus AMUNDARAIN, Kasra NIKOOYEH, Keivan KHALEGHI, Merouane KHAMMAR, Mohammad Javad AMANI, Nafiseh DADGOSTAR, Mildred BECERRA, and Sepideh Mortazavi MANESH in the Petroleum Thermodynamic group.

Mildred BECERRA : Your experience and knowledge of the lab was a must in operating and maintaining equipment. Thanks for your availability.

Sepideh Mortazavi MANESH : You were a reliable and essential team mate in preparing samples, executing tests and analysing raw data on the computer screen. That helps me a lot in generating experimental curves.

I am also thankful to my friend Robel Berhe TEKLEBRHAN for advising me on modelling approaches and Matlab encoding.

I would like to thank all our sponsors, the Alberta Innovates, the Alberta Energy Research Institute (AERI), ConocoPhillips Canada Inc., Imperial Oil Resources, Kellogg Brown and Root Energy and Chemicals (KBR), Natural Sciences and Engineering Research Council of Canada (NSERC), NEXEN Inc., Shell Canada Ltd. Halliburton Energy Services, and Total E&P Canada, for their financial support.

TABLE OF CONTENTS

LIST OF TABLES

LIST OF FIGURES

LIST OF SYMBOLS

PARAMETERS	DESCRIPTION
Parameters for the Structural Kinetic equations	
a b c d m	The regression parameters for the SKM
$\eta_{us}^{Tg,0}$ $\eta_{fs}^{Tg,0}$	The lower (unstructured) and upper (structured) limiting viscosity measured at atmospheric pressure and glass transition temperature **Tg.**
σ_0 σ_{0d}	The static and dynamic yield stresses respectively with their Arrhenius exponential constants
$G_{fs}^{Tg,0}$	The upper (structured) limiting shear modulus as measured at atmospheric pressure and glass transition temperature **Tg.**
K n	The power law constants
$\kappa^{T,P}$	Is the structural characteristic time of change function of T and P [s]
Parameters for the TNM equation for the computing of the Fictive temperature	
l k_b	Respectively the structural unit average dimension and the Boltzmann constant $k_b = 1.3806503 \times 10^{-23} \left[m^2 kg/s^2 K \right]$
τ_0	Is the relaxation time τ of the structured phase when both T and T_f are formally infinity
ΔH_{fs}^*	Is the activation energy of the relaxation process of the structure phase
x	The nonlinearity parameter that partitions the activation energy ΔH^* into the relative effects of temperature and structure, on the relaxation time. $0 < x < 1$

q_j	Quenching (Heating or cooling) rate [K/s]
N, j, k	is an iteration index, and j and k are dumb indices
β	Is the stretched exponential parameter

Parameters for the Modified WLF shift function used to calculate the $a_{T,P}$

A_1 A_2	T_g pressure dependency parameter $A_1 = 1/b$ $A_2 = b/a$ where **a** and **b** are obtained from plotting $dP/dT_g = (a + b \cdot P)$ [1]
$C_1^{Tref\,0}$ $C_2^{Tref\,0}$	WLF constant, defined as the reciprocal of the fractional free volume at Tref [2]. At T_g $C_1^{g0} = 17.44$ and $C_2^{g0} = 51.6$ (universal values) indicating that the free volume at T_g is 2.5% of the total volume.
T_{g0}	The glass transition constant as measured at atmospheric pressure
f_0	fractional free-volume at the reference temperature;
$\alpha_f(P)$	free-volume expansivity, considered pressure dependent only
α_f^g	free-volume expansivity at atmospheric pressure and temperature of reference

Chapter I: INTRODUCTION

I. 1. APPLICATIONS AND RHEOLOGY OF PETROLEUM MATERIALS

Hydrocarbons are naturally occurring organic substances mainly composed of hydrogen and carbon. Depending on conditions, they may comprise gases, liquids or solids. In one form or another, petroleum has always been part of human history. The modern applications of hydrocarbons have become sophisticated but many do not differ fundamentally from those of ancient peoples. Olmecs, in Mesoamerica, extracted and processed "bitumen" not only as a trade item but as a structural material to produce watercraft, masks and ceramics [3]. The waterproofing and adhesive qualities of these materials were mentioned in ancient texts related to the bible through stories like the Noah's ark (Genesis 6.14), the Tower of Babel (Genesis 11.3) or Moses' cradle on the Nile (Exodus 2.3). Hydrocarbon fluids were used as disinfectants and insecticides in medical practice, and were used by ancient Egyptians to prepare mummification mixtures [4]. Neolithic artefacts from Humm El Tlel [5] reveal the use of "bitumen", in the manufacture of weapon, as hafting materials.

Hydrocarbon use has become ubiquitous in modern times. Our recent focus on heavy hydrocarbons and bitumen in particular concerns imbalances between global demand and inexpensive supply, but also the constraint to reduce energy inputs during production, transport and processing of such fluids, to minimize waste and environmental impacts.

Fluid "rheology" or "flow behaviour" is a critical decision variable. ***Chemical Process Engineers*** need accurate viscosity values to calculate head loss and therefore to size equipment, and to optimize surface or refining processes. ***Reservoir Engineers*** use mobility ratio (permeability/viscosity) to forecast production performance from reservoirs. In fact, the spatial distribution of fluid viscosity in a reservoir dominates the oil phase mobility ratio distribution which in turn controls production behaviour. Therefore, understanding the pattern and variation of the petroleum fluid viscosity before and during production is very important since the selection of a production method, the placement of wells, enhancing recovery, and estimating costs are some issues that depend heavily on viscosity. The ***Road Paving Industry*** relies on viscosity to assess the quality of paving asphalt. The material must be fluid enough at high temperature (around 433.15K (160°C)) to be pumpable and to coat aggregates consistently during mixing but stiff enough at the highest pavement temperature to resist rutting (around 333.15K (60°C)) and ductile enough at the lowest pavement temperature to resist cracking (around 275.15K (-20°C)) [6]. In the ***Process Simulation Industry***, viscosity is one of the most unreliable transport properties to be predicted. There is no satisfactory theories for the calculation of the viscosity for heavy oil and bitumen [7], in general, and at low temperatures in particular where **structure** varies with the intensive properties of these fluids.

I. 2. CONTEXT OF THIS WORK

The literature is full of theories, concepts and models to predict Newtonian rheological properties of hydrocarbon liquids. S.E. Quinones-Cisneros et al. [8] introduced the **f-theory** to describe the viscosity of dense fluids. The theory is based on the friction principles of classical mechanics and on the Van der Waals theory of fluids. Fluids must be single phase and Newtonian to apply the theory. Another approach, based on the **corresponding states** principle, has shown to

be reliable for viscosity prediction of mixtures with species similar to reference fluids. However, substantial deviations occur for mixtures with components having different sizes, shapes, and basic molecular structure [9]. Recently, H. W. Yarranton and M. A. Satyro [7] introduced a revolutionary idea for estimating the viscosities of heavy oils, mixtures of heavy oils, and mixtures of solvents and heavy oils. They combined the **corresponding state theory** with the **free space theory** to calculate viscosities**.** The free space theory was first illustrated by Batschinski in 1913 then reintroduced in 1978 by Hildebrand [10] in essentially the same form. According to the theory, the fluidity of a liquid is directly proportional to its free volume[11]. As a fluid expands, there is greater distance between molecules and its fluidity increases. H. W. Yarranton and M. A. Satyro reformulated the correlation as a viscosity departure-like function. Their approach appears to work well above ~330 K (60°C).

At lower temperatures, heavy oil and bitumen exhibit complex phase behaviour and are not Newtonian fluids. The rheology of such fluids is mainly dictated by the phase behaviour of their heavy constituents [12] [13], fluid thermal and shear history [14] and fluid structure [15] [16].

I. 3. THESIS OBJECTIVES

This work provides a mathematical description of phenomena underlying the rheological response observed in Maya crude oil, Athabasca bitumen [16] and Safaniya heavy oil. A set of equations which takes into account the effect of *shear*, *temperature* and *structural relaxation* to predict the flow of these hydrocarbon resources at low temperatures is derived, and tested against experimental rheological data.

I. 4. OUTLINE OF THIS THESIS

This thesis comprises 6 chapters. **Chapter 1** provides a general introduction, a brief historical survey, an explanation of the significance of rheological properties of hydrocarbons, and an overview of previous work done on rheology modeling. The objectives of the thesis are also outlined. **Chapter 2** establishes the framework of this work through a succinct literature review concerning the rheological properties of real fluids [17]. An attempt to explain the causes of the transition of flow responses (from Newtonian behaviour to non-Newtonian behaviour), is provided through a brief description of the governing physics and chemistry behind this evolution. The derivation of the Structural Kinetics Model (SKM) for the non-Newtonian rheology of hydrocarbon fluids, including a full description of parameters appearing in the equations, is presented. In **Chapter 3,** relevant experimental data collected from the literature and laboratory tests comprising the training set to fit the model to natural samples of hydrocarbon materials are presented. A justification for the simplification procedure that leads to the modified form of the Structural Kinetics Model with a reduced number of parameters is provided. The ability of the model to predict flow responses of native hydrocarbons (extrapolation) and their nano-filtered permeates (pure prediction) at constant shear conditions is evaluated in **Chapter 4**. The quality of the predictions for Maya crude oil, Athabasca bitumen, Safaniya heavy oil and related samples is discussed. Following this discussion, **Chapter 5** underlines the physical meaning associated with the variations of model parameters as observed among feedstocks. A simplistic model for the network structure of petroleum materials at low temperature is proposed. The concluding chapter, **Chapter 6**, summarizes the findings of the thesis, and suggests new research opportunities emerging from the key results.

Chapter II: RHEOLOGY OF HEAVY OIL AND BITUMEN AS COMPLEX FLUIDS

II. 1. INTRODUCTION

Complex fluids, also called structured fluids [18], exhibit uncommon rheological behaviours due to their mechanical properties that are intermediate between ordinary liquids and ordinary solids. They comprise a liquid phase and a structured phase [19-20]. When complex fluids are subjected to deformation beyond a threshold, their microstructure becomes altered which may cause remarkable drops in their apparent viscosity [18, 21-22]. A steady state is reached when these fluids are subject to a constant stress for a long enough period of time. At steady state the microstructure acquires a stable configuration, which results from a balance between microstructure build-up and breakdown rates. Microstructure alteration does not occur instantaneously and it is for this reason, structured fluids are said to be time-dependent fluids.

II. 2. RHEOLOGICAL TERMINOLOGY

Due to a lack of standardization in the literature[19, 23], it is critical to provide a clear explanation of the notion and terms used to for flow properties of hydrocarbons in this work. The nomenclature used here is consistent with usages

of the Society of Rheology and the International Union of Pure and Applied Chemistry (IUPAC) [24-26].

For **shear thinning/thickening** fluids, viscosity decreases/increases with increasing shear rate or shear stress during steady shear flow. After a sudden reduction in shear rate, **viscoelastic** fluids exhibit a monotonic decrease in the transient shear stress until a new plateau value is reached. During this stress relaxation, the microstructure is altered to a new steady state. By contrast, purely **thixotropic** fluids drop instantaneously to a new lower value, then increase gradually until a new steady state value is reached, under similar conditions [27]. In response to an applied shear stress, thixotropic fluids show a bifurcation in flow behaviour that depends on flow history, i.e., on its current structural state [28]. In **rheopexy**, the fluid structure builds up by deformation and breaks down when the fluid is at rest thus an increase of viscosity in time at constant deformation rate is observed. Even though rheopexy is rarely reported, it has been attributed to some crude oils [29]. Since structural changes take time to occur (either from rest or from some other configuration), thixotropy/rheopexy is to be expected from any shear thinning/thickening material. **Rheomalaxis** is a time-dependent behaviour in which time of deformation causes irreversible alteration in the fluid structure. The alteration can be negative, as when structural linkages are broken. Therefore the viscosity is permanently reduced. A positive alteration occurs when the fluid structure become entangled under deformation.

II. 3. FLOW BEHAVIOURS OF COMPLEX FLUIDS

When classical substances are above their freezing point, their resistance to flow is insensitive to deformation and time but varies with temperature and pressure.

In addition to that, they don't exhibit elastic effects or extensional anomalies. Classical fluids are idealizations describe by a constant shear viscosity η and a constant extensional viscosity η_e with a Trouton ratio Tr of 3 [30].

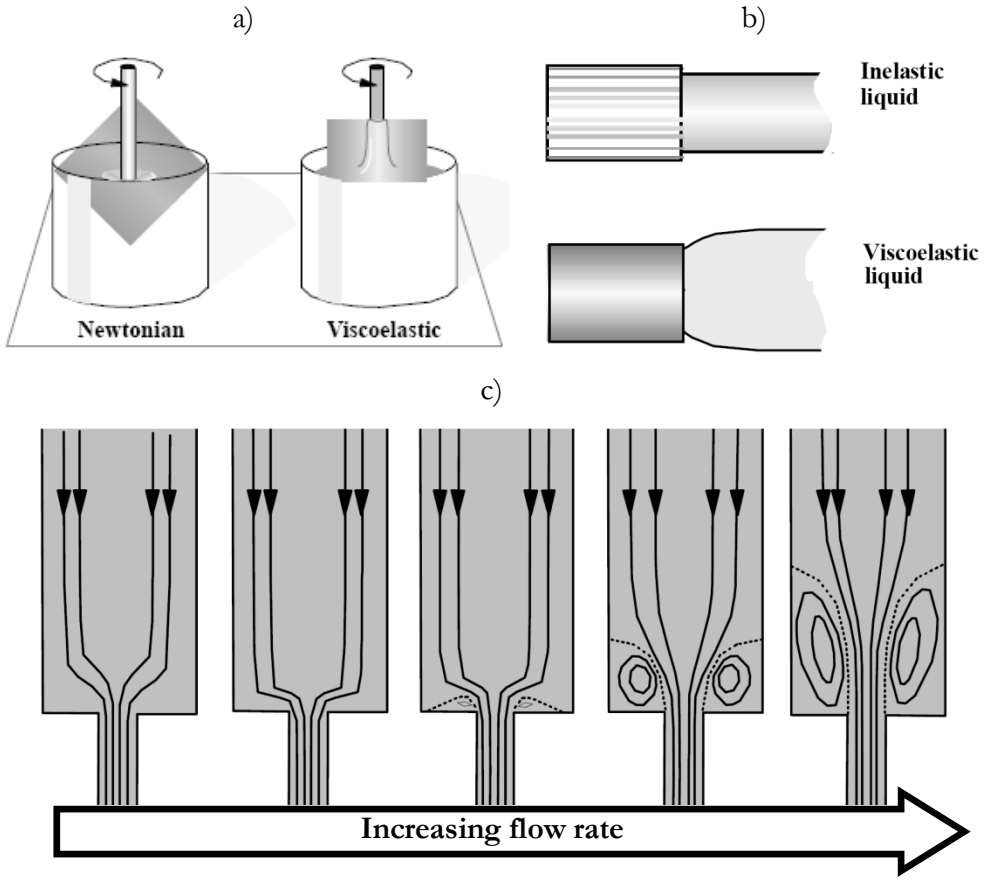

Figure II.1 : Common flow behaviour associated with the viscoelasticity of complex fluids: a) weissenbergeffect, b) extrudate swell c) recirculating vortices in contraction. ***these pictures are adapted from*[31-32]**

Real fluids are neither classical liquids nor solids. In many cases, the relationship between stress and deformation for these materials is nonlinear[33], unknown[34], or under dispute [35-36]. These "complex fluids" possess mechanical behaviours that are intermediate between those of liquids and solids.

They behave like "solids" at short time scales in that they maintain their shape and they are "liquids" at long time scales since they eventually flow. The characteristic time required for complex fluids to change from "solid-like" to "liquid-like" varies from fractions of a second to days, or even years, depending on the fluid and temperature. Glass-forming liquids, polymer melts, polymer solutions, and micellar solutions are examples of complex fluids with long structural or molecular relaxation times. Particulate and polymeric gels change from solid-like materials to liquid-like fluids, or vice versa, when subjected to a modest deformation. Some complex fluids even change to solids when an electric or magnetic field is applied; these are electrorheological and magnetorheological suspensions.

II. 4. FLOW BEHAVIOURS OF PETROLEUM MATERIALS

II.4.1. **Composition impact on the rheology of petroleum resources**

The heavy fraction of petroleum materials dictates the temperature susceptibility of their rheology.

At low temperatures (< 330 K), petroleum resources such as heavy oils and bitumen exhibit non Newtonian rheological behaviour. Nano-filtration [37], phase behaviour and rheological investigations [13, 16, 38] revealed that below a threshold temperature solids segregate in heavy oil and bitumen. This fraction increases as the temperature lowers, promoting viscosity raise, shear thinning and time dependency. When separated, filtrates show an almost Newtonian behaviour (**Figure II.2**) which characterizes rheology of heavy oils and bitumen at high temperature (typically higher than 60 °C) [39].

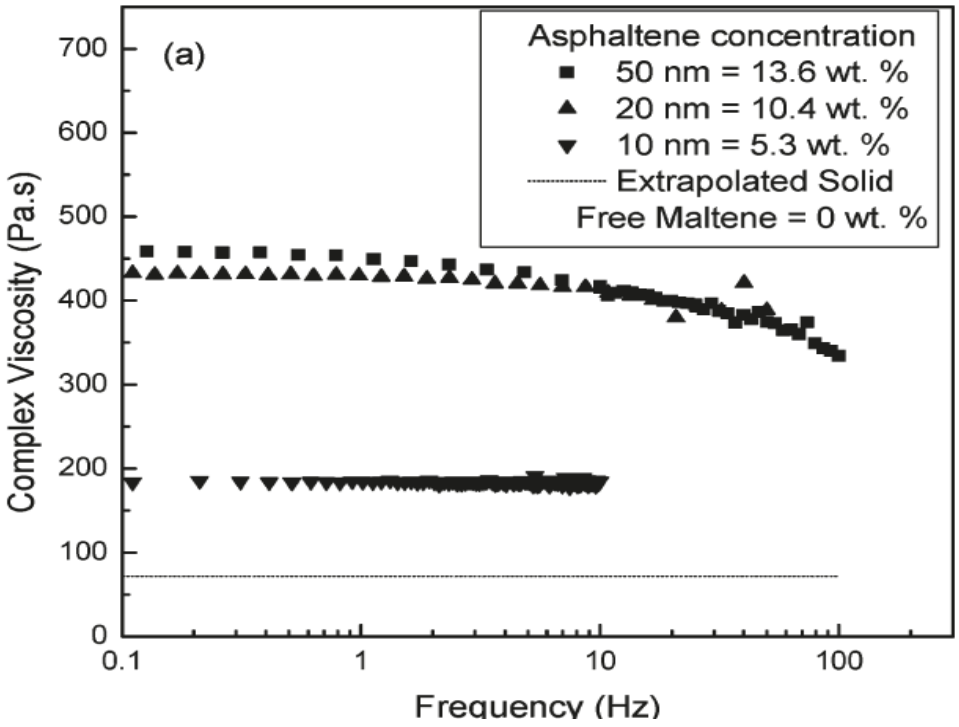

Figure II.2 : Complex viscosity for nano-filtered-permeate samples at 298 K (25C) Athabasca bitumen. *Image e from* Hasan, M.A., et al.[37]

II.4.2. **Temperature effects**

At high temperatures (typically above 60 °C), bitumen and heavy oil are viscous Newtonian liquids characterized by a temperature dependent Newtonian viscosity η_N. Below the glass transition temperature (typically below -20 °C), the shear modulus **G** and the viscosity η_0 , reach some limiting values independent of temperature corresponding to the glassy state (**Figure II.3**). In-between these two behaviours, their mechanical response is intermediate between that of an elastic solid and a viscous liquid said to be viscoelastic [20, 37, 40-41] .

As a consequence of viscoelasticity, petroleum materials **store** appreciable elastic energy and **dissipate** viscous energy when subjected to flow. Their rheological phenomenology is determined by their **elasticity** and the time dependent behaviour of their microstructure [19] .

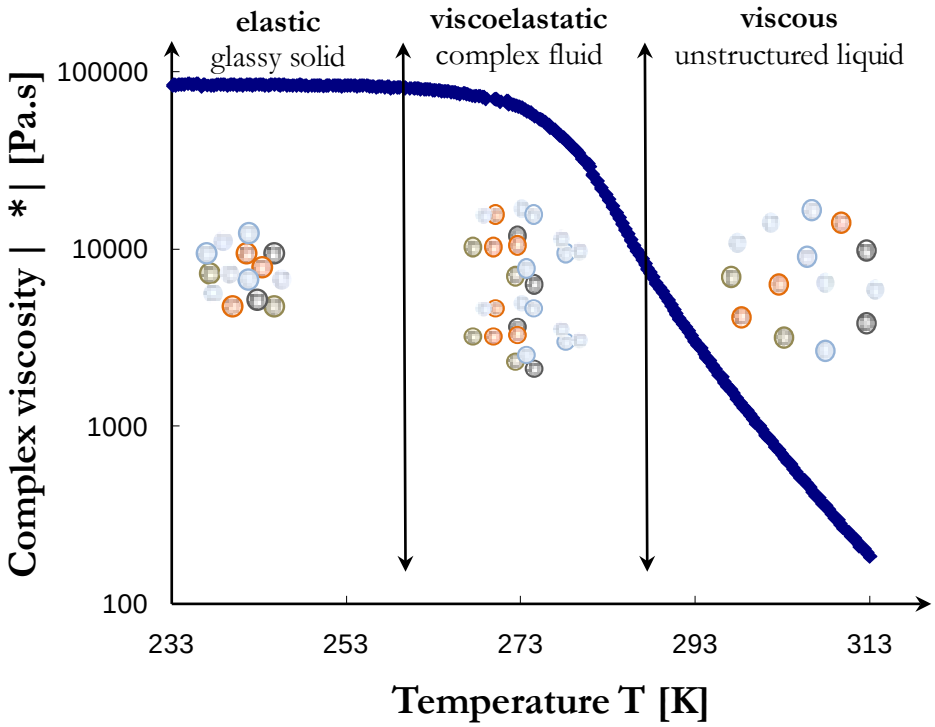

Figure II.3 : Complex viscosity for Athabasca Bitumen during a temperature sweep experiment. As temperature decreases, collision between elemental particles become more efficient and results in larger networked phase domains, that produce viscoelastic properties and others complex flow behaviours.

Common flow behaviours associated with **fluid elasticity** include **Normal stress effects**, **Secondary Flows**, **Elastic recoil**, **Die swell**, **Entry flow vortex, Pressure hole errors [31]** and the **Open-channel siphon**. Books by Barnes, H.A. [31], Macosko, C.W. [42], Larson, R.G. [43] and Riande, E., et al. [44] provide a wealth of information and are excellent resources for understanding these phenomena.

II.4.3. **Thermorheological simplicity**

Though out of context, experimental data related to the feedstocks employed in this study are included here to clarify how the Time-Temperature Superposition Principle (TTSP) holds for the feedstocks covered in this study. This principle, an important underlying assumption in the context of this study, states that the effect of increasing loading time (or decreasing the frequency) on the mechanical properties of a material is equivalent to that of raising the temperature [45]. Materials behaving in this way are said to be thermorheologically simple. An analogous requirement applies to piezorheological simple materials with all response times depend equivalently on pressure.

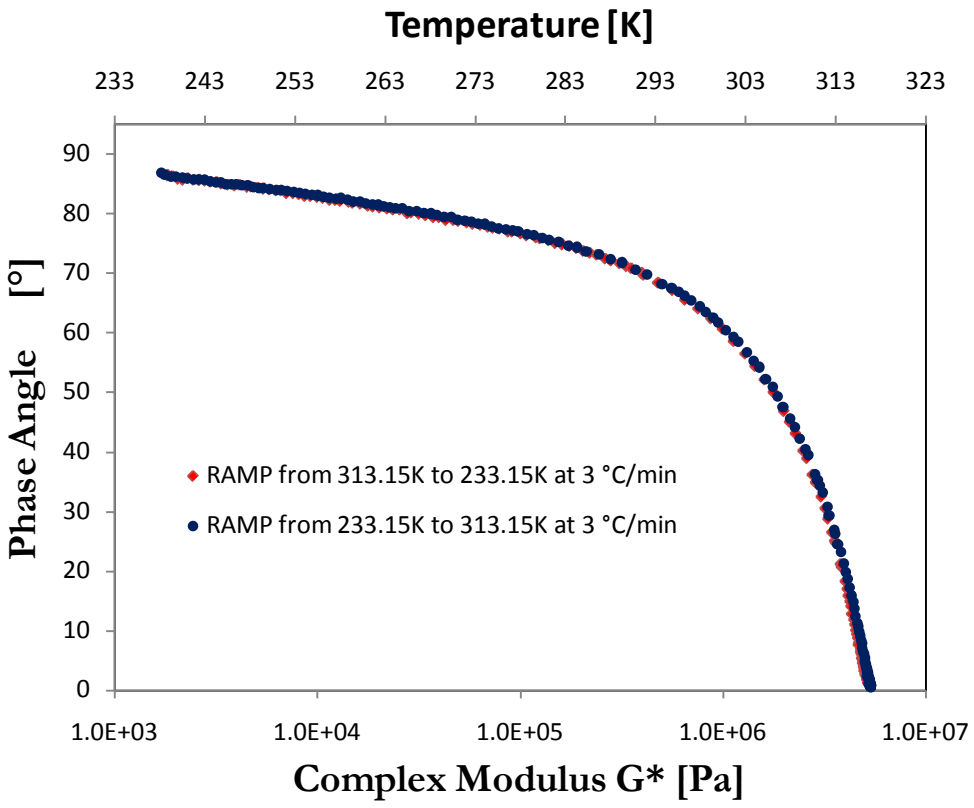

Figure II.4 : Black Diagram for Athabasca bitumen

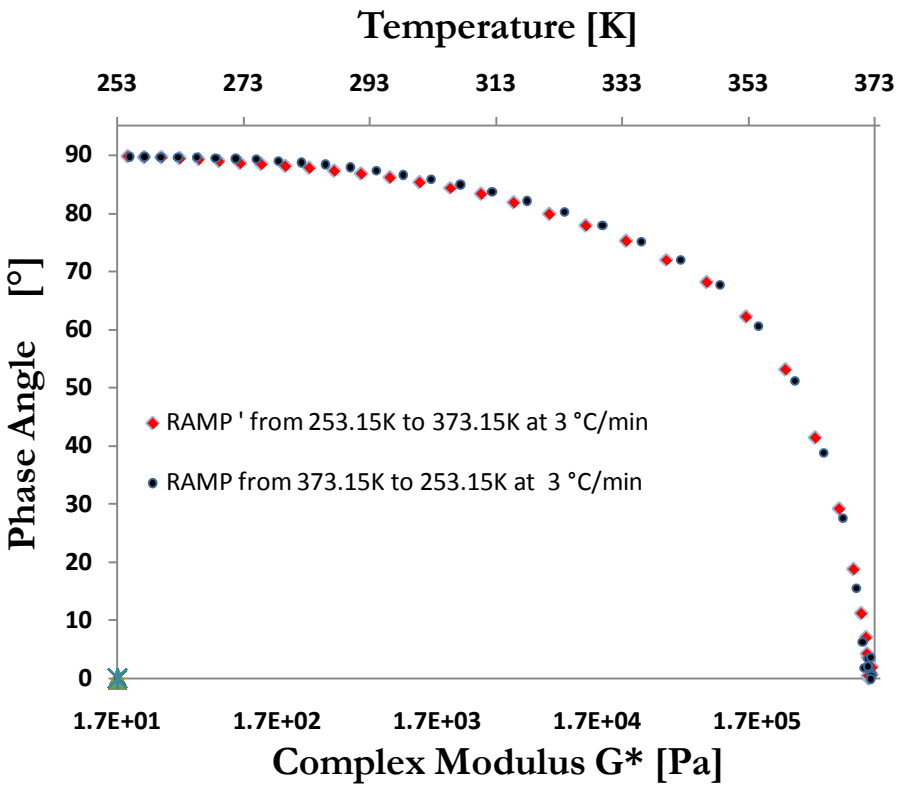

Figure II.5 : Black Diagram of a sample of Safaniya heavy oil

These statements can be expressed by the temperature-pressure shift function.

$$a_{TP} = \frac{\tau_i(T,P)}{\tau_i(T_0,P_0)}\,; \quad i = 1,2,3,\ldots$$

Whether TTSP holds for hydrocarbon materials is still debated [41, 46].

According to Mavridis [45], the time-temperature superposition principle holds for a given fluid if the Black diagram (plot of phase angle (**d**) versus the complex modulus($\mathbf{G}^*$)) obtained at different temperatures, match on a single curve. Since this diagram is obtained without any shifting procedure, it is chosen indicator for applicability of TTSP to Athabasca Bitumen and Maya Crude Oil in this work.

Figure II.4 , **Figure II.5** and **Figure II.6** represent, respectively, the Black Diagrams for unaged samples of Athabasca Bitumen, Safaniya Heaby Oil and Maya Crude Oil.

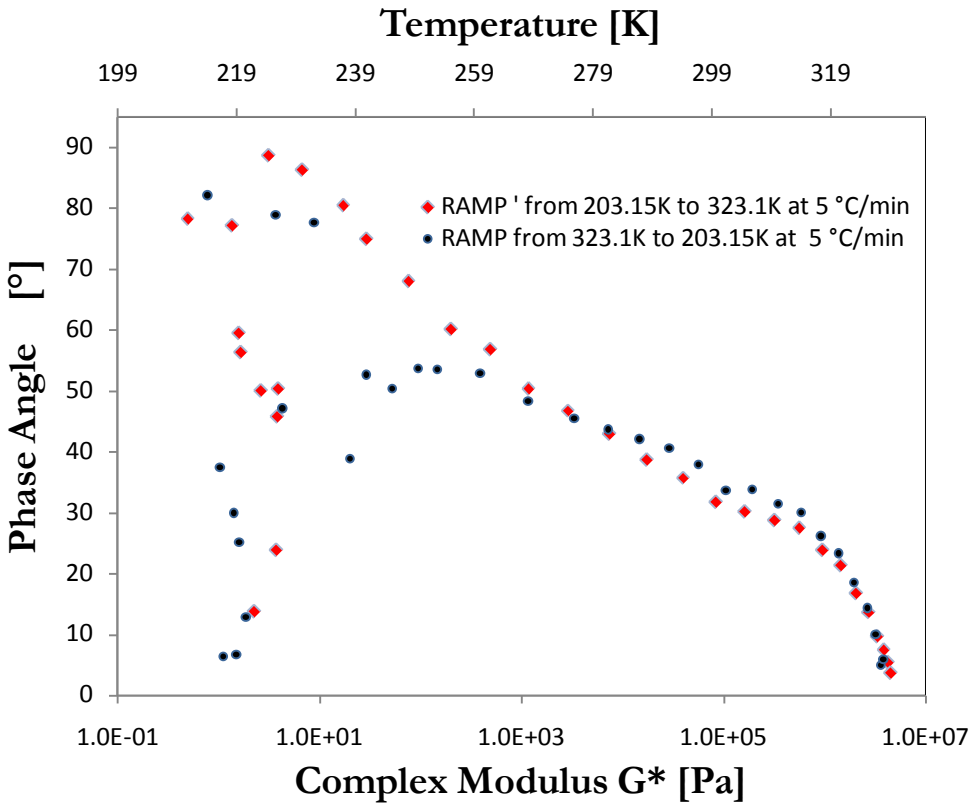

Figure II.6 : Black Diagram of an unaged sample of Maya Crude Oil

The superposition is obvious for Athabasca Bitumen and Safaniya heavy oil. Indeed **d** vs $\mathbf{G}^*$ lies on a single curve between 233.15K (-40°C) and 313.15K (40°C) for Athabasca Bitumen and between 248.15K (-25°C) and 373.15K (100°C) for Safaniya Heavy Oil.

Figure II.6 shows a scattered set of points below 243.15K (-30°C) but a consistent single curve from 243.15K (-30°C) to 313.15K (40°C) for Maya crude oil.

Athabasca Bitumen, Maya Crude Oil and Safaniya heavy oil, are thermorheological simple materials under the conditions relevant to this study - 275.15K (-20°C) and 333.15K (60°C).

II.4.4. **Structural relaxations in petroleum fluids**

The structures present in hydrocarbon liquids, at low temperatures have both temperature and time-dependent responses [47-48].

At the glass transition temperature of their heaviest fractions viscoelastic behaviour is not observable [37]. Indeed, the rheological behaviours of Athabasca Bitumen and Maya crude oil are those of hard spheres suspensions in a Newtonian liquid at temperatures well above 298K. For low temperatures (<330 K)**,** the structures begin to interact and to form a microstructure network (**Figure II.3**).

Two relaxation mechanisms have been reported in the literature [6]:

- The transition from viscoelastic flow to Newtonian flow (α-relaxation) is attributed to the relaxation process of the structured phase.
- A transition from elastic glassy behaviour to viscoelastic flow (β-relaxation) is attributed to the glass transition of the Newtonian liquid phase.

II. 5. PREDICTING THE RHEOLOGY OF HEAVY OIL AND BITUMEN

The non-Newtonian flow properties exhibited by heavy oils and bitumen, at low temperatures, have not been modeled previously. The f-theory by S.E. Quinones-Cisneros et al. [49] and the Expanded Fluid-Based theory by H. W. Yarranton and M. A. Satyro are expected to break down at temperatures significantly below

~ 300 K where these complex fluids exhibit significant structure. The current work evaluates the idea of coupling three theories to compute the rheometry of these complex fluids at low temperatures. The Structural Kinetics Model (SKM), the Williams Landel Ferry (WLF) equation and the Tool-Narayanaswamy-Moynihan (TNM) formalism are combined to track the rheology of the structured and liquid phases.

The phase behaviour of Athabasca bitumen, comprising four phases between 260K and 360K [16, 50-51] and Maya crude oil comprising a minimum of three phases over a comparable temperature range[13, 51], is lumped in the present context into a structured and a liquid phase. The number of phases present in Safaniya crude is currently under investigation, but it is expected to comprise a minimum of two phases at room temperature. Two phase lumping is however justified because unstructured Bitumen or Heavy oils have viscosities value up to 5 orders of magnitude lower that when they are structured [20, 39, 52].

II.5.1. **The Maxwell mechanical representation**

Structured Bitumen and Heavy oil generally do not respond instantaneously to an imposed rate of deformation because the structures act as bridges in the fluid [41]. Their characteristic response is predominantly viscoelastic [39]. The simplest rheological model to describe this property is the spring and a dashpot representation (**Figure II.7**) known as the Maxwell model[44, 53-54] is chosen here to represent the mechanics of the rheological behaviour of Maya Crude Oil, Athabasca Bitumen and Safaniya heavy Oil.

This model, described elsewhere in detail [44] was introduced during the 1860's when Maxwell abandoned the notion of “mean free path" to introduce the concept of "time relaxation" of stresses in gases. According to this concept :

$$\sigma = \int_{-\infty}^{t} G_0 e^{-(t-t')/\lambda} \dot{\gamma}(t')dt \qquad \text{[Eq. II.1a]}$$

the time derivation of [Eq. II.1a] gives:

$$\frac{d\sigma}{dt} = -\int_{-\infty}^{t} \frac{G_0}{\lambda} e^{-(t-t')/\lambda} \dot{\gamma}(t')dt' + G_0 \dot{\gamma}(t) \qquad \text{[Eq. II.1b]}$$

Integrating [Eq. II.1b], and then multiplying the result by λ yields:

$$\sigma + \lambda \frac{d\sigma}{dt} = \eta \dot{\gamma} \qquad \text{[Eq. II.1]}$$

since $\eta = \lambda G_0$.

To overcome poor descriptions of polymeric materials, the rheology community has adopted [Eq. II.1] as the Maxwell model that is often represented as a series combination of springs, elastic elements, and dashpots, illustrated in **Figure II.7**.

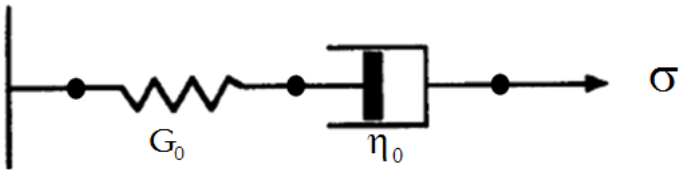

Figure II.7 : Spring and dashpot representation of the Maxwell element.

The Maxwell model, under its original form, predicts stress relaxation processes fairly well but handles creep and recovery processes poorly.

[Eq. II. 1] is applicable to soft solids, thermoplastic polymers in the vicinity of their melting temperature, fresh concrete (neglecting aging) and numerous metals. In this study, hydrocarbons fluids are considered to be **soft solids** at very low temperatures [55] instead of **hard solids** in the Hookean and Kelvin–Voigt sense

of the term. This assumption does not preclude the possibility of alternative approaches (**Figure II.8**) such as the Generalized Maxwell Model, Oldroyd Model, Kelvin–Voigt and their variants.

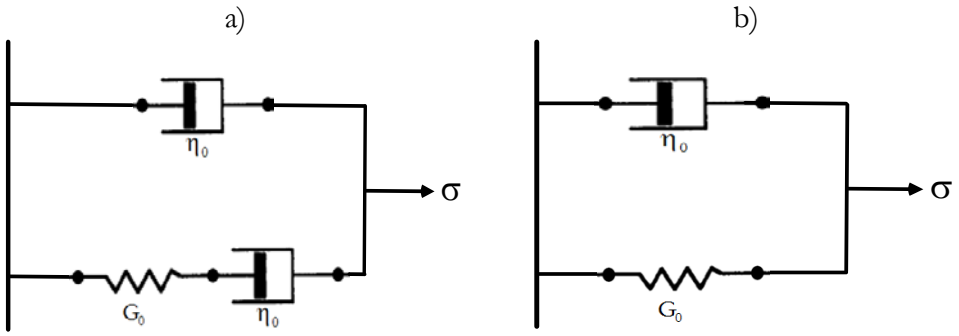

Figure II.8 : Some other viscoelastic models: (a) Oldroyd, (b) Kelvin–Voigt

II.5.2. **The Structural Kinetics Model (SK-Model)**

Denny and Brodkey [56] introduced a theory in 1962 based upon an assumption that the non-Newtonian behaviour of fluids can be linked to the structural changes occurring in them (**Figure II.9**). The theory supposed that the build up and break down of mechanical "bonds" in the material occurred according to a reaction kinetics scheme, with the number of bonds being related to viscosity.

$$(\textbf{Unbroken structured fluid}) \underset{k2}{\overset{k1}{\rightleftharpoons}} (\textbf{Broken unstructured fluid})$$

The rate of breakdown is calculated by assuming equal rupture probability for each bond between structural units. This theory has been used to develop several mathematical models for non-Newtonian fluids based on the numerical value of a scalar structural parameter $\boldsymbol{\lambda}$, which ranges from $\boldsymbol{\lambda}= 1$ for completely built structures to $\boldsymbol{\lambda}= 0$ for completely broken-down structures as illustrated in **Figure II.8** [14, 17, 22, 28, 57-60].

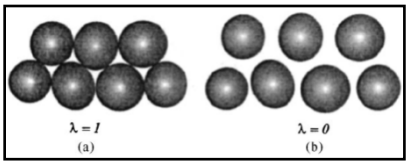

Figure II.9 : Schematic representation of a structured fluid accordion to the SKM theory

Time dependence is introduced via the time derivative of λ. The description of the shear induced breakdown is given by the product of the current level of structure and the shear rate, raised to some power **b**. The driving force for build up is controlled by how far the current value of λ is from its maximum value 1 rose to another power **a**:

$$\frac{d\lambda}{dt} = k_1\left(\text{Build up}\right)^a + k_2\left(\text{Breakdown}\right)^b = k_1\left(1-\lambda\right)^a + k_2\lambda\left(\dot{\gamma}\right)^b$$

where k1 and k2 are the rate constants for build-up and breakdown and the powers **a**, and **b** are either directly specified in the model or obtained by fitting rheological data.

On **Figure II.10**, a microstructure composes of a series of large flocks at rest. When the applied shear rate is increased progressively and sufficient time is allowed, the flock size decreases and then disintegrates at a high enough shear rates. Because large flocks trap more continuous-phase fluids they are responsible for the very high viscosity. As the shear rate is increased stepwise from point **1** to **2**, the flock size corresponds initially to the shear stress condition at point **1**. The flocks erode to a size appropriate to the higher rate. If the shear rate is then instantaneously decreased from **2** to **1,** the smaller flocks collide and flocculate until the size of the flocks formed is appropriate to the new, lower shear rate. The kinetics of this erosion and flocculation process underlies the shear susceptibility of the material and its time dependency.

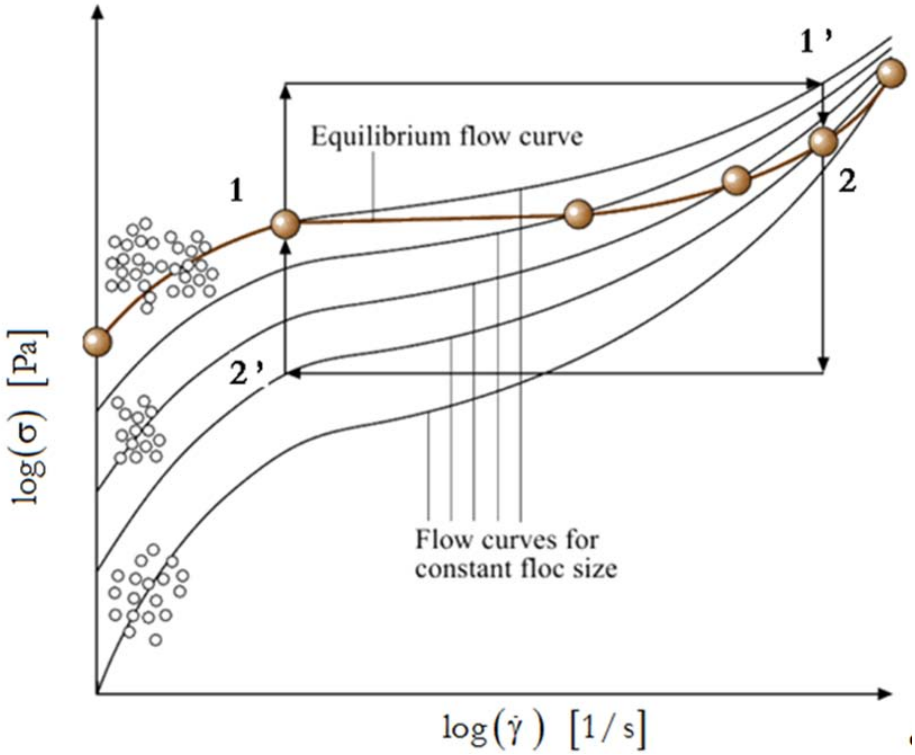

Figure II.10 : Schematic representation of microstructure kinetics and flow response for a structured suspension. ***Image is adapted from*** [31]

II.5.3. **The Williams Landel Ferry (WLF) equation**

The WLF model [61] is an expansion of kinetic theories based on the free volume [11, 62] and the Eyring [63] rate theories. The model deals with the temperature dependence of viscosity or viscoelastic relaxation.

In 1957, Doolittle and Doolittle [62] introduced the concept of free volume in their work on the viscosity of liquids. They assumed that the change in viscosity depends on the distribution of molecule-size holes in the fluid. The sum of these holes represents the free-volume, which directly affects the mobility of the liquid molecules. This was expressed by the semi-empirical expression for the viscosity, η, of liquids,

$$\eta = Ae^{B\left[\frac{V-V_f}{V_f}\right]} \qquad \text{[Eq. II.2a]}$$

where V_f is the free volume and V the total volume.

Williams et al. [61] modeled the effect of thermodynamic parameters such as temperature (T) and pressure (P) on the mechanical properties of amorphous homopolymers or random copolymers by considering that the fractional free volume f of such polymers increases linearly with temperature:

$$f = f_r + \alpha_f (T - T_r) \qquad \text{[Eq. II.2b]}$$

to obtain the temperature shift function:

$$\text{Log}(a_T) = \frac{C_1^g (T - T_g)}{C_2^g + (T - T_g)} \qquad \text{[Eq. II.2]}$$

where the reference temperature is taken at the glass transition temperature and $C_1 = B / f_g \ln(10)$ and $C_2 = f_g / \alpha_f^g$ with α_f^g the coefficient of thermal expansion as measured at the glass transition temperature; T_g [C^{-1}]. f_g is the fractional free volume (V_f / V) at the glass transition temperature T_g [–]. A major drawback is that at temperatures below Tg, the WLF equation in its original form does not account for steady state and relaxation/retardation processes occurring in structured phases.

II.5.4. **The Tool-Narayanaswamy-Moynihan (TNM) formalism**

Structural relaxation refers to the time-dependent change of any macroscopic property (volume, enthalpy, refraction index, electrical conductivity or viscosity)

of a liquid following perturbation (i.e. a change in temperature or pressure) [64]. When a structured fluid is subject to a rapid change in temperature, the macroscopic properties of the material exhibit an instantaneous change. This is followed by a slower structural relaxation toward a new equilibrium property value at the new temperature. Tool [65] proposed a model that sought to explain this aspect of structural relaxation. He introduced the concept of fictive temperature, $\mathbf{T_{eff}}$ as a measure of the structural state of a glass:

$$\frac{dTeff}{dt} = k\, e^{(T/g)}\, e^{(Teff/h)} \qquad \text{[Eq. II.3]}$$

Tool's equation was modified by Narayanaswamy [66] and Moynihan [64] to include both nonlinearity, memory effects and nonexponentiality in the relaxation process. Thus a continuous heating or cooling process at rate **q** is seen as a series of differential temperature steps, **dT**, followed by isothermal holds, **dt=dT/q** (**Figure II.11**). The TNM equation is expressed by the integral:

$$T_{eff}(T) = T_0 + \int_{T0}^{T} dT' \times \left[1 - \exp\left(-\left(\int_{T'}^{T} dT'' / q\tau \right)^{\beta} \right) \right] \qquad \text{[Eq. II.4a]}$$

where T_0 is a starting temperature well above Tg, and T' and T'' are dummy temperature variables. The value of τ, defined as the structural relaxation time, varies continuously with T and T_{eff} according to Tool-Narayanaswamy-Moynihan formalism [64] and is expressed as:

$$\tau = \tau_0 \exp \frac{\Delta H^*}{R} \left[\frac{x}{T} - \frac{(1-x)}{T_{eff}} \right] \qquad \text{[Eq. II.4b]}$$

with ΔH^* as the activation energy; τ_0 is the pre-exponential parameter equal to τ when both T and T_{eff} are formally infinity. The nonlinearity parameter $0 < x < 1$ is an empirical parameter that partitions the activation energy, ΔH^*, into two parts that characterize the relative effects of temperature and structure, respectively, on the relaxation time. The normalized relaxation function is written as $\Phi = \exp\left[-(t/\tau)^{\beta}\right]$, with $\boldsymbol{\beta}$ the stretched exponential parameter. t is the macroscopic time. Nonexponentiality parameter $\boldsymbol{\beta}$ is a direct measure of the breadth of the distribution of relaxation times. Smaller values of $\boldsymbol{\beta}$ correspond to increased nonexponentiality. Typically, $\boldsymbol{\beta}$ lies in the range 0.4-0.6 for glass transitions [67] . A dimensionless heat capacity is defined as $C_p^N(T) = dT_{eff}/dT$ corresponds to the usual DSC scans and therefore depends on both the heating rate and the previous cooling rate through Tg.

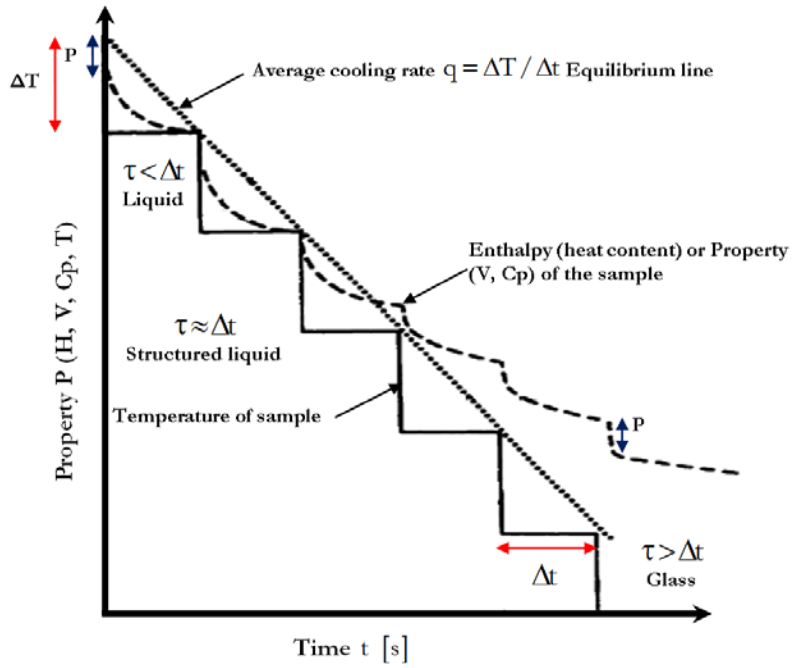

Figure II.11 : Schematic of the kinetic aspects of a glass transition, in which property change with time is considered as a sequence of temperature jumps ΔT.

II. 6. DERIVATION OF THE PROPOSED MODEL

II.6.1. **Framework**

- The fluid to be modeled is a viscous, incompressible and strain (shear or extension) degradable.
- The material is considered to be **complex fluid** comprising a **viscous matrix** and a **micro-structured phase (**network of aggregates**)**.
- The internal strain in the fluid is composed of a strain component arising from the **viscous fluid** and a strain component arising from the **structured phase (**Network of aggregates**)**.
- The **structured phase** contributes to the shear degradation and time-dependent behaviour of the material through a breakdown and recovery process when the fluid is subject to deformation (shear or extension).
- The structured phase can grow in size or be restored at rest after degradation. Thus, the fluid shows some degree of **reversibility**.
- Rate of structural degradation is a function of the instantaneous values of a structural parameter **λ**.
- Mechanical history of the fluid is stored and defined by the structure level (or value of the structure parameter) at a given time **t**.
- Thermal history is given by the value of a pseudo-temperature $\mathbf{T}_{\mathbf{eff}}$.
- Athabasca bitumen, Maya and Safaniya crude oil are treated as thermally simple fluids (assumption verified in **II.4.3**).

II.6.2. **Structural** kinetics **approach**

II.6.2.1. *Proposed mechanical representation*

The total strain $\dot{\gamma}_{tot}$ in a complex fluid under a constant stress σ_{tot} is assumed to have a viscous and an elastic component as proposed by the Maxwell Model in **Figure II.6**. This assumption can be expressed as:

$$\gamma_{tot} = \gamma_{el} + \gamma_{vis} \qquad \text{[Eq. II.5a]}$$

where γ_{el} is the elastic strain and γ_{vis} is the viscous strain. The differentiation with respect to time t gives the total strain rate:

$$\dot{\gamma}_{tot} = \dot{\gamma}_{el} + \dot{\gamma}_{vis} \qquad \text{[Eq. II.5b]}$$

If the stress is expressed as:

$$\sigma_{tot} = \eta(\dot{\gamma}, t)\ \dot{\gamma}(\lambda, \gamma) \qquad \text{[Eq. II.6]}$$

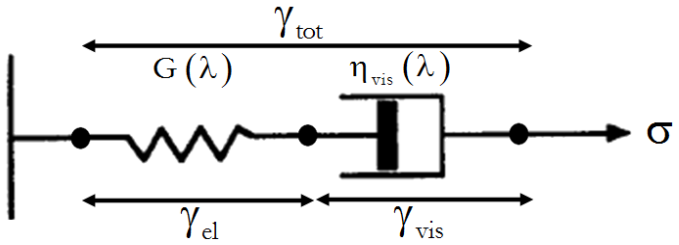

Figure II.12 : Proposed representation of the mechanical behaviour of petroleum materials at low temperatures.

$$\sigma_{tot} = \eta_{vis}(\lambda)\ \dot{\gamma}(\lambda, \gamma_v) \qquad \text{[Eq. II.6a]}$$

or

$$\sigma_{tot} = G(\lambda)\ \gamma_{el}(\lambda, \gamma_{el}) \qquad \text{[Eq. II.6b]}$$

The differentiation of equation [Eq. II.6b] with respect to time gives:

$$\dot{\sigma}_{tot} = \dot{G}(\lambda)\ \gamma_{el}(\lambda, \gamma_{el}) + G(\lambda)\ \dot{\gamma}_{el}\ (\lambda, \gamma_{el}) \qquad \text{[Eq. II.7a]}$$

By postulating that G depends only on $\boldsymbol{\lambda}$ so that its time derivative is zero yields:

$$\dot{\sigma}_{tot} = G(\lambda)\ \dot{\gamma}_{el}\ (\lambda, \gamma_{el}) \qquad \text{[Eq. II.7b]}$$

This relation shows that as $G(\lambda)$ decreases due to structural breakdown, the elastic strain γ_{el} increases at the same rate keeping total stress σ_{tot} unchanged.

Multiplying [Eq. II.5b] by $\eta_{vis}(\lambda)$ gives:

$$\eta_{vis}(\lambda)\dot{\gamma}_{tot} = \eta_{vis}(\lambda)\dot{\gamma}_{el} + \eta_{vis}(\lambda)\dot{\gamma}_{vis} \qquad \text{[Eq. II.7c]}$$

and re-arranging yields:

$$\eta_{vis}(\lambda)\cdot\dot{\gamma} = \sigma_{tot} + \dot{\sigma}_{tot}\left(\frac{\eta_{vis}(\lambda)}{G(\lambda)}\right) \qquad \textbf{[Eq. II.7]}$$

Which has the same form as the linear viscoelastic Maxwell constitutive equation [Eq. II.1] except that $\eta_{vis}(\lambda)$ and $G(\lambda)$ both depend on the structural parameter $\boldsymbol{\lambda}$.

II.6.2.2. *Modulus of rigidity function* $G(\lambda)$

Rigidity modulus $G(\lambda)$ should be constant (G_0) when the material is fully structured $\boldsymbol{\lambda = 1}$ until a critical strain $\boldsymbol{\gamma_c}$ is reached. Beyond $\boldsymbol{\gamma_c}$, $G(\lambda)$ should

increase monotonically with **λ** to infinity at **λ = 0** where elasticity is suppressed (**Figure II.12**). These considerations can be expressed as [17]:

$$G(\lambda) = \frac{G_0(T)}{\lambda^m} \qquad \textbf{[Eq. II.8]}$$

where larger values of **m** are associated with shorter relaxation times.

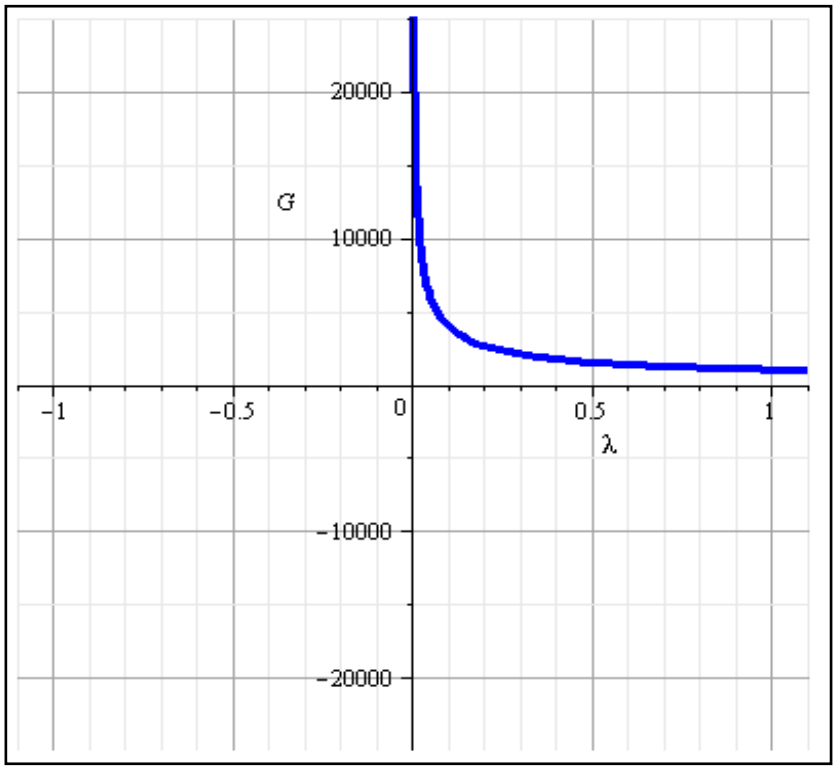

Figure II.13 : Evolution of elastic modulus as the structural parameter changes from 0 to 1

The elastic modulus G_0 is determined through oscillatory shear experiments in the linear regime. An oscillatory shear stress of amplitude is applied at a frequency of 1 Hz. The oscillatory shear stress is controlled, rather than an oscillatory shear strain, in order to get small and accurate deformations. The shear stress amplitude is chosen to ensure that the strain induced on materials is lower enough, so that they are tested in their linear regime.

II.6.2.3. *Transient viscosity function* $\eta(\dot{\gamma}_{tot}, t)$

In response to changing flow conditions, the microstructure of complex fluids relaxes toward a new steady state. Elastic effects appear when $\dot{\gamma}_{el} \neq 0$, i.e.: when the stress is varying [Eq. II.7], and vanish when $\dot{\gamma}_{el} = 0$, i.e. when the fluid is fully unstructured. Viscous effects vanish when $\dot{\gamma} = \dot{\gamma}_{el}$.

Thus [17]:

$$\eta(\dot{\gamma}_{tot}, t) = \left(1 - \frac{\dot{\gamma}_e}{\dot{\gamma}}\right).\eta_{vis}(\lambda) \qquad \text{[Eq. II.9]}$$

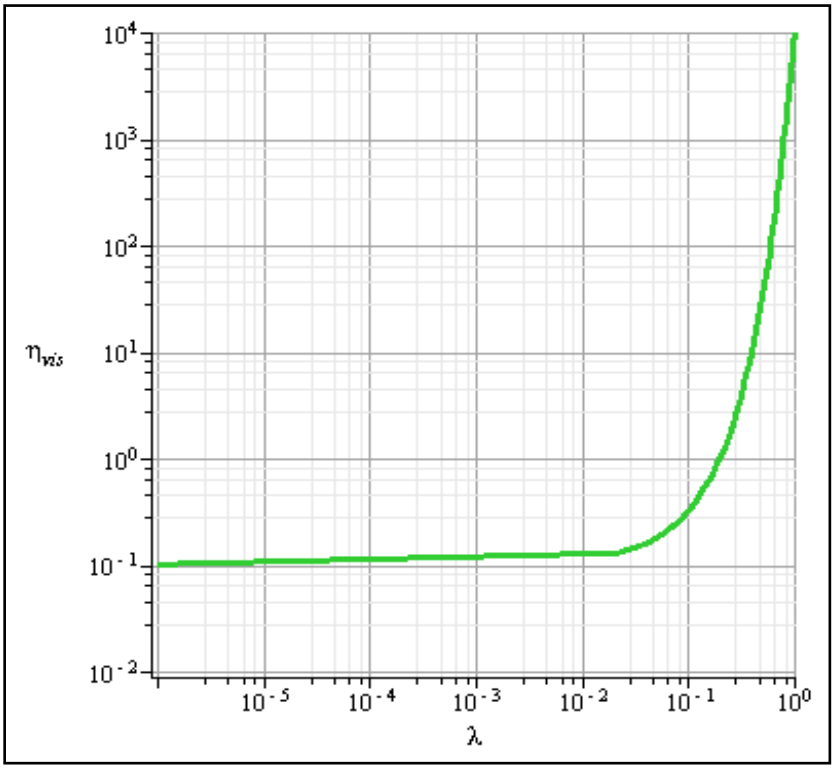

Figure II.14 : Impact of λ on steady state viscosity.

II.6.2.4. *Structural viscosity function* $\eta_{vis}(\lambda)$

As commonly agreed [16, 19, 27, 68], the viscosity of complex fluids varies from the fully structured (**λ=1**) viscosity η_{FS} to an unstructured (**λ=0**) equilibrium viscosity η_{US} with $\eta_{US} < \eta_{FS}$ (**Figure II.14**). For this case, as **λ** approaches 0 the viscosity is almost asymptotic to 10-1[Pa.s]. As λ approaches 1, fully structured fluid, the maximum value of viscosity is reached. These two characteristic properties (η_{US} and η_{FS}) are known to vary with temperature.

Since λ only describes structural degradation, two identical fluids with a same λ must have similar values of η_{US} and η_{FS} to have equal rheological properties under similar conditions (pressure, temperature, composition).

In order for a viscosity function to relate the interval of $0 \leq \lambda \leq 1$ to $[\eta_{US}; \eta_{FS}]$ at a given temperature, the following conditions must be fulfilled. If $\eta(\lambda)$ is the viscosity at a known λ, then $d\eta(\lambda)$ is a differential increase resulting from a differential increase $d\lambda$ in **λ**. The magnitude of the increase depends on the value of $\eta(\lambda)$ and how close it is to the maximum viscosity η_{FS} The viscosity evolves slowly with λ close to η_{us} and them more quickly as it approaches (λ=1). A linear progression is adopted by some authors [69], here the following equation is used to describe $\eta_{vis}(\lambda)$:

$$\eta_{vis}(\lambda) = \left(\frac{\eta_{FS}(T)}{\eta_{US}(T)} \right)^{\lambda} \eta_{US}(T) \qquad \text{[Eq. II.10a]}$$

This leads to:

$$\lambda(\dot{\gamma},t)=\left(\frac{\ln\left[\eta_{vis}(\dot{\gamma},t)\right]-\ln\left[\eta_{US}(T)\right]}{\ln\left[\eta_{FS}(T)\right]-\ln\left[\eta_{US}(T)\right]}\right) \qquad \text{[Eq. II.10b]}$$

which at steady state becomes :

$$\lambda_{SS}(\dot{\gamma})=\left(\frac{\ln\left[\eta_{SS}(\dot{\gamma})\right]-\ln\left[\eta_{US}(T)\right]}{\ln\left[\eta_{FS}(T)\right]-\ln\left[\eta_{US}(T)\right]}\right) \qquad \text{[Eq. II.10]}$$

II.6.2.5. *Steady state viscosity* $\eta_{SS}(\dot{\gamma})$

At lower temperatures, heavy oil and bitumen do not flow if the imposed stress does not affect their microstructure. Indeed they are yield stress fluids with shear degradation or thixotropic behaviour after yielding. To quantify the steady state flow properties of these fluids, their flow curve (a plot of the shear stress vs. the shear rate) should be measured. Several predictive equations are available to model the steady state viscosity of yield-stress thixotropic fluids [22, 28, 39, 70-71].

In the present approach, the energy flow per unit volume comprises a structural and a viscous contribution: $\dot{E}=\dot{E}_{str}+\dot{E}_{vis}$ which can be expressed as $\sigma\times\dot{\gamma}=\sigma_{str}\times\dot{\gamma}+\sigma_{vis}\times\dot{\gamma}$ or in terms of stress $\sigma=\sigma_{str}+\sigma_{vis}$. The transition from the unyielded fluid to the yielded material occurs progressively with an exponential stress growth before flow occurs [72-73]. A constitutive equation for stress can then be written as (for one-dimensional flows):

$$\sigma=\left(1-e^{-m_0\dot{\gamma}}\right)\sigma_{str}+\sigma_{vis} \qquad \text{[Eq. II.11a]}$$

where m_0 is a parameter controlling stress level .

In [Eq. II.11a], the viscous stress is due to the Newtonian liquid phase while the structural stress has a component related to bonds between the structural aggregates σ_{bn}, and another constituent related to the network of aggregates σ_{nt}.The σ_{nt} is responsible of the yield behaviour while σ_{bn} dominates the shear thinning behaviour.

Application of the Herschel–Bulkley, three parameters model, yields $\sigma_{str} = \sigma_{nt} + \sigma_{bn} = \sigma_{nt} + K\dot{\gamma}^{n}$.

The network induced stress σ_{nt} can be related to the static and the dynamic yield stresses through $\sigma_{nt} = \left(\sigma_0 - \sigma_{0d}\right)e^{-m_1\dot{\gamma}} + \sigma_{0d}$. Including these stresses in flow curve analysis arises from the fact that the static yield stress should be reached at steady state. If not, the structuring/ unstructuring process would be irreversible and thixotropy, for example, would not occur.

The above considerations can be summarized by a single expression for stress

$$\sigma = \left(1 - e^{-m_0\dot{\gamma}}\right)\left(\left(\sigma_0 - \sigma_{0d}\right)e^{-m_1\dot{\gamma}} + \sigma_{0d} + K\dot{\gamma}^{n}\right) + \sigma_{vis} \qquad \text{[Eq. II.11b]}$$

When divided by shear rate, [Eq. II.11b] yields an expression for steady state viscosity:

$$\eta(\dot{\gamma}) = \left(1 - e^{-m_0\dot{\gamma}}\right)\left(\frac{\left(\sigma_0 - \sigma_{0d}\right)e^{-m_1\dot{\gamma}} + \sigma_{0d}}{\dot{\gamma}} + K\dot{\gamma}^{(n-1)}\right) + \eta_{vis} \qquad \text{[Eq. II.11]}$$

where σ_0 and σ_{0d} are respectively the static and the dynamic yield stresses. This expression is similar to that proposed by De Souza [70] where $m_0 = \frac{\eta_{fs}}{\sigma_0}$

$m_1 = \frac{1}{\dot{\gamma}_{0d}}$ .and $\dot{\gamma}_{0d}$ are the shear rates marking the transition from dynamic yield stress to dynamic yield stress.

Figure II.15 illustrates the features of [Eq. II.11] with shows a high viscous plateau at lower shear rate follow by a viscosity transition to a power law region, then by a high shear transition to a Newtonian plateau.

In [Eq. II.11], K is the consistency index and **n** the power law, often called as flow index. Both indexes are functions of temperature [74]. But K is a much more sensitive function of temperature than is **n**. These two variables will be represented by :

$$K = K_{Tref0} \times \exp\left(-p_K\left(1 - \frac{T_{eff}}{T_{ref0}}\right)\right) \qquad \text{[Eq. II.12]}$$

$$n = n_{Tref0} + p_n \times \left(1 - \frac{T_{eff}}{T_{ref0}}\right) \qquad \text{[Eq. II.13]}$$

where p_K and p_n are temperature sensitivity parameters while K_{Tref0} and n_{Tref0} are power law parameters at reference temperatures and pressure

II.6.2.6. *Evolution equation for the structural parameter* λ

In modeling shear degradation and time dependency behaviours of complex fluids, the rate of structural change is a key phenomenon. Several approaches are available for modeling this phenomenon [14, 75]. These options are well presented by Barnes [19].

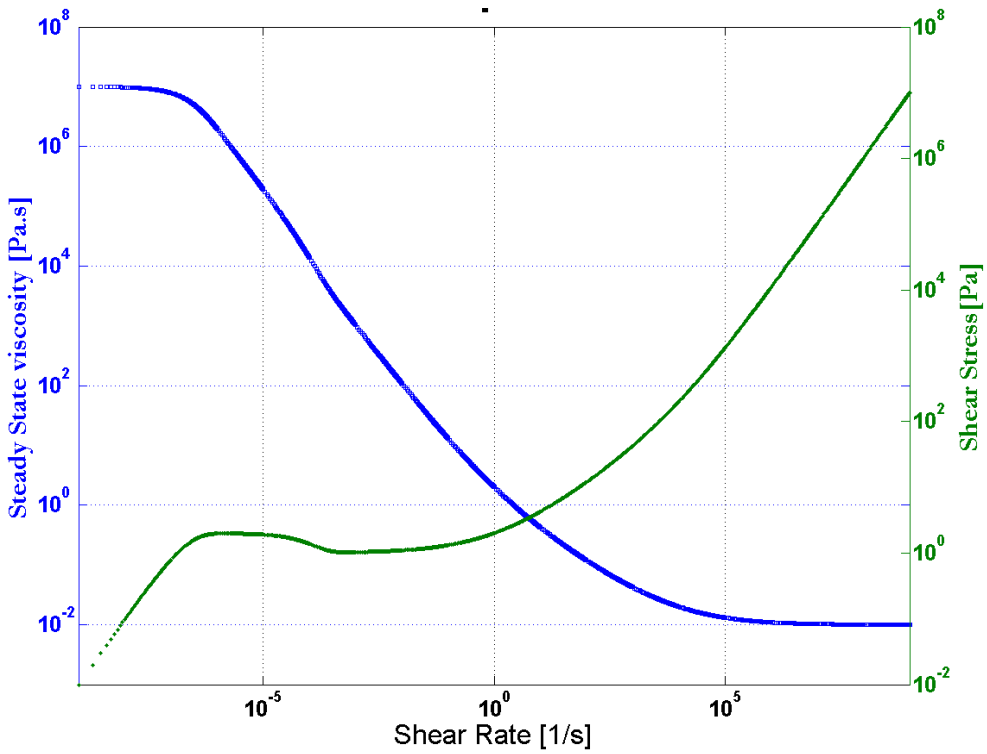

Figure II.15 : Steady State flow properties (flow curve and viscosity curve) as predicted by [Eq. II.11] at constant temperature.

Structure can change according to three basic mechanisms[76] :

- Brownian motion (perikinetic)
- Flow deformation (orthokinetic)
- and differential settling.

The evolution equation for structural change contains terms to cover flow-induced aggregate breakdown and build-up resulting from Brownian motion.

$$\frac{d\lambda}{dt} = \left(\frac{1}{t}\right)^{\beta} \left[Br(1-\lambda)^{a} - f(\sigma)\lambda^{b} \right] \qquad \text{[Eq. II.14a]}$$

By supposing that the elemental structures (particles/aggregates) are of similar sizes [76], the Brownian collision rate is :

$$Br = \kappa = \frac{k_b \cdot T}{6\pi \cdot \eta_{us} \cdot a^3} \qquad \text{[Eq. II.14b]}$$

If the break down term is taken to be proportional to the shear stress [17]:

$$f(\sigma) = \frac{(1-\lambda_{ss})^a}{\lambda_{ss}^b} \kappa \frac{\sigma}{\eta_{vis}(\lambda_{ss})\dot{\gamma}} \qquad \text{[Eq. II.14c]}$$

Combining equations [Eq. II.14b] and [Eq. II.14c] into [Eq. II.14a] yields:

$$\frac{d\lambda}{dt} = \frac{1}{\kappa^{T,P}} \left[(1-\lambda)^a - \left((1-\lambda_{ss})^a \left(\frac{\lambda}{\lambda_{ss}} \right)^b \left(\frac{\sigma}{\eta_{vis}(\lambda_{ss})\dot{\gamma}} \right)^c \right) \right] \qquad \text{[Eq. II.14]}$$

where $\kappa^{T,P} = \frac{k_b \cdot T}{6\pi \cdot \eta_{us} \cdot a^3}$

II.6.3. **Free-volume theory approach**

Many theories for modeling the effect of intensive thermodynamic variables such as temperature (T) or pressure (P) on the rheological behaviour of complex fluids are available in the literature [7, 40, 77]. In this work, the effect of pressure and temperature is based on the free-volume concept. The dependence of flow behaviour on temperature and pressure is introduced through the piezo and thermo dependency of the WLF model.

In the structured phase, the free volume can be considered to have of an equilibrium part $\left(V_f\right)$ and a non-equilibrium part $\left(\omega_f\right)$. The total free volume $\left(V_{f\_Tot}(T)\right)$ at temperature T controls the overall relaxation process:

$$V_{f\_Tot}\left(T\right) = V_f\left(T\right) + \omega_f\left(T\right) \qquad \text{[Eq. II.15]}$$

II.6.3.1. *Temperature dependency*

Several attempts have been made to describe the dependence of viscosity on temperature mathematically. By 1951, Partington had listed nearly 50 [78] of them. Remarkably successful predictions have been achieved by models hybridizing rheological equations (Cross, Carreau, Power-Law) and temperature dependent equations (Arrhenius, WLF) in order to model the temperature dependence of viscosity [79]. The WLF model [61] has proven very reliable. However, at temperatures in the range of Tg, the WLF equation in its original form does not account for non-equilibrium effects occurring in the structured phase. Therefore, following the concept introduced by Tool and then adopted by Rusch et al. [80] the range of validity of the free-volume concept can be extended to include the low-temperature region and account for the thermal history of the structured phase responsible for the non-equilibrium state.

The "effective temperature" T_{eff} is a time and temperature dependent parameter used by Toll [65] to describe the state of a glass. It is the hypothetical temperature at which the glass would have an equilibrium free volume equal to the total free volume of the non-equilibrium glass at temperature T. The concept of fictive temperature is illustrated **Figure II.16** and helps define the non-equilibrium state of the resulting glass [65-66].

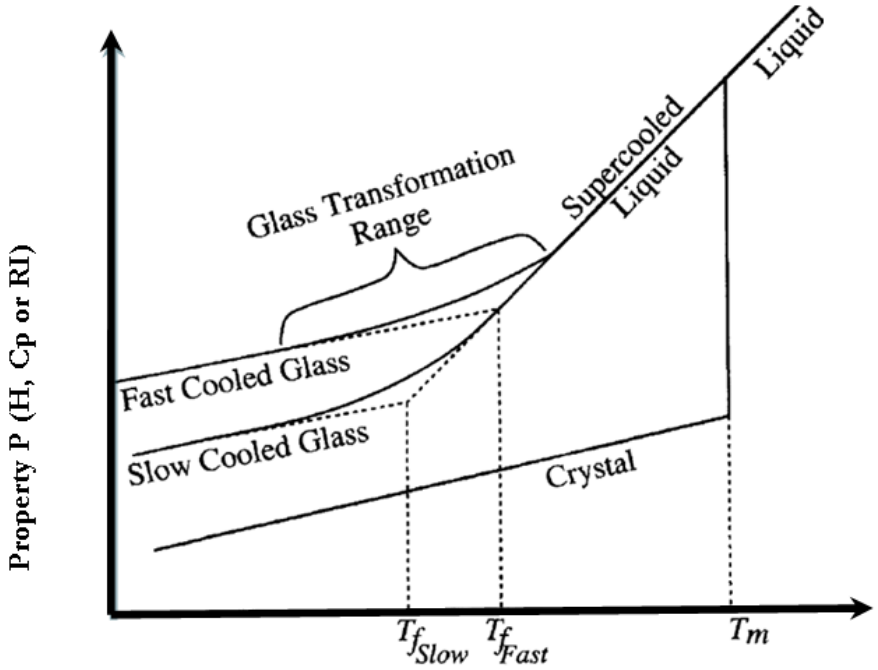

Figure II.16 : As the liquid initially at equilibrium is cooled, different pathways are followed that depend on the cooling rate **q**.

To account for the discrete nature of numerical calculations the following form of the TNM equation is adopted in this work:

$$T_{eff}(T) = T_0 + \sum_{i=1}^{N} \Delta T_i \left[1 - \exp\left(-\left(\sum_{j=i}^{N} \frac{\Delta T_j}{q_j \tau_{pj}} \right)^{\beta} \right) \right] \qquad \text{[Eq. II.16]}$$

where ΔT_i and ΔT_j are temperature increment. N is an iteration index, and i and j are dumb indices. q_j is the heating or cooling rate [K/s].

$$\tau_{pj} = \tau_0 \exp \frac{\Delta H^*}{R} \left[\frac{x}{T} - \frac{(1-x)}{T_{eff(j-1)}} \right] dx \qquad \text{[Eq. II.17]}$$

[Eq. II.17], is the glassy structural relaxation time according to Tool-Narayanaswamy-Moynihan formalism [64] . Caution must be exercised in that (T_0) the starting temperature for the simulation, must be sufficiently high, so that the fluid is initially in equilibrium at that temperature. This is a necessary condition since the properties of glasses are route dependent and every step in the thermal history affects subsequent responses.

II.6.3.2. *Pressure dependency*

Pressure dependency of the rheological properties is expressed in terms of variation of the glass transition temperature $T_g(P)$ and the thermal expansivity of free volume $\alpha_f(P)$ which have a direct effect on C_1 and C_2 . Indeed, as assumed by many authors [1, 61] and demonstrated experimentally (**Figure II.17**), $C_1 = B_g(P)/\left(f_g(P)\ln(10)\right)$ doesn't depend on pressure [81] while $C_2 = f_g(P)/\alpha_f(P)$ does. One possible reason can be the similar dependency on pressure of $f_g(P)$ (the fractional free volume) and $B_g(P)$ (a constant for the dependency of liquid viscosity on temperature in Doolittle equation [62]). However, $f_g(P)$ and $\alpha_f(P)$ are differently affected by pressure.

The glass transition temperature, T_g, increases with increasing pressure. At low pressure, the increase in Tg approximates a linear function [21], whereas at higher pressures dTg/dP gradually decreases as seen in. Although some thermodynamic analysis has been performed to predict dTg/dP [22, 23], details remain unclear. In a study of pressure effects on Tg [24], Oels and Rehage showed that dP/dTg for Polystyrene is a linear function of pressure:

$$\frac{dT_g}{dp} = a + b.P \qquad \text{[Eq. II.18]}$$

Integration of equation [Eq. II.18] yields:

$$T_g(P) = T_{g0} + A_1.\ln(1 + A_2.P) \qquad \text{[Eq. II.19]}$$

where $T_g(P)$ and T_{g0} are respectively the glass transition temperature measured at pressure P and atmospheric pressure. A_1, and A_2 are constants.

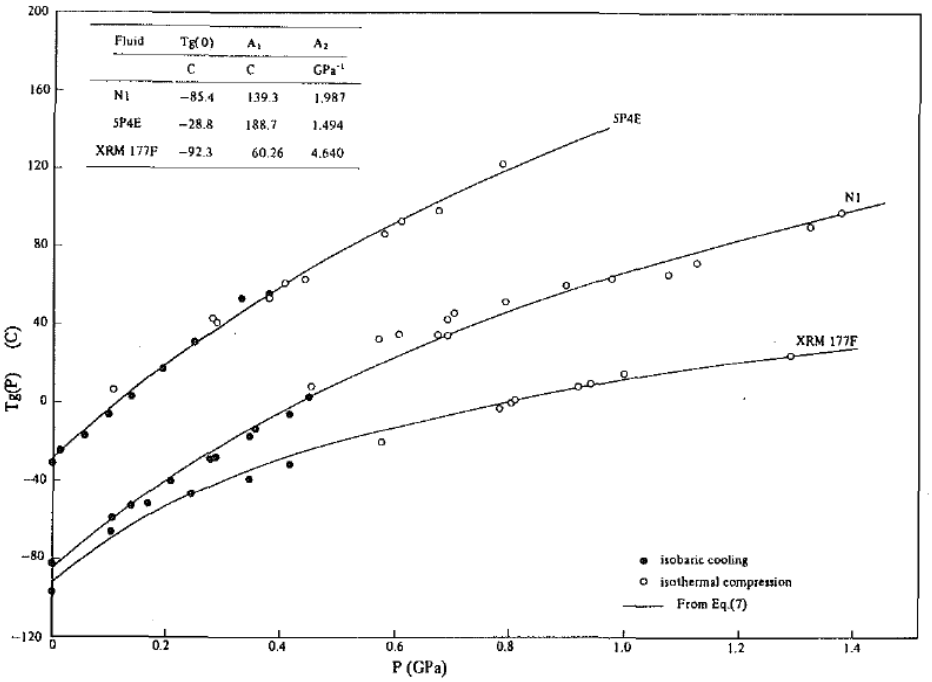

Figure II.17 : Evolution of $T_g(P)$ with pressure using [Eq. II.16]. Data and image source [1].

The free volume doesn't change linearly with pressure as initially assume by Williams et al. [61]. In this work, we account for this non-linearity in terms of the pressure dependency of the thermal expansion coefficient $\alpha_f(P)$ given

$f = f_{ref} + \alpha_f(P).(T - T_{ref})$. According to works by Breuer and Rehage [82] the variation of the thermal expansion coefficient of liquids with pressure can be described by $\alpha_f(P) = \alpha_{f0} \cdot F(P)$ with $F(P) = 1 - B_1.\ln(1 + B_2.P)$, yielding :

$$C_2 = f_{Tref}(P) / (\alpha_{f0} \cdot F(P)) = C_2^{Tref\,0} / F(P)$$

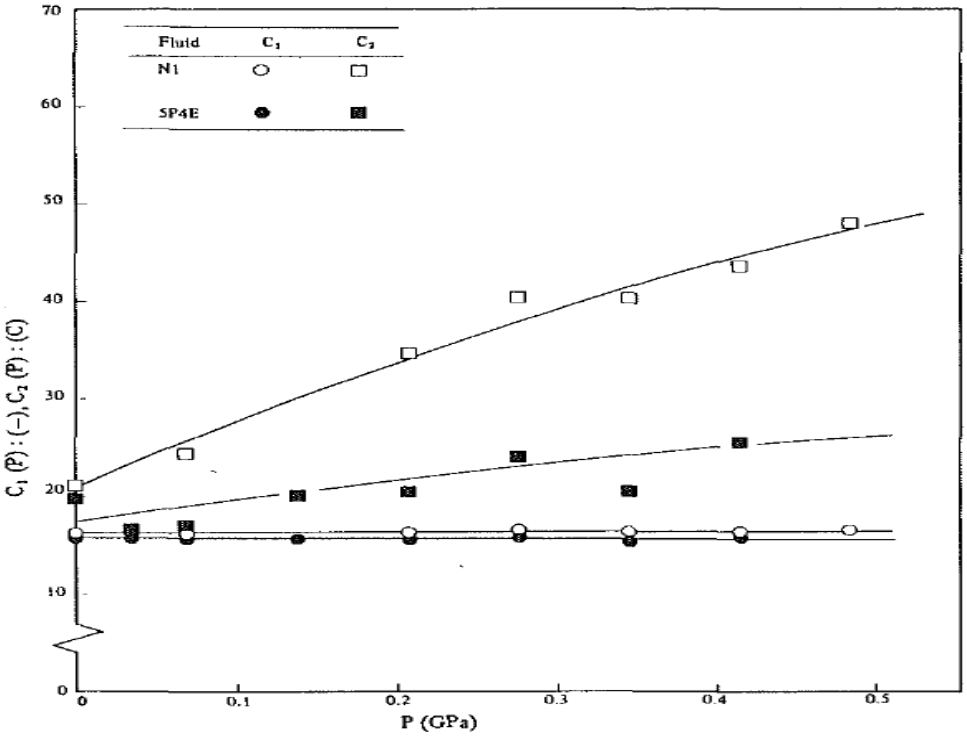

Figure II.18 : Illustration of Pressure dependence of WLF constants, C1 and C2 from [1].

II.6.3.3. *Pressure and Temperature shift function*

Models describing the combined effect of temperature and pressure on the rheological properties of complex fluids can be found in the literature. Many of them are empirical functions of temperature and pressure [9, 83-84] while some are based on the free-volume concept [15].

A modified WLF model introduced by Tschoegl et al. [85] describes the variation of the Newtonian viscosity of heavy petroleum fractions in the temperature range 60 C and 160 C from 1 to 400 bar [86]. In order to extend this model to lower temperatures, where structural relaxation dictates flow behaviour, the concept of fictive temperature[65] is incorporated into this equation.

The modified WFL model, employed in this work is:

$$\mathrm{Log}\left(a_{P,T}\right)=\frac{C_1^{ref0}\left(T_{eff}\left(T,t\right)-T_{ref}\left(P\right)-F\left(P\right)\right)}{C_2^{ref}\left(P\right)+T_{eff}\left(T,t\right)-T_{ref}\left(P\right)-F\left(P\right)} \qquad \text{[Eq. II.20]}$$

where :

$$T_{ref}\left(P\right)=T_{ref0}+A_1.\ln\left(1+A_2.P\right) \qquad \text{[Eq. II.20a]}$$

$$F\left(P\right)=1-B_1.\ln\left(1+B_2.P\right) \qquad \text{[Eq. II.20b]}$$

$$T_{eff}\left(T\right)=T_0+\sum_{i=1}^{N}\Delta T_i\left[1-\exp\left(-\left(\sum_{j=i}^{N}\frac{\Delta T_j}{q_j.\tau_{pj}}\right)^{\beta}\right)\right] \qquad \text{[Eq. II.16]}$$

$$\tau_{pj}=\tau_0\exp\frac{\Delta H^*}{R}\left[\frac{x}{T}-\frac{\left(1-x\right)}{T_{efff(j-1)}}\right] \qquad \text{[Eq. II.17]}$$

$T_{ref}\left(P\right)$ and $F\left(P\right)$ are functions for describing the pressure dependence of the reference temperature T_{ref} and the thermal expansion coefficient $\alpha_f\left(P\right)$ of the free-volume, considered pressure dependent and temperature independent. A1, A2, B1 and B2 are constants. C_1 and C_2 are WLF constants.

II.6.4. **Colloidal structure of hydrocarbons and its effects on rheometry**

The colloidal composition of hydrocarbon materials has been discussed extensively in the literature [6, 87-88]. In Figure II.18, it evident that lowering temperature increase the solid content in hydrocarbon resources such as Maya Crude Oil and Athabasca Bitumen.

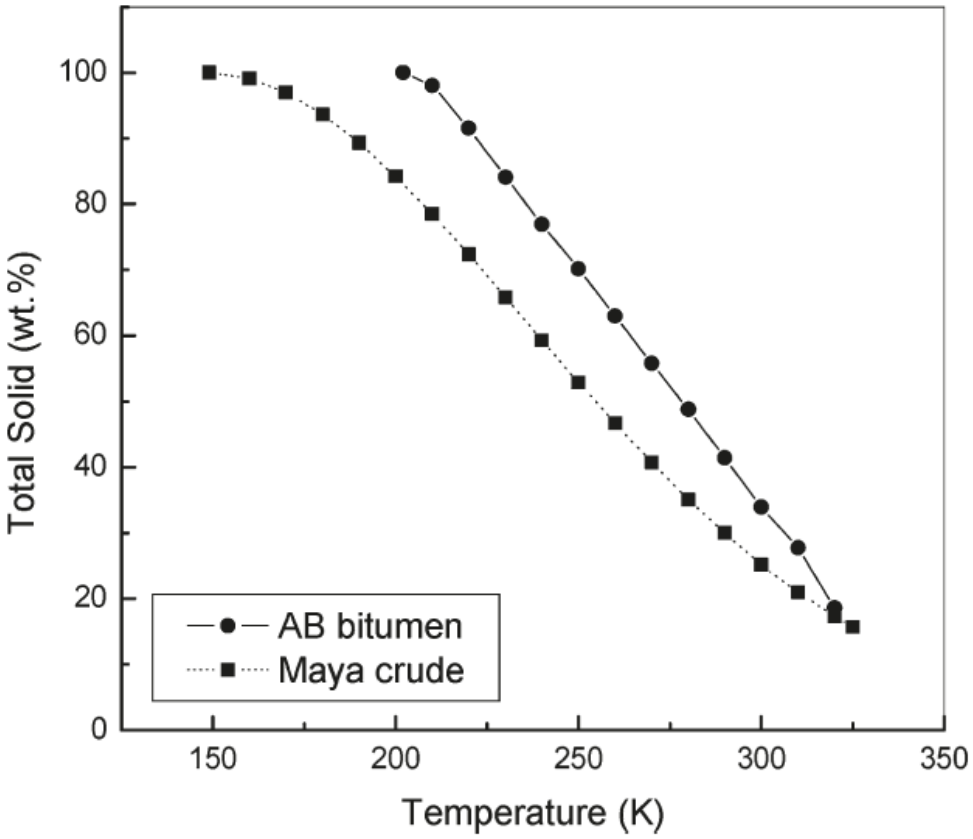

Figure II.19 : Total solids content (wt %) for Athabasca Bitumen and Maya crude oil. Image from [37].

The rheology build-up role of this solid fraction in hydrocarbon fluids is well described by the generalized suspension viscosity equation introduced by R.D. Sudduth in 1993 [89]. This viscosity-concentration equation includes variables

strongly related to the fluid composition and fluid-particle mixtures and was formulated as:

$$\ln\left(\frac{\eta_{fs}}{\eta_{us}}\right)=\frac{\phi_m[\eta]}{i_k-1}\left(\left(1-\frac{\phi}{\phi_m}\right)^{(1-i_k)}-1\right) \qquad \text{for } i_k \neq 1 \qquad \text{[Eq. II.21]}$$

where i_k is the particle interaction constant, ϕ_m is the particle maximum packing fraction, ϕ is the suspension particle volume fraction, η_{fs} is the suspension viscosity, η_{us} is the suspending medium viscosity, $[\eta]$ is the intrinsic viscosity of the solid fraction. In the perspective of this modeling effort the zero-shear viscosity in η_{fs} of the hydrocarbon will be related to that of its maltene phase η_{us} through [Eq. II.21]. Similarly, the network induced stress σ_{nt}, the elastic modulus G_{fs}, the consistency index **K** and the flow index **n** depend on the suspension particle volume fraction ϕ. In this regard, works by Coussot et al. [90] on the yield stress and elastic modulus of non-colloidal particles suspensions has shown that the $G_{fs}-\phi$ relationship follows a Krieger-Dougherty law and can be related to the $\sigma_{nt}-\phi$ relationship [91]. Their observation is extended in this work using the Sudduth equation for the solid fraction dependency of the elastic modulus.

$$\ln\left(\frac{G_{fs}}{G_{us}}\right)=\frac{\phi_m[\eta]}{i_k-1}\left(\left(1-\frac{\phi}{\phi_m}\right)^{(1-i_k)}-1\right) \qquad \text{for } i_k \neq 1 \qquad \text{[Eq. II.21a]}$$

and

$$\frac{\sigma_{st}}{\sigma_{us}}=\sqrt{(1-\phi)\frac{G_{fs}}{G_{us}}} \qquad \text{[Eq. II.21b]}$$

II. 7. SUMMARY

II.7.1. **The system**

Bitumen and Heavy oils are complex fluids at low temperatures. Their flow behaviour depends mainly on the time and temperature response of their structured phase to shear.

At high temperatures their flow response is Newtonian. At temperatures below glass transition region, their rheology is characterized by limiting values of viscosity and shear modulus.

Although this chapter concentrates on time dependent behaviours, from a practical perspective, it is the steady state properties which govern the flow in most fields, transport and process applications as these involve steady shear flow environments. Exceptions include storage tanks and multi-use pipelines where fluids are batch transported. But in most cases where flow is observable, steady state is reached in a matter of minutes. As a result, an accurate predictive tool for steady state flow properties is the prime concern. It is for this reason, that the development of a model for the relaxation of the structured phase, α-relaxation, is the focus of this work.

As the phenomena responsible of the complex flow responses observed in heavy oils and bitumen with deformation and temperature are complex, a combination of relevant models has been adopted from the literature:

1. A Maxwell Mechanical representation (**Figure II.12**) is used to define these fluids as a structured phase within a Newtonian fluid matrix.
2. In the Maxwell like construction, each element in the model is a function of λ **[Eq.** II.7**]**.

3. A structural kinetics model is adopted to describe the rheological behaviour of these fluids with deformation **[Eq.** II.14**]**.
4. The effects of intensive thermodynamic variables (temperature and pressure) are accounted through a free-volume based theory.
5. Using a colloidal theory by Sudduth [89], steady state material functions can be expressed as function of solid volume fraction.

The equations, coefficients, and properties comprising the model are summarized in **Table II-1**. A total of **17** parameters must be identified from experimental rheological data or taken from the literature. These topics and the model simplification are addressed in **Chapter 3** where the modified Structural Kinetics model is presented in detail.

II.7.2. **Summary of the Structural Kinetics Model**

The SKM-WLF model

The Structural Kinetic equations (λ-Model)

$$\eta_{vis}(\lambda)\cdot\dot{\gamma} = \sigma_{tot} + \dot{\sigma}_{tot}\left(\frac{\eta_{vis}(\lambda)}{G(\lambda)}\right) \quad \textbf{[Eq. II.7]}$$

$$G(\lambda) = \frac{G_{fs}}{\lambda^{m}} \quad \textbf{[Eq. II.8]}$$

$$\eta_{vis}(\lambda) = \left(\frac{\eta_{fs}}{\eta_{us}}\right)^{\lambda}\eta_{us} \quad \textbf{[Eq. II.10a]}$$

$$\lambda_{ss}(\dot{\gamma}) = \left(\frac{\ln\left[\eta_{ss}(\dot{\gamma})\right]-\ln\left[\eta_{us}\right]}{\ln\left[\eta_{fs}\right]-\ln\left[\eta_{us}\right]}\right) \quad \textbf{[Eq. II.10]}$$

$$\eta_{ss}(\dot{\gamma}) = \left(1-e^{-\frac{\eta_{fs}\cdot\dot{\gamma}}{\sigma_0}}\right)\left(\frac{(\sigma_0-\sigma_{0d})e^{-\frac{\dot{\gamma}}{\dot{\gamma}_{0d}}}+\sigma_{0d}}{\dot{\gamma}}+K\dot{\gamma}^{(n-1)}\right)+\eta_{us} \quad \textbf{[Eq. II.11]}$$

$$\frac{d\lambda}{dt} = \frac{1}{\kappa^{T,P}}\left[(1-\lambda)^{a}-\left((1-\lambda_{ss})^{a}\left(\frac{\lambda}{\lambda_{ss}}\right)^{b}\left(\frac{\sigma}{\eta_{vis}(\lambda_{ss})\dot{\gamma}}\right)^{c}\right)\right] \quad \textbf{[Eq. II.14]}$$

with $\kappa^{T,P} = \frac{k_b\cdot T}{6\pi\cdot\eta_{fs}^{T,P}\cdot\iota^{3}}$

The T and P dependent shift function ($a_{T,P}$)

$$Log\left(a_{T,P}\right) = \frac{C_1^{Tref0}\cdot\left(T_{eff}(T)-T_{ref}(P)\right)\cdot F(P)}{C_2^{Tref0}+\left(T_{eff}(T)-T_{ref}(P)\right)\cdot F(P)} \quad \textbf{[Eq. II.20]}$$

$$T_{ref}(P) = T_{ref0} + A_1.\ln\left(1+A_2.P\right) \quad \textbf{[Eq. II.20a]}$$

$$F(P) = 1 - B_1.\ln\left(1+B_2.P\right) \quad \textbf{[Eq. II.20b]}$$

$$C_1^{Tref0} = cte$$

$$C_2^{Tref0} = cte$$

$$T_{eff}(T) = T_0 + \sum_{i=1}^{N}\Delta T_i\left[1-\exp\left(-\left(\sum_{j=i}^{N} rt_j\right)^{\beta}\right)\right] \quad \textbf{[Eq. II.16]}$$

with

$$rt_j = \begin{cases}\Delta T_j/(q_j\cdot\tau_{pj}) & \text{during temperature jump}\\ \Delta t_j/(\tau_{pj}) & \text{during annealing step}\end{cases}$$

$$\tau_{pj} = \tau_0\exp\frac{\Delta H^{*}}{R}\left[\frac{x}{T}-\frac{(1-x)}{T_{eff-1}}\right] \quad \textbf{[Eq. II.17]}$$

Material properties

Functions

$$\eta_{fs}^{T,P} = \eta_{fs}^{Tref,0}\cdot a_{T,P} \qquad \eta_{us}^{T,P} = \eta_{us}^{Tref,0}\cdot a_{T,P} \qquad G_{fs}^{T,P} = G_{fs}^{Tref,0}\cdot a_{T,P}$$

$$n = n_{Tref0} + p_n\times\left(1-\frac{T_{eff}}{T_{ref0}}\right) \qquad K = K_{Tref0}\times\exp\left(-p_K\left(1-\frac{T_{eff}}{T_{ref0}}\right)\right)$$

Constants

ΔH_{fs}^{*}; τ_0; x; q_j; N; β

A_1; A_2; B_1; B_2; C_1^{Tref0}; C_2^{Tref0}

$\eta_{fs}^{Tref,0}$; $\eta_{us}^{Tref,0}$; $G_{fs}^{Tref,0}$; σ_{0d}; σ_0; K; n

n_{Tref0}; p_n; K_{Tref0}; p_k

Chapter III: IDENTIFICATION OF MODEL PARAMETERS

III. 1. EQUIPMENT AND MATERIALS

III.1.1. **The Rheometer**

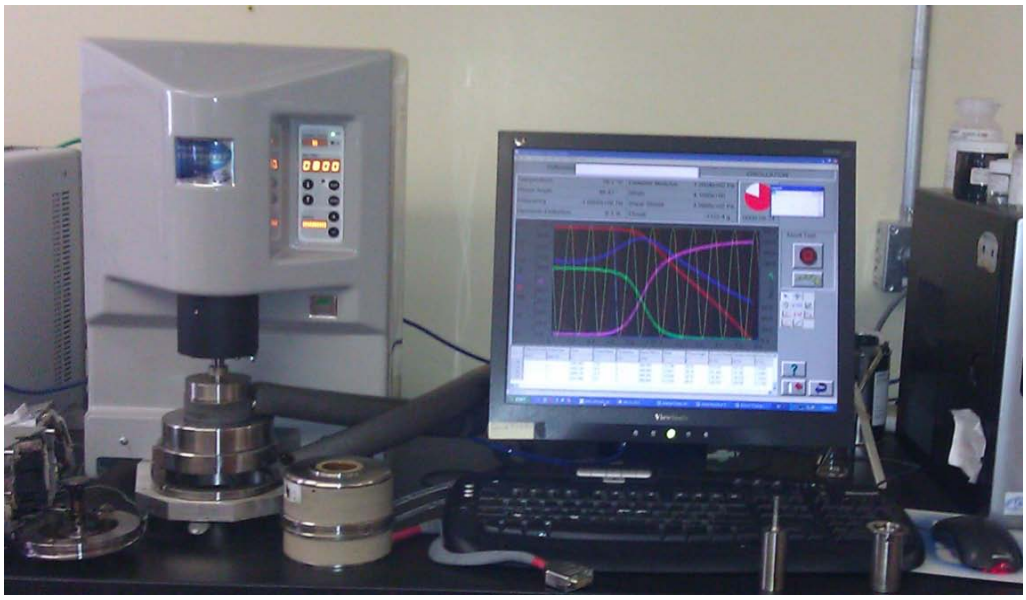

Figure III.1 : The Gemini HR NanoRheometer equipped with Double Gap geometry and a Peltier assembly for temperature control

The Malvern Bohlin Gemini HR NanoRheometer is a compact Rheometer with a capability of testing both fluids and solids. The equipment is optimized for strain controlled and stress controlled operations and can work with various types of temperature control devices in steady, dynamic as well as in transient modes. It

provides torque in the range of 10nNm to 200mNm for controlled stress/rate viscometry and 3nNm to 200mNm for controlled stress/strain oscillations and has a torque resolution better than 1nNm. In its controlled stress mode(used in this study), the Rheometer applies, defined shear stresses to the test sample by means of an extremely low inertia, drag cup motor. The drive shaft of the Bohlin Gemini HR NanoRheometer is centered by an air bearing which ensures an almost "frictionless" transmission of the applied stress to the tested fluid. The resulting deformation on the sample placed into a sensor system is detected with a digital encoder processing **1 million impulses per revolution**. This resolution makes it possible to measure even the smallest yield values as well as extremely low strains or shear rates.

The Bohlin Gemini HR NanoRheometer is computer controlled to swap between both the CS and CR-modes and can provide oscillating stress inputs. A controlled lifting system, with variable speed, axially positions rotor versus a cup or a cone versus a plate.

A built-in standard procedure provides10-point flow- and viscosity curves which "finger-print" the rheological behaviour of a given material. During this test, the time required to reach steady state depends on the "strength" of the viscous and elastic elements as well as the value of the applied "stress". Considerable length of time may be required until the material is sufficiently deformed to remove all elastic deformation and just measuring the pure viscous flow. When this state is achieved, the measured shear rate is constant and the slope of the compliance curve as a function of time is 45° i.e. 1.00. This is the number shown by the Bohlin software. Under these conditions the measured viscosity of the material doesn't contain any effects due to elasticity.

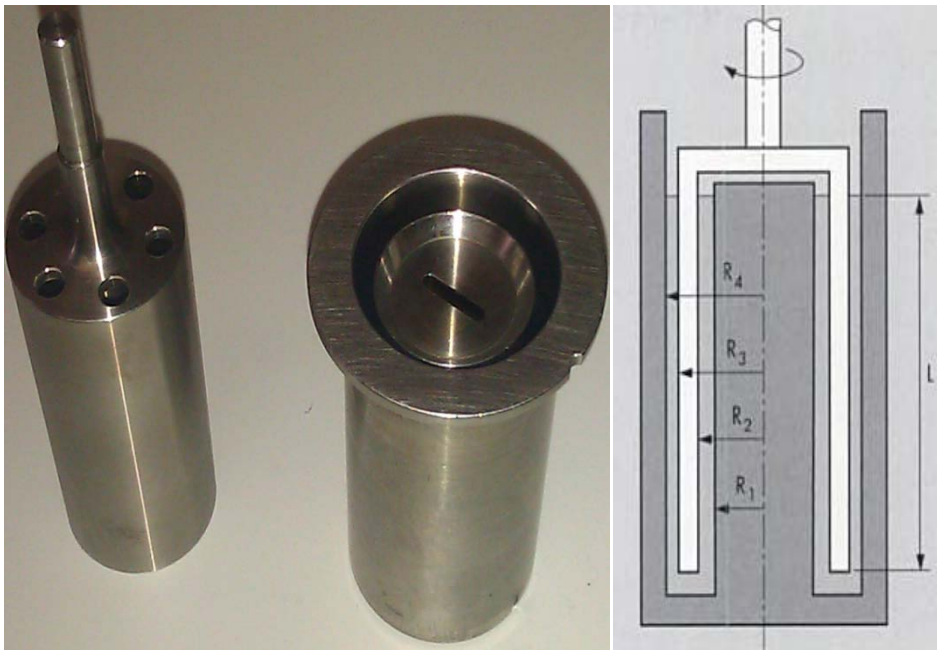

Figure III.2 : Representation of the double gap assembly DG24/27 Ti used during the measurements

III.1.2. **Double-gap measuring systems (DG MS)**

The double-gap measuring system comprises concentric cylinders designed for low-viscosity liquids. According to the standard geometry (DIN 54453), an inner cylinder is mounted in the center of the cup and the gap is annular as shown on **Figure III.2**, where $R4 / R3 = R2 / R1 \leq 1.15$. The bob is a hollow cylinder. Both the inner and outer surfaces are exposed to the fluid. The goal is to reach a uniform shear condition in the inner and outer gap concerning the shear rates. The analysis was performed on 10 ml samples, injected from the fridge, using a syringe (which provides a pre-shear condition). A toluene gas blanket surrounds the assembly to prevent the release of light hydrocarbon upon heating. The Peltier assembly is used to control temperature. Operating procedures,

measurement quality, calibration methods, and other experimental details related to this equipment can be find in the DIN 54453, the "Bohlin Help System" and are briefly explained in III.3.2 and reported elsewhere [16] .

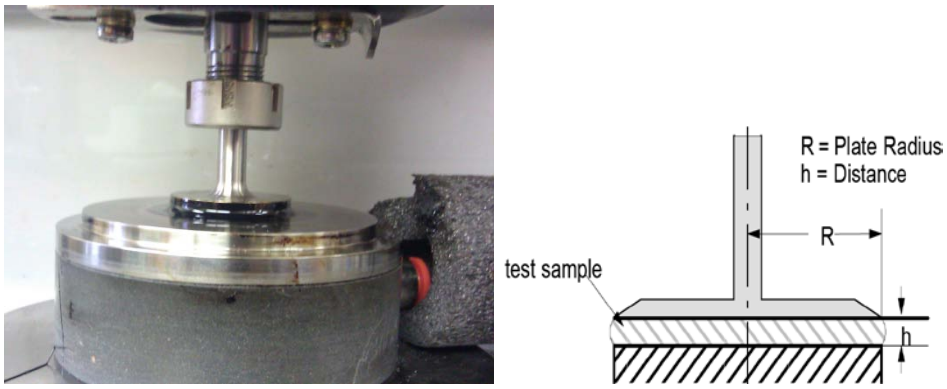

Figure III.3 : Representation of a sample as loaded on a parallel-plate/cone-plate geometry used during the measurements.

III.1.3. **Samples**

Rheological data on structured fluids are hard to reproduce and are sensitive to sample preparation, physical history, and experimental protocol. In this work Maya crude oil (commercial-blend heavy oil from Mexico), Athabasca bitumen (Alberta, Canada) and Safaniya vacuum residue are the main hydrocarbon fluids assessed. It has been reported that upon heating above 360K (86 °C), thermal irreversibility of viscosity, due to slowly reversing or irreversible phase transitions of the heavy fractions and/or evaporation of light components occurs for Maya crude oil [16]. In this work, measurements were performed at temperatures far below this temperature. In order to have a defined shear and temperature history, all samples used in this work were pre-sheared and pre-heated before testing. The flow curve ($\sigma \times \dot{\gamma}$) and steady-state shear viscosity ($\eta_{ss} \times \dot{\gamma}$) curve were measured

at 268.15K for Maya Crude Oil, 308.15K for Athabasca Bitumen and 313.15K for Safaniya Heavy Oils.

III. 2. FLUID CHARACTERIZATION

In order to better model a given complex fluid, under the scope of this study, a full characterization of the material is crucial. Indeed, three behaviours need to be captured in order to simulate the complex rheological behaviour of bitumen and heavy oil at low temperatures.

- The *transient flow* responses are described by **[Eq. II.14']** with parameters $(G_{fs}, m, a, b, c$ a dh ι$)$ adopted from literature [17, 22, 92].
- The kinetics of structural behaviour with temperature is assessed through *temperature sweep test* $\left(\Delta H^{*}_{fs};\ \tau_0;\ x; \beta; T_{ref\,0}; C_1^{Tref\,0};\ C_2^{Tref\,0}\right)$, under low shear rate conditions.
- After identifying the reference temperature (**Tref)** from the viscosity-temperature plot, the second experiment that describes the kinetics of structural behaviour with shear (steady-state shear sweep) is performed by *flow curve measurements* $(n,\ K,\ \sigma_0,\ \sigma_{0D},\ \eta_{fs},\ \eta_{us})$.

III. 3. LABORATORY MEASUREMENTS

III.3.1. **Overview**

The SKM model is under constrained. Some parameters are determined experimentally only and some are defined through the literature. Experimental data provide a training data set, used to fit model parameters, and two test data sets. The first test data set comprises data for the same fluids as in the training

data set but at conditions outside the training conditions (the extrapolation data set). The other data set comprises rheological data for nanofiltered permeates and retentates derived from the fluids comprising the training set but possessing different ratios of structured to unstructured fluid phases (the prediction data set). The fluids tested are Athabasca bitumen, Maya crude oil and Safaniya crude oil. The shear rheometry of the samples was measured in oscillatory and rotational modes using a CS/S Bohlin Gemini HR nano-Rheometer (**Figure III.1**) available in the Petroleum Thermodynamics laboratory at the University of Alberta. Supplemental calorimetric measurements were also performed. The modelling approach is based on fundamental principles and assumptions (II.6.1). It requires the input of two set of variables. The first set of parameters (shear rate, shear stress, and cooling rate, annealing time) is independent of experiment and defines the process conditions being simulated. The second set of parameters depends on experiments and is determined from literature but also by regression of observed data as applied through the model equations. The parameters pertaining to this set of variables are obtained from a ***temperature sweep test*** $\left(\Delta H_{fs}^{*};\ \tau_0;\ x;\ \beta;T_{ref\,0};C_1^{Tref\,0};\ C_2^{Tref\,0}\right)$, and detailed ***flow curve measurements*** $\left(n,\ K,\ \sigma_0,\ \sigma_{0D},\ \eta_{fs},\ \eta_{us}\right)$ at a reference temperature.

III.3.2. **Validity of rheological measurements**

The measurements done in this study were carried out using a controlled stress/strain Bohlin Gemini HR nano rheometer (Malvern Instruments Limited, U.K.). The measuring configurations used are :

1- a double gap 24/27 mm concentric cylinder equipped with a Peltier assembly using the principle of the Peltier heat pump. That allowed measurements from (253 K to 453 K) with stability of 0.2 K;

2- parallel plates and cone-plate (25 mm and 40 mm diameter) with an extended temperature cell (ETC) using a forced gas system to heat and cool the sample. The ETC can also be fitted with a low temperature extension (LTE), cooled with a stream of liquid nitrogen, in cases where measurements below ambient temperatures are required. The ETC in these two complementary configurations (with and without LTE) covers temperature range from 123 K to 823 K with a stability better than 0.2 K.

In the ETC, temperatures are measured with a thermocouple (calibrated to ITS 90 using a PT100 resistance thermometer) inserted into the middle of the lower plate. Similar setting is used in the Peltier cylinder and calibrated in same way. Temperature errors in both cases are estimated to be less than 0.2 K. Assuming a Williams-Landel-Ferry type of temperature dependency of viscosity, these deviations in temperature will contribute in 2% to 3% inaccuracy for viscosity readings. All experiments were conducted under a nitrogen atmosphere to avoid oxidation.

The space between the parallel plates and cone-plate were set between 500 μm to 1000 μm depending on the range of viscosity values studied. The double gap cylinder was set at default value of 150 μm.

The experimental conditions and the operating parameter values for the rheological experiments were validated by measuring the viscosity of the Cannon certified viscosity standards N2700000SP, N74B, N1400B, and N115B (from

Cannon Instrument Company, U.S.A.) and PRA standard oils#12 and U3600 (from Paint Research Association, U.K.). The agreement with the recommended data in the certified temperature range of 244K to 349K are within 5 % error for both the double gap cylinder in the Peltier assembly and the parallel plates in the ETC without cooling. A 10 % error is obtained for the parallel plates in the ETC with nitrogen cooling. The data pertaining to this validation procedure are summarized in **Table III-1** and published in [16].

Standards	T [K]	η_{stand} [Pa.s]	η_{exp} [Pa.s]		100 (η_{exp} - η_{stand})/η_{stand} [-]%	
			DGC-PA	PP-ETC	DGC-PA	PP-ETC
PRA standard oil #12	293.2	1.449	1.425	1.419[c]	-1.7	-2.1
	298.2	0.972	0.961	0.997[c]	-1.1	2.6
PRA standard oil U3600	293.2	15.33	15.31	15.80[c]	-0.1	3.1
	296.2	11.63	11.55	11.94[c]	-0.7	2.7
	298.2	9.705	9.623	9.936[c]	-0.8	2.4
	303.2	6.287	6.203	6.343[c]	-1.3	0.9
Cannon certified viscosity standard N2700000SP	325.2	604.9		582.1[c]		-3.8
	331.2	397.6		391.1[c]		-1.6
	337.2	267.3		259.0[c]		-3.1
	343.2	183.1		180.4[c]		-1.5
	349.2	128.1		124.0[c]		-3.2
Cannon certified viscosity standard N74B	273.2	3.502	3.383	3.551[d]	-3.4	1.4
Cannon certified viscosity standard N1400B	260.2	168.9	169.6	174.4[d]	0.4	3.3
	262.2	135.2	137.2	142.9[d]	1.5	5.7
Cannon certified viscosity standard N115B	244.3	140.2		146.9[d]		4.8
	247.0	94.10		96.65[d]		2.7
	249.8	64.45		69.73[d]		8.2
	255.4	31.93	32.41	33.64[d]	1.5	5.4
	260.9	17.00	16.84	17.44[d]	-0.9	2.6
	266.5	9.575	9.496	10.16[d]	-0.8	6.1

Table III-1: Table showing the measured viscosities against standards values. This procedure is used to assess the validity of the rheological measurements. DGC-PA stands for the double gap cylinder in a Peltier assembly; PP-ETC is for the parallel plates in an ETC; η_{stand} refers to the reference viscosity value; η_{exp} is the experimental viscosity. The gaps between, 25mm diameter, plates in the PP-ETC configuration are: 750µm for PRA standard oil #12 and PRA standard oil U3600, 700µm for Cannon certified viscosity standards N74B, N115B, and N1400B, and 1000µm for Cannon certified viscosity standard N2700000SP. Shear strain range of tests: 1% to 50 % for PRA standard oil #12 and PRA standard oil U3600, 0.1% to 50% for Cannon certified viscosity standards. N74B, N115B, and N1400B, and 0.3% to 1% for Cannon certified viscosity standard N2700000SP. [c] for values measured in the ETC without nitrogen cooling. [d] for data measured in the ETC with nitrogen cooling.

III.3.3. **The Temperature sweep test**

The temperature sweep test is used to follow changes in state, such as a melting phenomenon, glass transition and curing in samples. When cooling under constant shear conditions, it is important to follow the kinetics of structure build-up in real time, without disrupting the process itself. For this reason, a very low frequency (1Hz or 10rad/sec) or shear rates (10^{-3} 1/s) are used. The temperature is ramped at a meaningful rate (-3K/min) to minimize temperature gradients effects in samples. Parallel-plates and cone-plate geometries mounted with an extended temperature cell (ETC) are used for Athabasca Bitumen and Safaniya Heavy Oil. Indeed those two samples a very stiff at room temperatures compared to Maya crude oils where a syringe is used to sample the material. For Maya crude oil, a double-gap geometry equipped Peltier assembly (DGC-PA) is used for measurement. Since the relaxation processes in petroleum materials decelerate as temperature decreases, a longer equilibrium time is set for measurements in the low temperatures region. From the viscosity-temperature curves on **Figure III.7**, the reference temperature is chosen in the region where the material response is equally dominated by both the **a** and the **b** relaxation processes[46]. The region is characterized by the end of the linear increase of viscosity with temperature when cooling. It points better the bimodal rheology [46]of heavy oil and bitumen.

From these curves on **Figure III.7**, temperature dependency parameters $C_1^{Tref\,0}$ and $C_2^{Tref\,0}$ are obtained by regressing the experimental data (III.4.2) with the linear form of **[Eq. II.20]** while ΔH^*, $\ln(\tau_0)$, x, β are determined by fitting with the TNM equations (III.4.3).

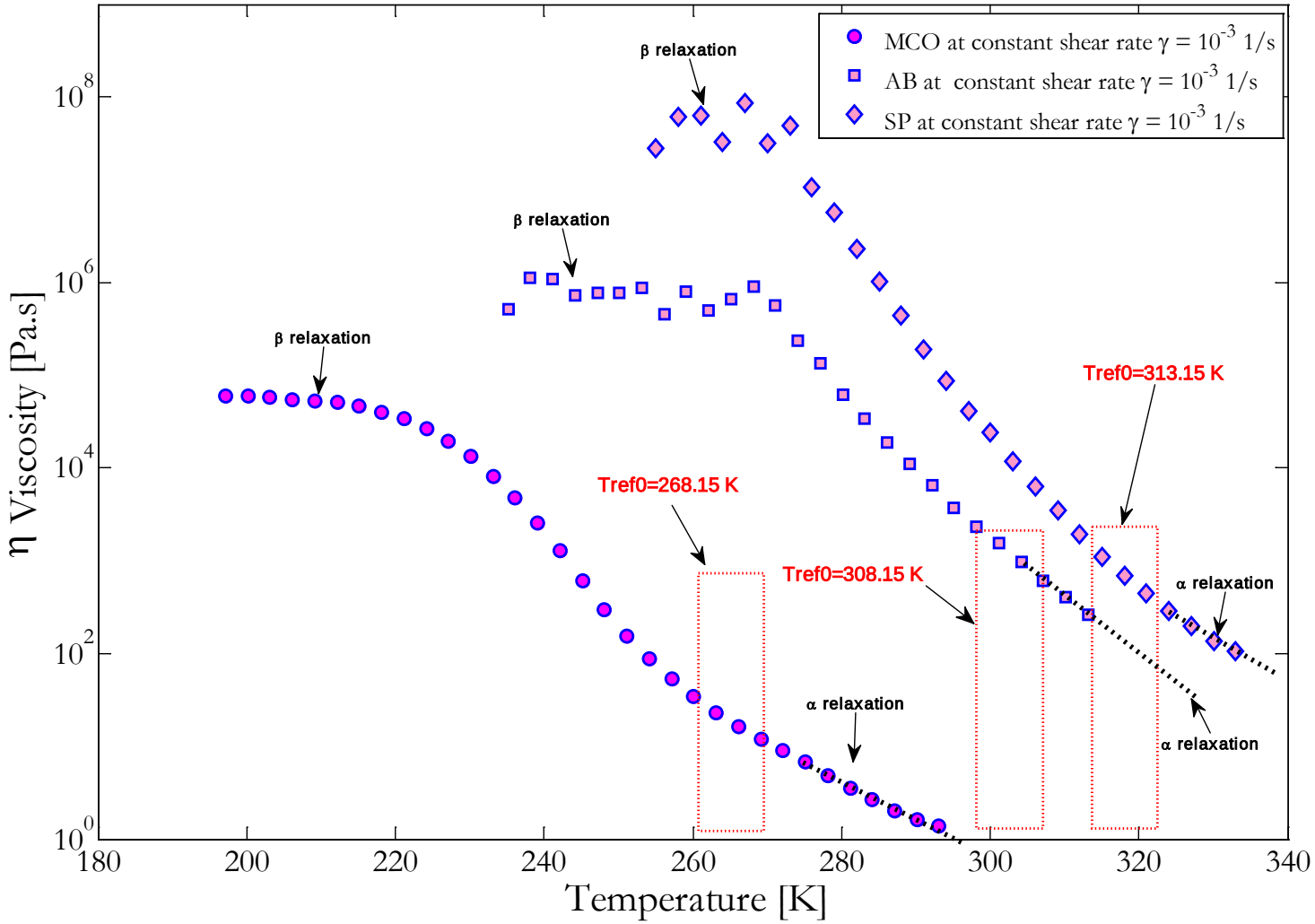

Figure III.4 : Temperature sweep curve for Maya crude oil(MCO), Athabasca Bitumen (AB) and Safaniya vacuum residue(SP) obtained under iso-shear condition.

III.3.4. **Flow ($\sigma \times \dot{\gamma}$) and viscosity curves ($\eta_{ss} \times \dot{\gamma}$) measurements**

A step shear process, using a table of preset shear values, was performed. Before each test, samples are pre-sheared at 1600Pa for 300s, and annealed for 300s at 268.15 K to ensure a common shear and thermal history. Then shear, rates ranging from 0.001 to 100 $\mathbf{s^{-1}}$**,** were applied, with a logarithmic increase over a period of 10 minutes (this period was varied) at respective $\mathbf{T_{ref0}}$ (268.15 K for Maya Crude Oil, 308.15 for Athabasca Bitumen and 313.15K for Safaniya Heavy Oils). The DGC-PA set-up is used for flowing materials such as Maya crude oil while cone-plate-ETC and PP-ETC assemblies are used for stiff materials like Athabasca Bitumen and Safaniya Heavy Oil. From flow curves, estimative values of parameters $(n, K, \sigma_0, \sigma_{0D}, \eta_{fs}, \eta_{us})$ are determined graphically using the procedure illustrated on **Figure III.5**. From these tests, flow curves such as those in **Figure III.6, Figure III.7** and **Figure III.8** were obtained and the estimated values are recorded in **Table III-3**. A summary of the procedures used to collect those data is shown on **Table III-2**.

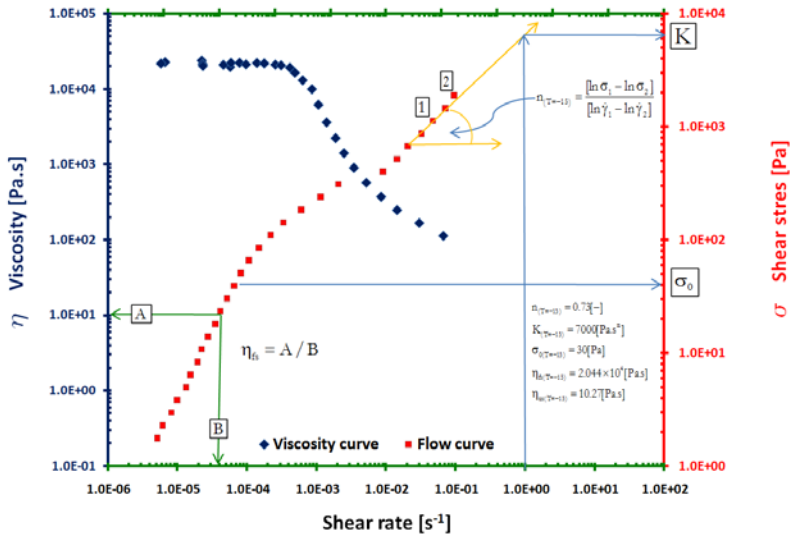

Figure III.5 : Steady state viscosity and flow curve of Maya crude oil at reference temperature of 258.15K (-15C). The physical meaning of the flow curve parameters is illustrated.

Imprinting a defined shear and thermal history on samples				
1- Sample Pre-conditioning Cooling to 248K(-25°C) Shear at 1600Pa for 5 min wait time 5 min	**2- Temperature ramp up to 345K (72°C)** The shear is 1600Pa Thermal equilibrium time is 60s Ramp rate 3°C/min	**3- Temperature ramp down to 248K (-25°C)** The shear is 1600Pa Thermal equilibrium time is 60s Ramp rate 3°C/min		
Performing the shear sweep tests				
1- Shear Stress Ramp to 1600Pa at 248K (-25C) Min Shear= 6mPa Max Shear= 1.6kPa Sample= 2000 Delay Time= 60s Timeout= 900s	**2- Shear Stress Ramp to 1600Pa at 258K (-15C)** Min Shear= 6mPa Max Shear= 1.6kPa Sample= 2000 Delay Time=60s Timeout=900s	**3- Shear Stress Ramp to 1600Pa at 273K (0C)** Min Shear=6mPa Max Shear=1.6kPa Sample= 2000 Delay Time=60s Timeout=900s	**4- Shear Stress Ramp to 1600Pa at 293K (20C)** Min Shear=6mPa Max Shear=1.6kPa Sample= 2000 Delay Time=60s Timeout=900s	**5- Shear Stress Ramp to 1600Pa at 323K (50C)** Min Shear=6mPa Max Shear=1.6kPa Sample= 2000 Delay Time=60s Timeout=900s

Table III-2 : Summary of the procedures used to collect data for the flow curve and viscosity curve. A preconditioning procedure is used to imprint a defined thermal and deformation history to the sample before testing and data collection.

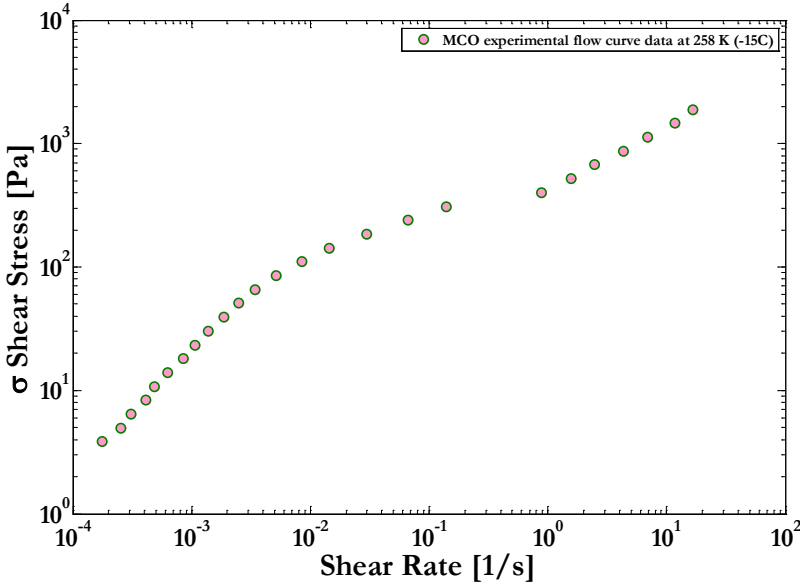

Figure III.6 : Experimental flow curves of Maya crude oil measured at reference temperature Tre0=258.15K**.**

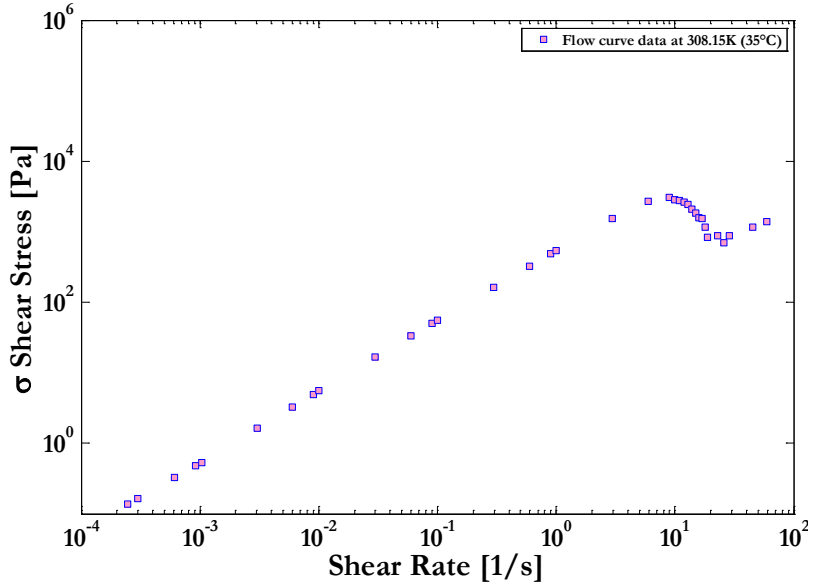

Figure III.7 : Experimental flow for Athabasca Bitumen obtained under isothermal conditions Tref0=308.15K**.**

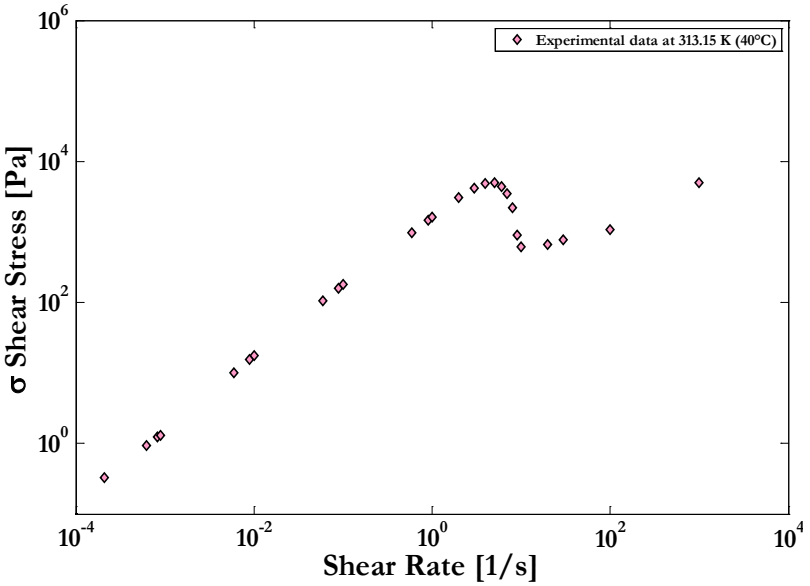

Figure III.8 : Measured flow curve of Safanyia Vacuum Residue. Tref0=313.15K**.**

Material	Reference temperature		Power Law indexes		Yield stresses		Limiting viscosities	
	T [C]	T [K]	n	K	σ_0 [Pa]	σ_{0D} [Pa]	η_{fs} [Pa.s]	η_{us} [Pa.s]
AB	35	308.15	0.2	25	3000	709	560	24
MCO	-15	258.15	0.74	16.99	13	10	21	5
SP	40	313.15	0.7	20	4930	635	1600	1

Table III-3: Preliminary flow curve parameters estimated graphically according to the illustration of **Figure III.5 .**

In order to reduce uncertainties associated with their graphical estimations, the parameters in **Table III-3** will be optimized using a Levenberg–Marquardt [93] fitting procedure. The idea is to get the set of value that fit better the experimental flow curve to **[Eq. II.11]**.

III. 4. DSC DATA

The thermal history effects are assessed through DSC analysis of petroleum heavy fractions at various heating/cooling rates. The DSC data used in this work are of different experimental sources and physically consistent.

Figure III.9 : The TG-DSC 111 thermoanalyzer used in the worl by Bazyleva, A.B., et al. [16]

In the work by Bazyleva et al [16] thermo gravimetric analysis (TGA) of bitumen and heavy oil samples was performed using a TG-DSC 111 thermoanalyzer pictured in **Figure III.9**. Thermo grams of asphaltenes from Athabasca Bitumen and Maya Crude Oil are shown in **Figure III.10**. A phase transition region for unaged samples of asphaltenes from Athabasca Bitumen and Maya Crude Oil occurs at approximately 423.15K (150°C). Glass transition and melting point temperatures of asphaltenes have been investigated by a few numbers of researchers using DSC [6, 48]. Kopsch [94] claimed that asphaltenes precipitated with the same solvent react relatively uniformly regardless of the origin of the crude oils.

Asphaltenes	**Glass Transition Temperature Tg [K]**	**Limiting fictive Temperature T'_{eff} (K)**	**Heating/ Cooling rate [K/min]**
Maya Crude Oil C5 [16]	423 ± 10	140	5
Athabasca Bitumen C5 [16]	423 ± 10	140	5
Kirkuk crude oil [94]	586 ± 6	307	10
Kirkuk crude oil [94]	604 ± 9	3329	20
Kirkuk crude oil [94]	626 ± 11	342	50

Table III-4 : Limiting Fictive temperature and glass transition data for asphaltenes as obtained from experimental results and the literature review.

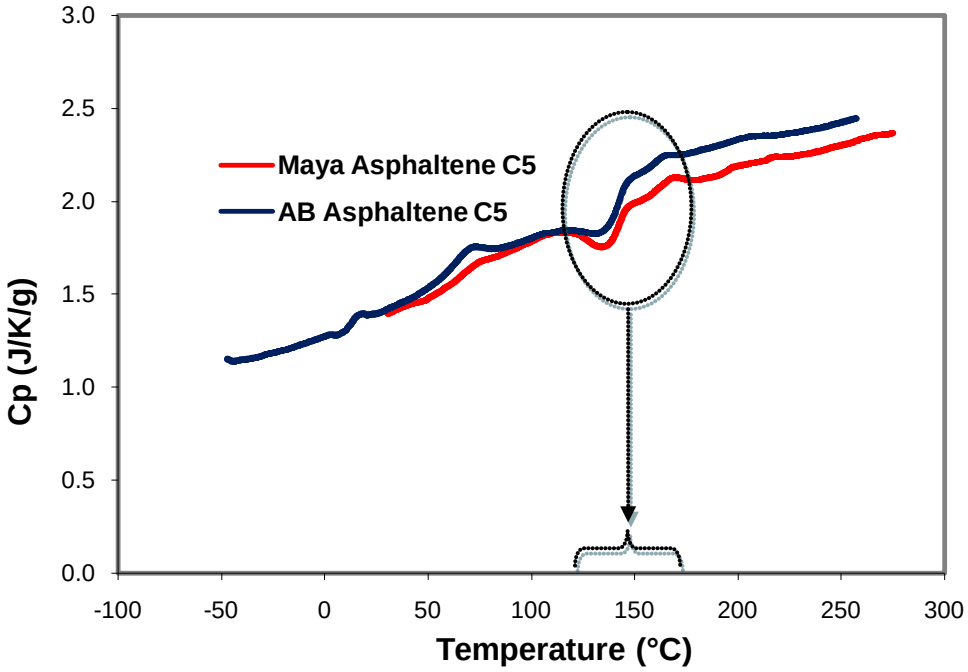

Figure III.10 : Thermo gram for unaged C5 asphaltenes from Athabasca bitumen and Maya crude oil cooled and reheated at q=5K/min

This observation was confirmed by Zhang et al.[95] and reinforces the remark of this work shows on **Figure III.10** where the glass transition region of the C5 asphaltenes from Maya Crude Oil and Athabasca Bitumen is located around 423.15K (150°C). The limiting fictive temperatures in **Table III-4** are determined using the method of Richardson and Savill [96] .

III. 5. MODEL PARAMETERS

The versatility of the proposed model relies on a set of parameters determined by DSC and steady stated rheometry. A least square fitting of experimental data, by the model using those parameters as initial values, helped in obtaining a set of optimized values, then used in the predictive simulation.

III.5.1. **Flow curve parameters** $(n, K, \sigma_0, \sigma_{0D}, \eta_{fs}, \eta_{us})$

From the experimental steady state flow curves, preliminary values of the SK-Model parameters were identified and summarized in **Table III-3**. These values serve as initial inputs to the Levenberg–Marquardt [93] algorithm implemented in MATLAB. Less than 3000 iterations were needed to identify a set of optimized parameters for the Maya Crude Oil, Athabasca Bitumen and Safaniya heavy oil. Graphically determined values and regressed data for all experiments are summarized in **Table III-3**. The fitted curves are illustrated in **Figure III.11**, **Figure III.12** and **Figure III.13**.

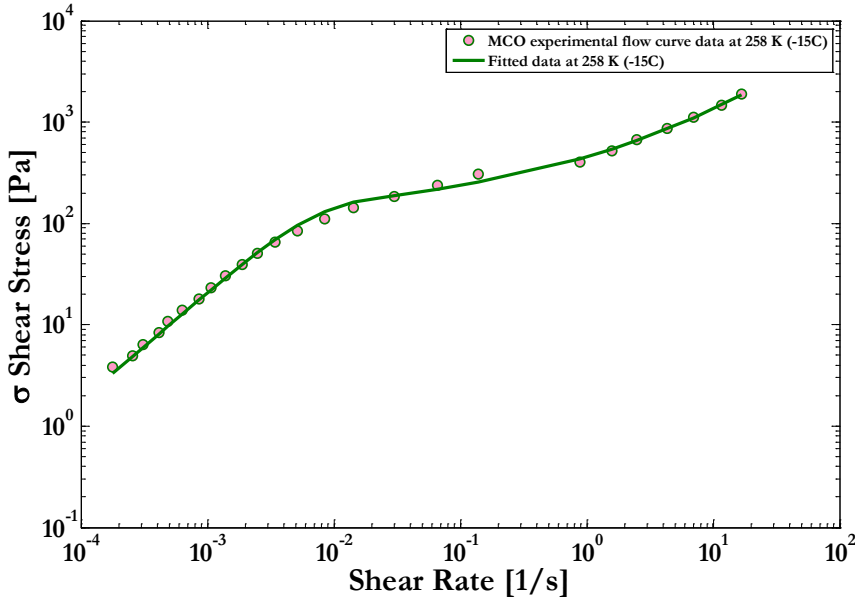

Figure III.11: Modified SK-Model fit to experimental flow curves of Maya crude oil. (Symbols are data; lines are simulated**).**

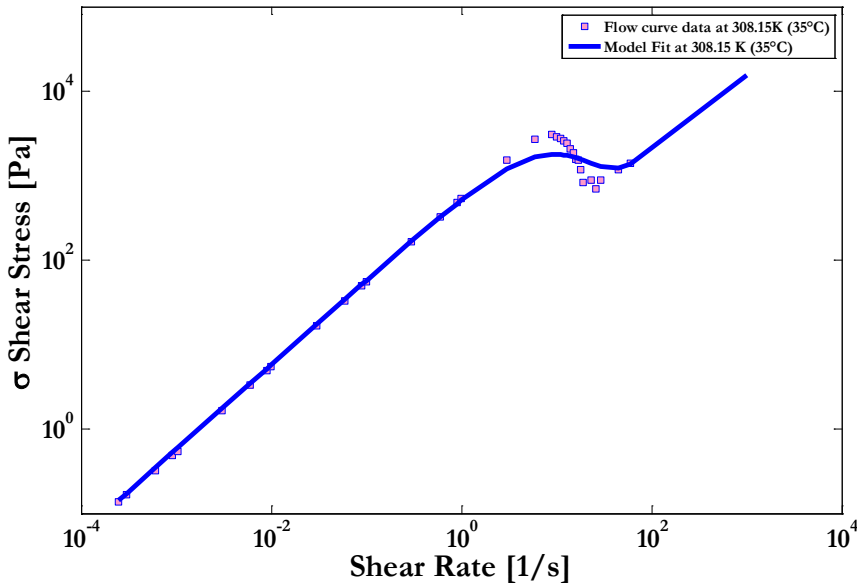

Figure III.12 : Experimental flow for Athabasca Bitumen. (Symbols are data and lines is model fitting**).**

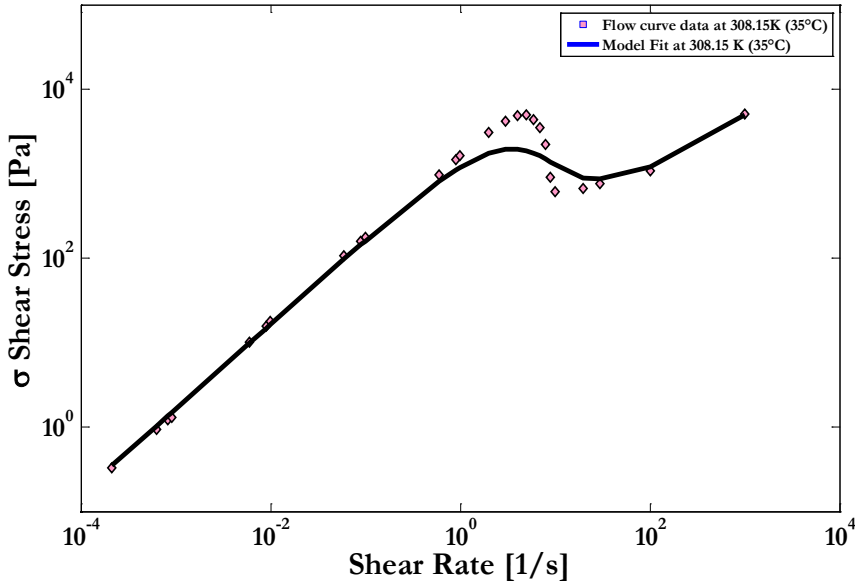

Figure III.13 : Model fit to experimental flow curve of Safanyia Vacuum Residue. (Symbols are data; lines are simulated**).**

Material	Reference temperature		Power Law indexes		Yield stresses		Limiting viscosities		R^2
	T [C]	T [K]	n	K	σ_0 [Pa]	σ_{0D} [Pa]	η_{fs} [Pa.s]	η_{us} [Pa.s]	
AB	35	308.15	0.485	55.78	3720	847.7	565	13.77	**0.969**
MCO	-15	258.15	0.701	17	13	1	18	1	**0.997**
SP	40	313.15	0.373	29	4960	637	1650	4.009	**0.898**

Table III-5: Optimized flow curve parameters for the hydrocarbon materials covered in this study. **They resulted from a fitting procedure** using a Levenberg–Marquardt algorithm implemented in MATLAB .

The three figures above show that the fittings are generally of good quality. Indeed the qualitative behaviour of [Eq. II.11] throughout the whole range of shear rate is essentially the same as that of the experimental data. However, the abrupt yield behaviour of hydrocarbons with high content of heavy components is roughly fitted. In fact, the transition from the static (local maximums) to the dynamic (local minimum) yield stresses is modelled in [Eq. II.11] to have an exponential form as observable with Maya Crude Oil. When this transition happens sharply, at low temperatures for feedstock with high content of heavy components (Athabasca Bitumen and Safaniya Heavy Oil), deviations in the flow curve calculations can occur. However, there is no need to discard data pertaining to this transition because they represent a tiny fraction of the flow curve and don't affect too much the model parameters nor the quality of the fit ($\mathbf{R^2}$ is well above 0.9).

In **Table III-5**, the optimized parameters vary slightly from the values determined graphically except for the dynamic yield stress σ_{0D} for Maya Crude Oil. Indeed, as opposed to the static yield stress σ_0, the values of σ_{0D} obtained graphically diverge by several units from those fitted due to experimental difficulties to capture dynamic yield behaviour on flow curves where a minimum is not obvious as reported in [28] and observable as on **Figure III.12** and **Figure III.13**.

III.5.2. **Williams Landel Ferry (WLF) parameters** $\left(C_1^{Tref0}, C_2^{Tref0}, T_{ref} \right)$

In this study, all measurements and simulations are carried at atmospheric pressure. Therefore pressure effects are not assessed. The values for A_1, A_2 B_1, B_2 are adopted from literature [1] to zero the logarithmic part of the pressure dependency functions [Eq. II.20a] and [Eq. II.20b]. This way, $T_{ref}(P) = T_{ref0}$, $F(P) = 1$ and no pressure effect is accounted for in WLF equation.

The WLF parameters C_1^{Tref0} and C_2^{Tref0} are obtained by fitting the steady state shear viscosity data, of a temperature sweep process, with the WLF-Model equation.

SAMPLES	C_1^{Tr}	C_2^{Tref0}	**Tref [K]**	**R^2**	**Pref [Pa]**	A_1 **[1/K]**	A_2 **[1/K]**	B_1 **[Pa]**	B_2 **[Pa]**
Athabasca Bitumen 1	**10.62**	**78.20**	308.15	0.97	101325	826.85	$0.2958*10^9$	0.1696	$45.92*10^{-6}$
Athabasca Bitumen 2	16.11	94.46	308.15	0.96	101325	826.85	$0.2958*10^9$	0.1696	$45.92*10^{-6}$
Maya Crude Oil 1	**10.80**	**98.41**	273.15	0.98	101325	826.85	$0.2958*10^9$	0.1696	$45.92*10^{-6}$
Maya Crude Oil 2	8.44	37.12	273.15	0.95	101325	826.85	$0.2958*10^9$	0.1696	$45.92*10^{-6}$
Safaniya heavy oil 1	**14.78**	**78.23**	313.15	0.99	101325	826.85	$0.2958*10^9$	0.1696	$45.92*10^{-6}$
Safaniya heavy oil 2	14.34	80.95	313.15	0.99	101325	826.85	$0.2958*10^9$	0.1696	$45.92*10^{-6}$

Table III-6 : The WLF-model parameters for Athabasca Bitumen, Maya Crude heavy oil samples studied and Safanyia Heavy Oil.

A linearized form of the WLF equation [Eq. II.20] is used to plot, $-1/\log(\mathbf{a_{TP}})$ versus $1/(T-T_{ref})$.

$$-\frac{1}{\log(a_{TP})} = \frac{1}{C_1^{Tref0}} + \frac{C_2^{Tref0}}{C_1^{Tref0}} \times \frac{1}{(T - T_{ref0})} \qquad \text{[Eq. III.1]}$$

The **y**-intercept equal to $1/C_1^{Tref0}$ and a slope proportional to C_2^{Tref0}/C_1^{Tref0}. The plots of this analysis are given in **Figure III.15**, **Figure III.16**, **Figure III.17**. For consistency purpose, two curves where fitted for every hydrocarbon material. The values of all C_1^{Tref0} and C_2^{Tref0} are summarized in **Table III-6**.

The quality of the fits is satisfactory with $\mathbf{R^2}$ values greater than **0.9**. Also, C_1^{Tref0} and C_2^{Tref0} are in the range reported by Lesueur, D. [6] for hydrocarbons. They are used in [Eq. II.20] with the fictive temperature **Teff** to calculate the shifting factor $\mathbf{a_{TP}}$ corresponding to a given temperature **T**.

III.5.3. **Tool-Narayanaswamy-Moynihan (TNM) parameters** $(\Delta H^*, \ln(\tau_0), x, \beta)$

The TNM parameters are determined for the C5 Asphaltenes. Indeed, as the heavier fraction in Maya Crude, Athabasca Bitumen and Safaniya Heavy Oil, they do play a determining role in the enthalpy relaxation process of those materials.

a)

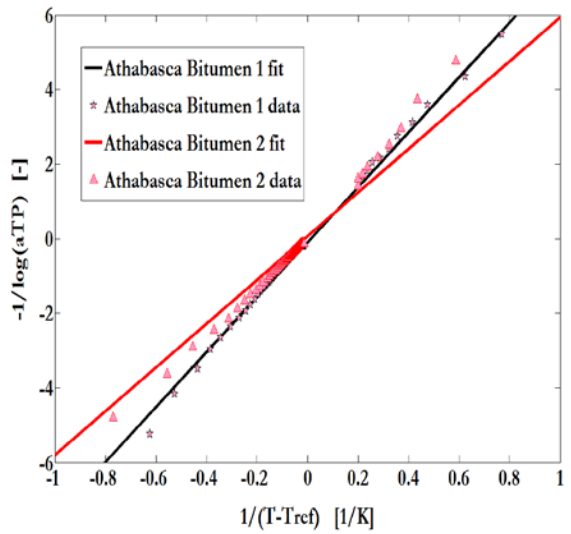

b)

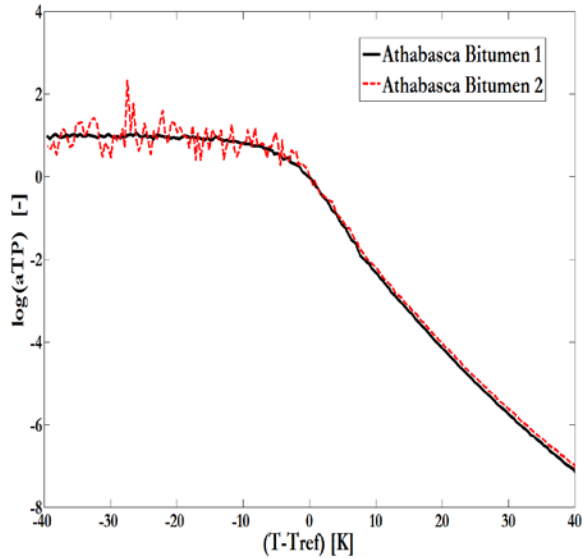

Figure III.14 : Linearized WLF equation fitted **a)** and representation of the experimental shift factor **b)** for Athabasca Bitumen.

c)

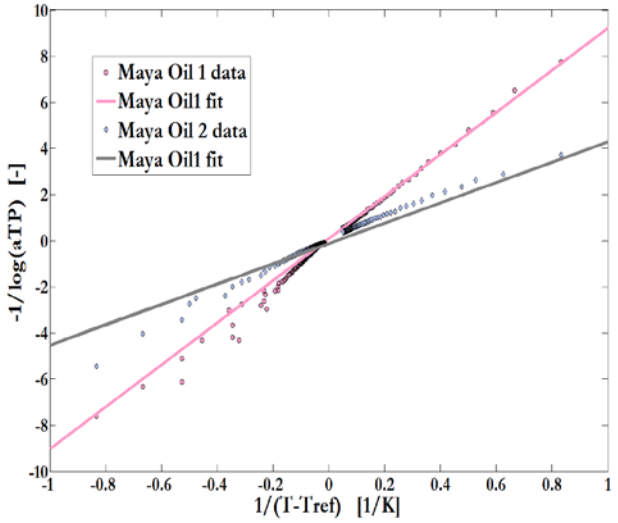

d)

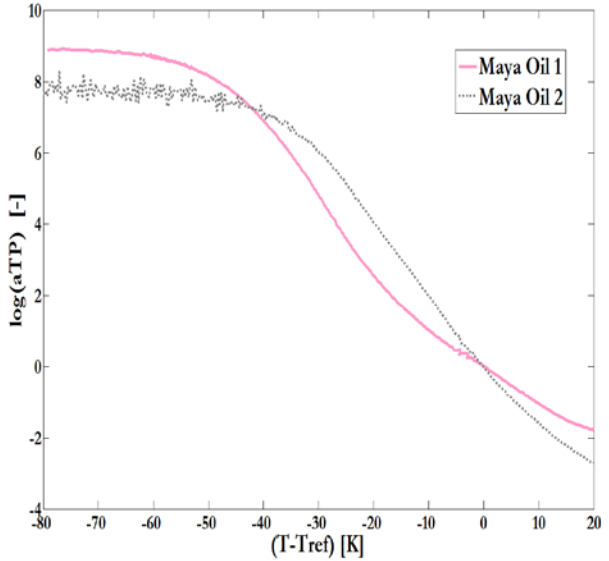

Figure III.15 : Linearized WLF equation fitted **c)** and experimental shift factors **d)** for Maya Crude Oil.

e)

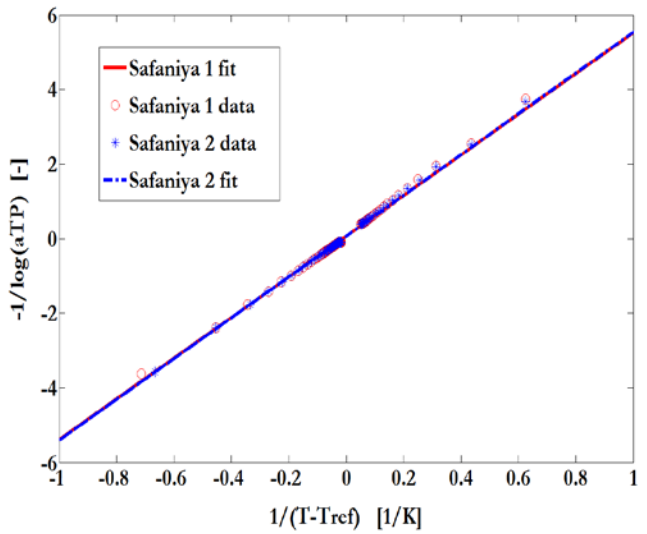

f)

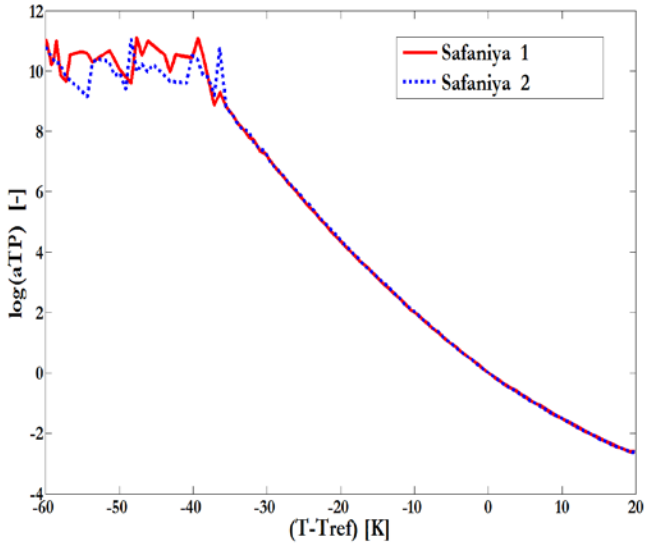

Figure III.16:: Plot of WLF equation fitted **e)** and experimental shift factors **f)** for Safaniya Heavy Oil

The initial values for the TNM parameters are determined in the following steps:

1. $\Delta H^*/R$, the apparent activation energy, is obtained experimentally from the dependence of the limiting fictive temperature T'_{eff} on the cooling rate **q**. By Plotting **ln|q|** versus the reciprocal of the limiting fictive temperature $1/T'_{eff}$ (**Figure III.18**) the slope provides:

$$-\Delta H^*/R = d\ln(q)/d(1/T'_{eff}) \qquad \text{[Eq.III.2]}$$

2. $\ln(\tau_0)$ is determined from [Eq. II.4b] assuming that in the glass transition region, τ is of order of 1 min and $T=T'_{eff}$ (= T_g). With ΔH*/R obtained in **step1**, $\ln(\tau_0) = \Delta H^*/RT_{ref} + Ln(\tau_{ref})$.

x and β are reported by many researchers in the literature [64, 67]: x = 0.45 [-] and β = 0.67 [-].

The four parameters $\Delta H^*/R = 15.8\times10^3$ K, $\ln(\tau_0) = -53.8$[s], x=0.45 and β=0.85 are assumed to be temperature independent in this work. They are very sensitive to thermal history.

In order to get specific $\Delta H^*/R$, $\ln(\tau_0)$, x and β for Maya Crude Oil, Athabasca Bitumen and Safaniya Heavy Oil, the C5 Asphaltenes data obtained experimentally are used as initial guesses in a Levenberg-Marquardt algorithm coded in MATLAB. The algorithm uses a Nonlinear Least Squares Minimization approach to provide a set of optimized parameter that allows a best fit.

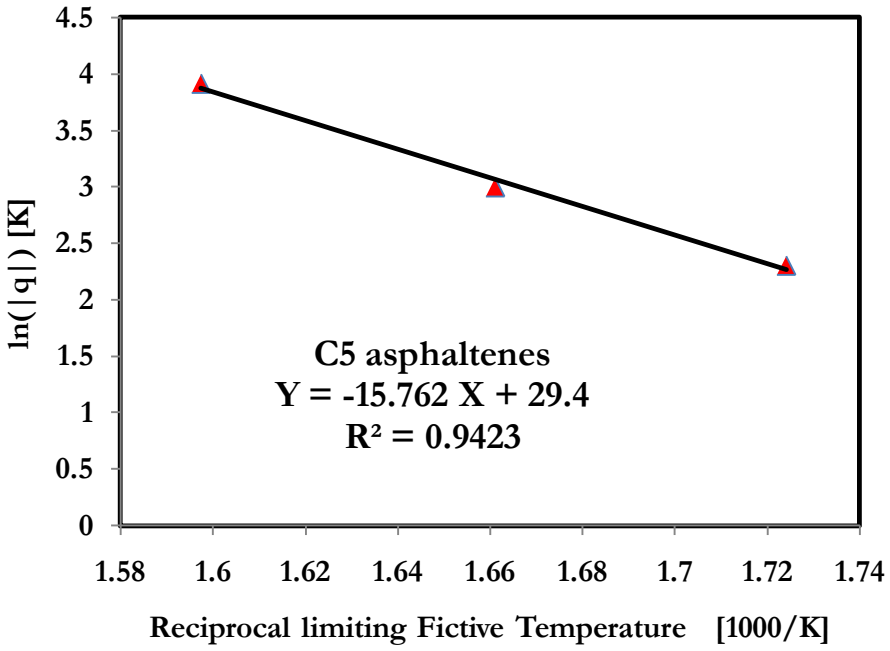

Figure III.17 : Plot of ln|q| versus the reciprocal of the limiting fictive temperature T'_{eff} of C5 asphaltenes. The slope represents the values of ΔH*/R

To achieve that goal, training data set are collected from temperature sweep tests under constant shear conditions. They are arranged into independent variable **T** and dependent variables $\eta_{exp}(T)$. The algorithm optimizes the parameters ψ for the model curve $\eta_{mod}(x,\psi)$ so that the objective function, which is the sum of squares of the deviations

$$S(\psi) = \sum_{i=1}^{m} \left(\eta_{exp,\,i} - \eta_{mod,\,i}(T_i,\psi)\right)^2 \qquad \text{[Eq.21]}$$

becomes minimal.

Optimum fitting data are summarized in **Table III-7** below and illustrated on **Figure III.19**, **Figure III.20** and **Figure III.21**.

SAMPLES	ΔH^* [J/mol]	$\ln(\tau_0)$	**x**	β
Athabasca Bitumen	15.8*10^3 **1.682*10^5**$^+$	-53.8 **-68.302**$^+$	0.45 **0.4525**$^+$	0.85 **0.9**$^+$
Maya Crude Oil	15.8*10^3 **1.67*10^5**$^+$	-53.8 **-80.900**$^+$	0.45 **0.32**$^+$	0.85 **0.53**$^+$
Safaniya Heavy oil	15.8*10^3 **1.641*10^5**$^+$	-53.8 **-65.754**$^+$	0.45 **0.715**$^+$	0.85 **0.86**$^+$

Table III-7 : Values of the different parameters for the TNM model from heavy oil samples **+** *are optimized data obtained computationally. They are used as parameters for the simulation.*

The three fluids have their activation enthalpy ΔH^* close to that of the C5 Asphaltenes.

The pre-exponential factors $\ln(\tau_0)$ roughly similar for all three petroleum materials, but are smaller compare to that of their heaviest constituents. That means annealing temperature $\mathbf{T_a}$ will affect equally the peak of heat capacity in these hydrocarbons but a higher $C_P^N(T)$ peak is expected for C5 Asphaltenes. β measures the nonexponentiality or the breadth of the distribution of relaxation times. Maya Crude Oil has smaller values of β and **x**. Therefore, the structure in Maya Crude Oils has lower exponentiality (higer linearity) in their structural relaxation process[67]. That means the average relaxation time of the system will be faster for the structure in Maya Crude Oil but slower for the structure in Athabasca Bitumen when compared to the C5 Asphaltenes. The physical meaning of these four parameters and the structural consequences of their variation is better covered in **Chapter V**.

These parameters will be used in [Eq. II.16] and [Eq. II.17] to compute the fictive temperature $\mathbf{T_{eff}}$ in simulating thermal histories. $\mathbf{T_{eff}}$ is then used, instead of thermodynamic temperature **T**, in the Williams-Landel-Ferry equation to calculate the temperature shift factors $\mathbf{a_{TP}}$ at a given **T**.

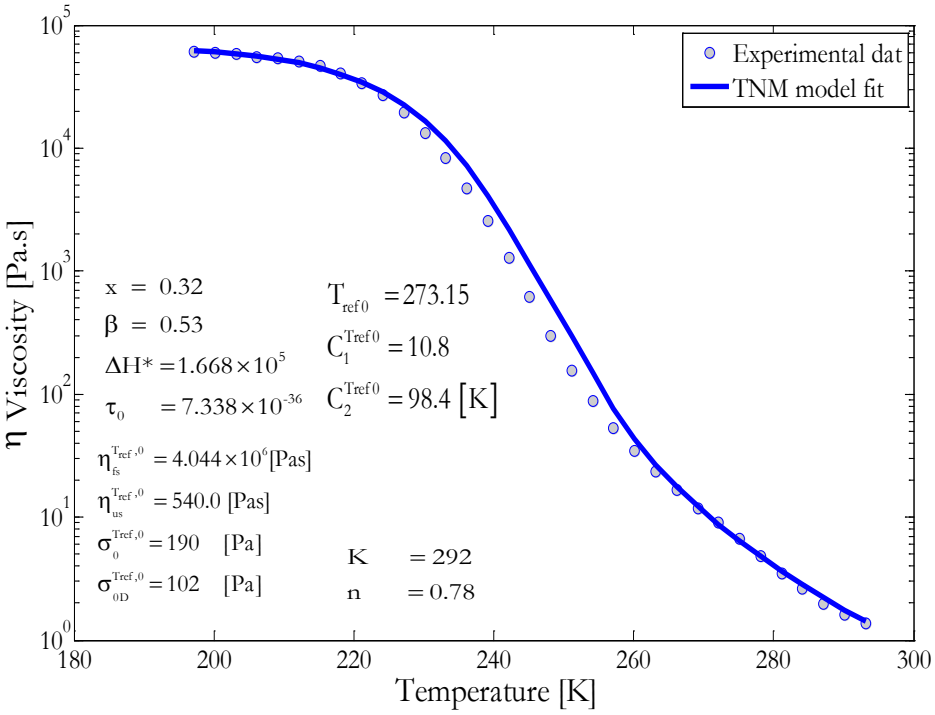

Figure III.18 : Curve fitting for Maya Crude Oil to determine the 4 parameters of the TNM model . Refer to **Appendix 1** for the data set (Symbols are data; line is fitted).

As seen on **Figure III.19** above, the modified SK-Model is able to consistently fit experimental data for Maya Crude Oil rheology over a broad range of temperature within experimental errors. The large number of parameters required to achieve this fitting underlies the complexities associated with structural changes and phase transitions when cooling.

The regression of Athabasca Bitumen (**Figure III.20**) shows an overall good fit with a slight divergence, between 290K and 270K, where the calculated viscosity are, to some extent, higher than experimental data. Issues associated with thermal equilibrium during measurements causes the lower temperature viscosity to vary erratically.

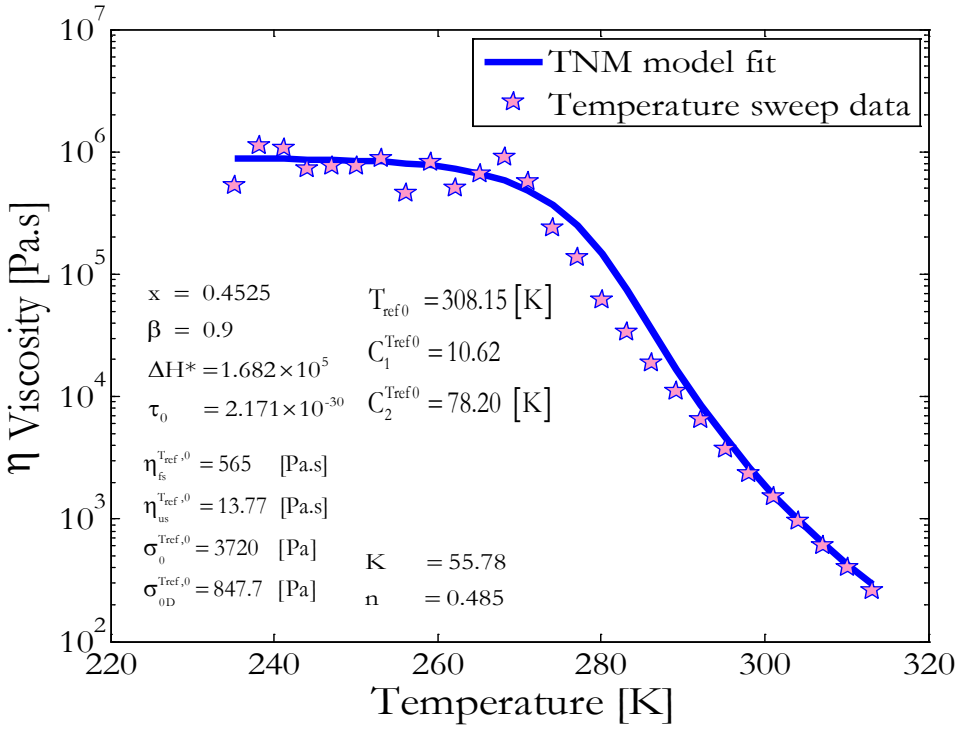

Figure III.19 : Temperature Sweep curve fitting for Athabasca Bitumen to determine the 4 parameters of the TNM model. Refer to **Appendix 2** for the data set (Symbols are data; line is fit).

Similar, random variation, issue is observable on **Figure III.21** with Safaniya Heavy Oil and is probably due to phenomenon associated with the high amont of heavy constituents in both AB and SP samples.

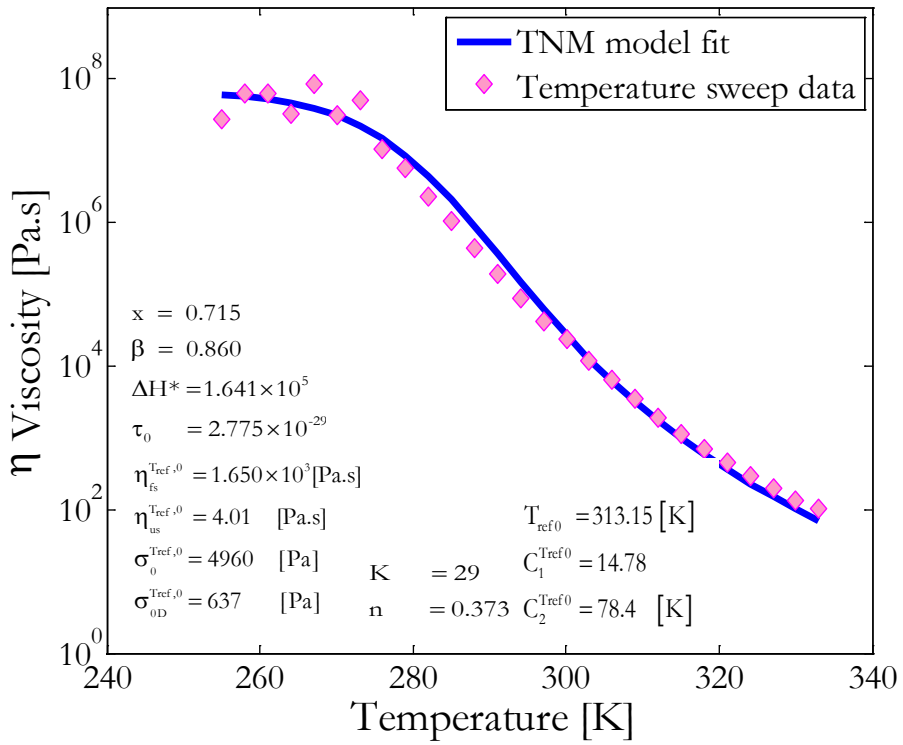

Figure III.20 : Curve fitting for Safaniya Oil to determine the 4 parameters of the TNM model. Refers to **Appendix 3** for the data set (Symbols are data; line is fitted).

In the three cases above the model was able to fit the measured apparent viscosity by precisions within experimental error. **Table III-8** shows a very low %AAD with a regression coefficient close to 1.

Material	Data points	% AAD	R2	RMSE [Pa.s]
Maya Crude Oil	33	2.3	1.000	222
Athabasca Bitumen	27	3.5	0.999	281
Safaniya heavy Oil	27	3.8	0.999	299

Table III-8 : Summary of errors for model fitting of the native sample data (training set) using the Modified SK-Model

The training data set, used in these fittings, are available in **Appendices** 1, 2 and 3, marked with a start (*) symbol.

MODEL	PARAMETERS	OIL SAMPLES			PROPOSED VALUES	COMMENTS
		AB	MCO	SP		
WLF (Williams - Landel - Ferry)	**Tref [K]**	**308.15** [e]	**273.15** [e]	**313.15** [e]	-	In the literature [6], temperature-dependency of the relaxation processes in bitumen and heavy oils are modelled using constants values of C_1 and C_2, with **Tref** as fluid dependent parameter. Here, the values of C_1 =11 and C_2 =80 are in the range proposed by Lesueur et al [41]. **Tref** is the value that allow a better regression of the temperature sweep data with [Eq. III.1]
	$C_1^{Tref\,0}$	**10.62** [e,f]	**10.8** [e,f]	**14.34** [e,f]	**11** [l]	
	$C_2^{Tref\,0}$	**78.2** [e,f]	**98.41** [e,f]	**80.95** [e,f]	**80** [l]	
Flow curve	**n**	**0.485** [e,f]	**0.701** [e,f]	**0.373** [e,f]	-	The flow curve parameters portray the fingerprint of the fluid being modeled. They are fluid specific and need to be determined experimentally at **Tref** where the material is structure and manifests yield behaviours. The model accuracy depends on the quality of the method used to collect these data. The method used in this work is detailed in III.2.4.
	K	**55.78** [e,f]	**17** [e,f]	**29** [e,f]	-	
	σ_0 **[Pa]**	**3720** [e,f]	**13** [e,f]	**4960** [e,f]	-	
	σ_{0D} **[Pa]**	**847.7** [e,f]	**1** [e,f]	**637** [e,f]	-	
	η_{fs} **[Pa.s]**	**565** [e,f]	**18** [e,f]	**1650** [e,f]	-	
	η_{us} **[Pa.s]**	**13.77** [e,f]	**1** [e,f]	**4.009** [e,f]	-	
TNM (Tool-Narayanaswamy-Moynihan)	ΔH^* **[kJ/mol]** [e,f,l]	**168.2** [f]	**167** [f]	**164.1** [f]	-	The pre-exponential parameter (τ_0) and ΔH^* are linearly related [67] therefore τ_0 will be keep constant while using ΔH^* as adjustable parameter. The chosen values of τ_0 and β are in close to those reported by many researchers in the literature [64, 67, 97] for amorphous materials.
	τ_0	**2.17*10^{-30}** [f]	**7.34*10^{-36}** [f]	**2.78*10^{-39}** [f]	**1.75*10^{-30}** [l]	
	x	**0.45** [f]	**0.32** [f]	**0.72** [f]	-	
	β	**0.9** [f]	**0.53** [f]	**0.86** [f]	**0.9** [l]	
Structural kinetics	**a**	**1** [l]	**1** [l]	**1** [l]	**1** [l]	The six parameters of the thixotropic equation **[Eq. II.14]**, namely: G_{fs}, **m**, **a**, **b**, **c**, and **i** are chosen form literature. The kinetics orders for the build up and break-up processes follows usually a simple order kinetics[57] giving a=b=1. Since the shear modulus G and the yield stress **s** are related to the structure of the un-yielded material they are assumed be equal as reported in [17].
	b	**1** [l]	**1** [l]	**1** [l]	**1** [l]	
	c	**0.1** [l]	**0.1** [l]	**0.1** [l]	**0.1** [l]	
	$G_{fs}^{T_{ref},0}$	σ_0 [e]	σ_0 [e]	σ_0 [e]	σ_0 [e]	
	m	**0.1** [l]	**0.1** [l]	**0.1** [l]	**0.1** [l]	
	l [nm]	**5** [l]	**5** [l]	**5** [l]	**5** [l]	

Table III-9 : List of parameter values determined from experimentation [e] and fitting [f] or from literature [l]. **AB** is for Athabasca bitumen, **MCO** represents Maya crude oil and **SP** if for Safaniya vacuum residue**.**

III. 6. THE MODIFIED – STRUCTURAL KINETICS MODEL FOR HYDROCARBON MATERIALS

III.6.1. **Reduction of model constants**

From analysis done above on the three feedstocks (Maya Crude Oil, Athabasca Bitumen and Safaniya Vacuum Residue) , it appears that some parameters are fluid specific $\left(\eta_{fs}^{T_{ref},0}; \eta_{us}^{T_{ref},0}; G_{fs}^{T_{ref},0}; \sigma_{0D}^{T_{ref},0}; \sigma_{0}^{T_{ref},0}; n_{Tref0}; K_{Tref0}\right)$ and change with the type of fluid, while others can be considered material dependent $\left(C_1^{Tref0}, C_2^{Tref0}, T_{ref0}, \Delta H^*/R, \ln(\tau_0), x, \beta\right)$, as they are similar for petroleum materials. A summary of those parameters and simplification comments are shown on **Table III-9 .**

The WLF coefficients $\left(C_1^{Tref0}, C_2^{Tref0}\right)$ are more or less the same for Athabasca Bitumen and Safaniya Vacuum Residue but diverge, to some extent, from the values for Maya Crude Oil. This suggests that hydrocarbon materials with high content of heavy-components behave, somewhat, differently from those with lower content of heavy-constituent. To account for these differences, temperature dependency parameters will be compensated by adjusting the value of the reference temperature (T_{ref}) while using $C_1^{Tref0} = 11$ and $C_2^{Tref0} = 80$ for the three fluids.

Among the TNM parameters $\left(\Delta H^*/R, \ln(\tau_0), x, \beta\right)$, supposing that $\ln(\tau_0)$ is constant and the same for the feedstock analysed in this study, implies "thermorheological simplicity" [64]. This was confirmed earlier with the black diagram on **Figure II.4** , **Figure II.6** and **Figure II.5** in accordance with the Mavridis criteria [45]. Therefore, $\tau_0 = 1.75 \times \mathbf{10}^{-30}[s]$ will be used as material constant. The dimensionless parameter β is a direct measure of

nonexponentiality or, equivalently, the breadth of the distribution of relaxation times. Smaller values of β corresponds to increased nonexponentiality. Typically, β lies in the range of 0 to 1 [67]. Therefore the value of $\beta = 0.9$ common to Athabasca Bitumen and Safaniya Heavy Oil will be adopted. However, because of their considerable differences and their respective effects on the fitting procedure, the nonlinearity parameter **x** and the relaxation enthalpy ΔH^* will be used as adjustable parameters in the TNM model.

From the above assertions, it results that in addition to the flow curve parameters $\left(\eta_{fs}^{T_{ref},0}; \eta_{us}^{T_{ref},0}; G_{fs}^{T_{ref},0}; \sigma_{0D}^{T_{ref},0}; \sigma_{0}^{T_{ref},0}; n_{Tref\,0}; K_{Tref\,0}\right)$, there are three parameters in the Modified SK Model, namely : $(T_{ref}, x, \Delta H^*)$.

III.6.2. **The modified Structural Kinetics equation**

As explained in **II.4.2** and illustrated in **Figure II.3**, three regions have to be separated when modelling the temperature effects on the flow behaviour of hydrocarbon materials. At high temperatures, the near Newtonian behaviour is dominated by the flow response of the structure-free liquid matrix. At low temperatures the flow response is an elastic one, dominated by a soft-solid material response. The transition from one plateau to the other is where time-dependent and shear-thinning rheology occurs. In modelling these transitions, one can use the temperature dependency of all 7 parameters $\left(\eta_{fs}^{T_{ref},0}; \eta_{us}^{T_{ref},0}; G_{fs}^{T_{ref},0}; \sigma_{0D}^{T_{ref},0}; \sigma_{0}^{T_{ref},0}; n_{Tref\,0}; K_{Tref\,0}\right)$ from the steady state flow curve, measured at reference temperature $\mathbf{T_{ref0}}$. This approach is laborious and amplifies errors associated with inaccuracies in the temperature dependency of these 7 fluid properties.

A more straightforward approach consists of considering that the **a** and **b** transitions occur according to a sigmoid like behaviour [98]. The following form is proposed:

$$\eta_{FS}^{T,P}(\dot{\gamma},T)=\eta_{US}^{T,P}+\frac{\eta_{SS}^{TP}(\dot{\gamma})}{1-\exp\left(-S\left(1-\frac{T_{eff}}{T_{ref0}}\right)\right)} \qquad \text{[Eq. III.4]}$$

where the high limiting viscosity plateau (shear dependent) is $\eta_{SS}^{TP}(\dot{\gamma})=a_{TP}\cdot\eta_{SS}^{Tref0}(\dot{\gamma})$, the low limiting viscosity value (shear independent) is $\eta_{US}^{T,P}=a_{TP}\cdot\eta_{US}^{Tref0}$ and the rate of transition process is given by **S**.

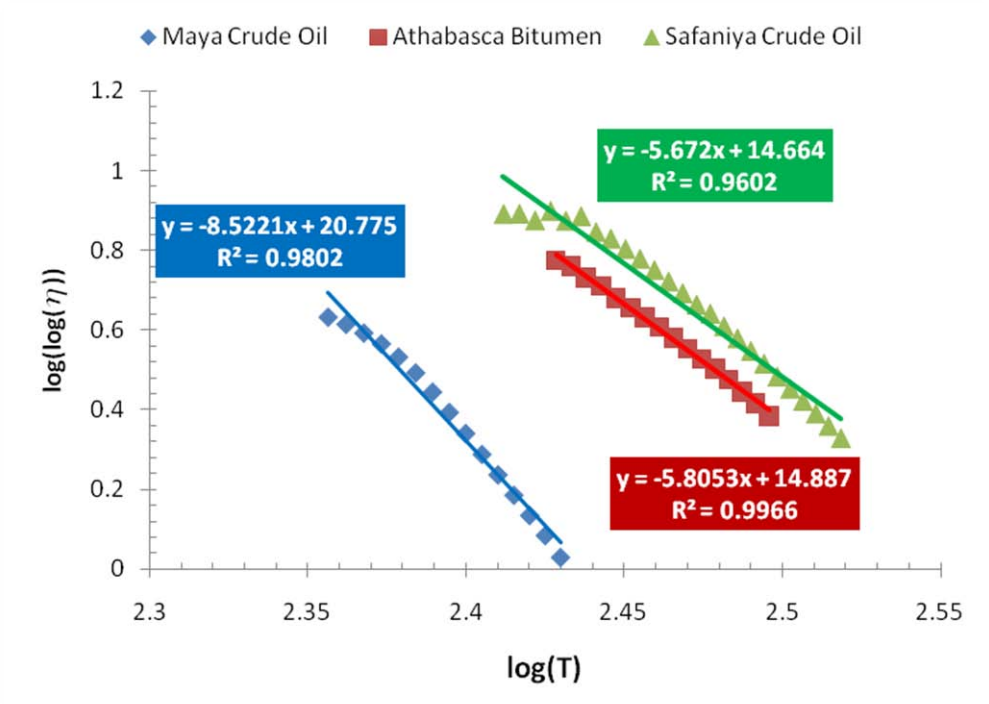

Figure III.21 : Representation of the viscosity-temperature susceptibility of the bitumen and heavy oils

S is the viscosity-temperature susceptibility coefficient and is represented by the slope the $\log\left(\log\left(\eta_{SS}^{TP}\right)\right)$ vs $\log(T)$ plot. The literature report, S to vary from -3.36 to -3.98 for 50 asphalt binders [99] and measures the rate of change of viscosity with temperature.

The plots in **Figure III.16** suggest that Maya crude oil (**S=-8.5**) is less susceptible to temperature than Athabasca Bitumen (**S=-5.7**) and Safaniya materials (**S=-5.8**) but the impact of this parameter is slight and a common value of **S=-7** was adopted.

In this way, by measuring rheological flow curve data at a reference temperature, $\mathbf{T_{ref0}}$, and knowing the temperature dependency parameters as well as the kinetics of the structural parameters, one can predict the rheological response at any other temperature under any shear condition.

The modified Structural Kinetics Model has the following form:

$$\eta_{FS}^{T,P}\left(\dot{\gamma},T\right)=a_{TP}\cdot\left(\frac{\eta_{SS}^{Tref0}(\dot{\gamma})}{1-\exp\left(-S\left(1-\frac{T_{eff}}{T_{ref0}}\right)\right)}+\eta_{US}^{Tref0}\right) \qquad \text{[Eq. III.5]}$$

with:

- a_{TP} the temperature shift function at obtained by **[Eq. II.20']** .
- $\eta_{SS}^{Tref0}(\dot{\gamma})$ the shear dependent viscosity as calculated using **[Eq. II.11'] .**
- η_{US}^{Tref0} the unstructured viscosity from flow curve measurement at $\mathbf{T_{ref0}}$.
- T_{ref0} the reference temperatures as reported on **Table III-9**.
- T_{eff} the pseudo temperature from the TNM equation **Eq.II.16']**.
- S the rate of viscosity transition (from η_{US}^{Tref0} to η_{FS}^{Tref0}) with temperature.

III. 7. SUMMARY

III.7.1. **Overview**

The training data set was used to fit preliminary parameter values, for the three feedstocks. Some of these parameters were easily determined experimentally but many of them were a challenge to identify and were estimated computationally through an optimisation procedure based on a Levenberg-Marquardt fitting algorithm coded in MATLAB. The similarity of some of these parameters, among feedstocks, allowed a simplification and generalization of the rheological model. This led to a reduction of the adjustable parameters, per feedstock, to three (T_{ref}, x, $\Delta H*$). A modified Structural Kinetics Model was elaborated and summarized below in **Table III-7**. Consequently, by measuring rheological flow curve data $\left(\eta_{fs}^{T_{ref},0}; \eta_{us}^{T_{ref},0}; G_{fs}^{T_{ref},0}; \sigma_{0D}^{T_{ref},0}; \sigma_{0}^{T_{ref},0}; n_{Tref0}; K_{Tref0}\right)$ at a reference temperature, $\mathbf{T_{ref0}}$, and knowing the temperature shift function $\mathbf{a_{TP}}$ as well as the kinetics of the structural parameters λ, rheological responses can be predicted at any other temperature under several shear conditions.

III.7.2. **The proposed rheological model for hydrocarbon materials**

MODEL FEATURES	**THE MODIFIED STRUCTURAL KINETICS MODEL**	
VISCO-ELASTICITY (TIME DEPENDENCY)	$\eta_{vis}(\lambda)\cdot\dot{\gamma} = \sigma_{tot} + \dot{\sigma}_{tot}\cdot\left(\frac{\eta_{vis}(\lambda)}{G(\lambda)}\right)$ **[Eq. II.7]**	$G(\lambda) = \frac{G_{fs}^{T,P}}{\lambda^{0.1}}$ **[Eq.II.8]** $\eta_{vis}(\lambda) = \left(\frac{\eta_{fs}}{\eta_{us}}\right)^{\lambda}\cdot\eta_{us}$ **[Eq. II.10a]**
THIXOTROPY (TIME DEPENDENCY)	$\frac{d\lambda}{dt} = \frac{1}{20}\cdot\left[(1-\lambda) - \left((1-\lambda_{ss})\cdot\left(\frac{\lambda}{\lambda_{ss}}\right)\cdot\left(\frac{\sigma}{\eta_{vis}(\lambda_{ss})\cdot\dot{\gamma}}\right)^{0.1}\right)\right]$ **[Eq. II.14']**	$\lambda_{ss}(\dot{\gamma}) = \left(\frac{\ln\left[\eta_{ss}(\dot{\gamma})\right]-\ln\left[\eta_{us}\right]}{\ln\left[\eta_{fs}\right]-\ln\left[\eta_{us}\right]}\right)$ **[Eq. II.10]**
STEADY STATE (SHEAR DEPENDENCY)	$\eta_{ss}^{Tref0}(\dot{\gamma}) = \left(1-e^{-\frac{\eta_{fs}^{Tref0}\dot{\gamma}}{\sigma_0}}\right)\cdot\left(\frac{\sigma_{str}^{Tref0}}{\dot{\gamma}} + K^{Tref0}\cdot\dot{\gamma}^{(n-1)}\right) + \eta_{us}^{Tref0}$ **[Eq. II.11']**	where $\sigma_{str}^{Tref0} = \left(\sigma_0^{Tref0} - \sigma_{0D}^{Tref0}\right)\cdot e^{-\frac{\dot{\gamma}}{\dot{\gamma}_{0d}}} + \sigma_{0D}^{Tref0}$ $\eta_{fs}^{Tref,0}; \eta_{us}^{Tref,0}; G_{fs}^{Tref,0}; \sigma_{0D}^{Tref,0}; \sigma_0^{Tref,0}; n_{Tref0}; K_{Tref0}$ are obtained from flow curve at reference temperature
THERMAL HISTORY	$T_{eff}(T) = T_0 + \sum_{i=1}^{N}\Delta T_i\cdot\left[1-\exp\left(-\left(\sum_{j=i}^{N} rt_j\right)^{0.9}\right)\right]$ **Eq.II.16']** $Log(a_{T,P}) = \frac{11\left(T_{eff}(T)-T_{ref}\right)}{80+T_{eff}(T)-T_{ref}}$ **[Eq. II.20']**	$rt_j = \begin{cases}\Delta T_j/(q_j\tau_{pj}) & \text{during temperature jump}\\ \Delta t_j/(\tau_{pj}) & \text{during annealing step}\end{cases}$ $\tau_{pj} = 1.75\times\mathbf{10}^{-30}\cdot\exp\left(\frac{\Delta H^*}{R}\cdot\left[\frac{x}{T}-\frac{(1-x)}{T_{eff-1}}\right]\right)$ **[Eq. II.17']**
MODIFIED STRUCTURAL KINETICS EQUATION	$\eta_{FS}^{T,P}(T,\dot{\gamma},\lambda) = a_{TP}\cdot\left(1-e^{-S\left(1-\frac{T_{eff}}{T_{ref0}}\right)}\right)^{-1}\cdot\eta_{SS}^{Tref0}(\dot{\gamma},\lambda) + \eta_{US}^{T,P}$ **[Eq. III.5']**	$\sigma_{str}^{Tref0} = \left(\sigma_0^{Tref0} - \sigma_{0D}^{Tref0}\right)\cdot e^{-\frac{\dot{\gamma}}{\dot{\gamma}_{0d}}} + \sigma_{0D}^{Tref0};$ $\eta_{FS}^{T,P} = \eta_{FS}^{Tref,0}\cdot a_{T,P}; \eta_{US}^{T,P} = \eta_{US}^{Tref,0}\cdot a_{T,P}; G_{FS}^{T,P} = G_{FS}^{Tref,0}\cdot a_{T,P}$
MODEL PARAMETERS ΔH^*; x; T_{ref0}		

Table III-10 : modified Structural Kinetics Model for petroleum fluids. The apostrophe **(')** beside the equations numbers help distinguish from those in the primary form.

Chapter IV: ROBUSTNESS OF MODEL PREDICTIONS

IV. 1. INTRODUCTION

The model proposed in **Table III-10** is intended to evaluate the effects of shear and temperature on flow properties of complex materials in which structural mutations are taking place.

The set of parameters pertaining to Maya Crude Oil, Athabasca Bitumen and Safaniya Heavy Oil were adopted form literature $\left(\mathbf{G_{fs}}, \mathbf{m}, \mathbf{a}, \mathbf{b}, \mathbf{c} \text{ a } \mathbf{d} \mathbf{t}\right)$ and through experimentation and fitting procedures $\left(n, K, \sigma_0, \sigma_{0D}, \eta_{fs}, \eta_{us}\right)$, $\left(C_1^{Tref0}, C_2^{Tref0}, T_{ref}\right)$ and $\left(\Delta H^*/R, \ln(\tau_0), x, \beta\right)$. Using those parameters, a series of flow simulations will be run to assess the aptitudes of the proposed model.

Preliminarily, the basic features, of the proposed model, will be assessed through transient and steady state calculation for Maya Crude Oil. The goal is to have an idea about the model capability to eventually compute such flows. Therefore the model will be run to calculated the start-up of flow (at 268.15K (-5°C)) and the steady state viscosity curve (at 265.15K (-8°C)) of Maya Crude Oil.

Subsequently, the ability of the modified SK-Model to simulate the resistance to flow, for Maya Crude Oil (MCO), Athabasca Bitumen (AB) and Safaniya Heavy Oil (SP) and their nano-filtered fractions are evaluated.

To assess the extrapolation capability for the feedstocks, the model was run under flow conditions, not used to determine model parameters, and the results are compared with the extrapolation data set. Two stars (**) are used to distinguish these data from the training data set. The prediction capability of the model was evaluated through the calculation of flow properties for nano-filtered fractions obtained from the feedstocks which possess more or less structured phase than the feedstocks but are otherwise similar. Three stars (***) designate the predictions data sets. Absolute Average Deviation (AAD), Coefficient of Determination ($\mathbf{R^2}$) and Root Mean Square Errors (RMSE) are the statistical tools used to determine calculation quality.

$$\%AAD = \sum_i^n \frac{\left| y_i^{exp} - y_i^{pred} \right|}{y_i^{exp}} \times \frac{1}{n} \times 100 \quad \left| \quad R^2 = 1 - \frac{\sum_i^n \left(y_i^{exp} - y_i^{pred} \right)^2}{\sum_i^n \left(\bar{y}_i^{exp} - y_i^{exp} \right)^2} \right| \quad RMSE = \sqrt{\frac{\sum_i^n \left(y_i^{exp} - y_i^{pred} \right)^2}{n}}$$

The extrapolation data sets, for samples of Maya Crude Oil, Athabasca Bitumen and Safaniya Heavy Oil, as well as the prediction data sets, for nano filtered samples, were culled from tests done in the context of this thesis but also from results of previous tests available in the laboratory, many of which have been reported in the literature [16] and [37]. These data were also obtained using the Gemini HR NanoRheometer. Calculated and experimental values are represented graphically in this chapter and organized in tables through **Appendices 1, 2** and **3**. The raw laboratory data (training, extrapolation and prediction data sets) as

well as the computer code use for the calculation are provided as supplementary materials to this thesis.

IV. 2. BASIC FEATURES OF THE MODEL

IV.2.1. Simulation Algorithm

The calculation approach for this *isothermal process* is as follow:

Step 1 The thermal history leading to the isothermal condition are input in the TNM model (Heating or cooling rate; Initial and annealing temperatures; Annealing Time after each temperature step and at annealing temperature).

Step 2 Base on these data the TNM model will generate a value of fictive temperature $\mathbf{T_{fic}}$ corresponding to the isothermal state.

Step 3 The WLF parameters ($C_1^{Tref\,0}$ and $C_2^{Tref\,0}$) and the pressure dependency parameters (A1; A2; B1; B2) are specified to the WLF model.

Step 5 Using the value of fictive temperatures (instead of the thermodynamic temperature), the WLF Model computes a shift function $\mathbf{a_{TP}}$ for the isothermal condition **T**.

Step 6 The corresponding flow curve parameters $(n, K, \sigma_0, \sigma_{0D}, \eta_{fs}, \eta_{us})$ are then calculated using $\mathbf{a_{TP}}$.

Step 7 SK-Model is then integrated to calculate the flow properties for the corresponding temperature and shear stresses (*shear stress sweep*) or shear rates (*shear rate sweep*).

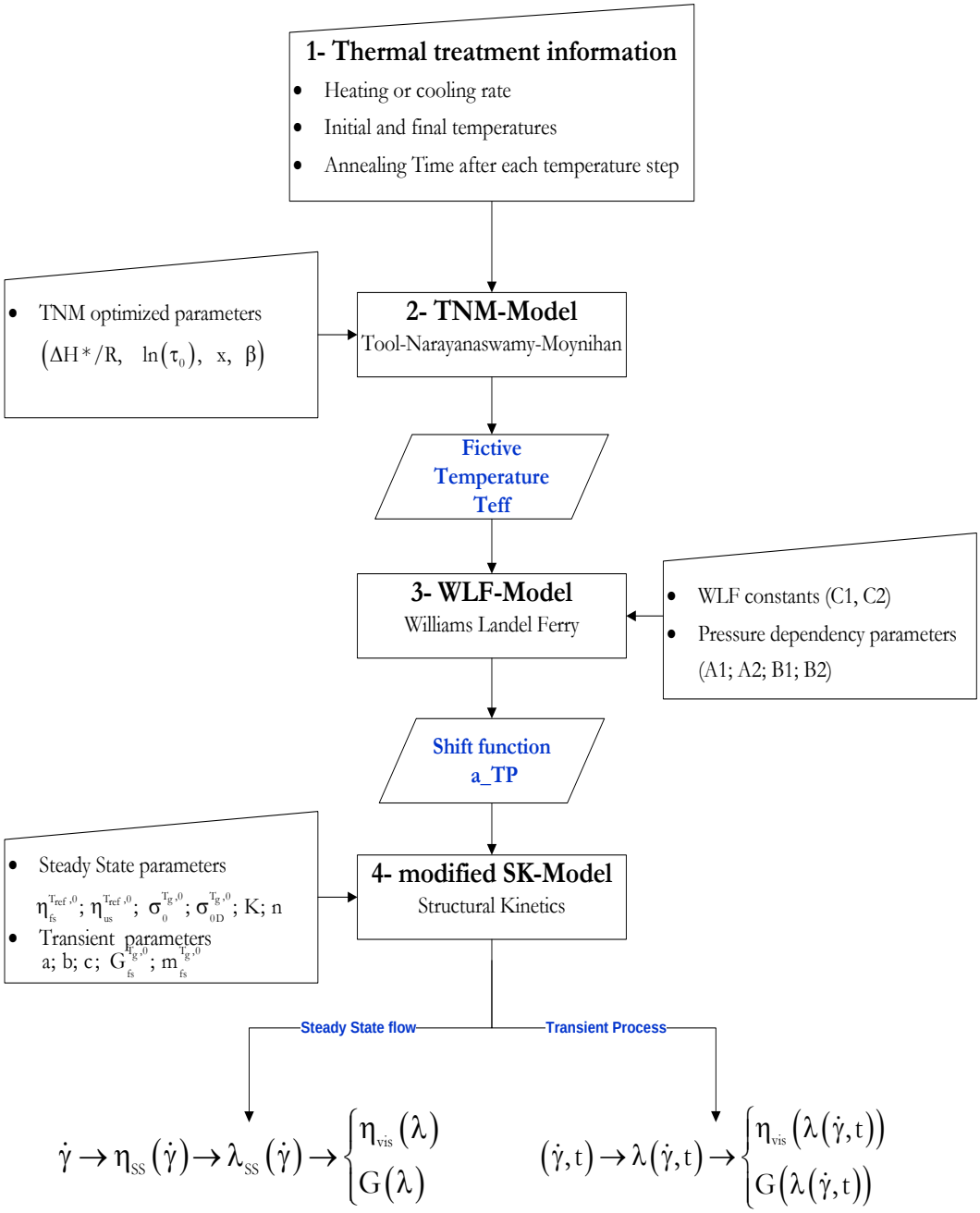

Figure IV.1 : Simplified diagram of steps for the calculation of steady state and transient flow properties of complex fluids using the Modified SK-Model.

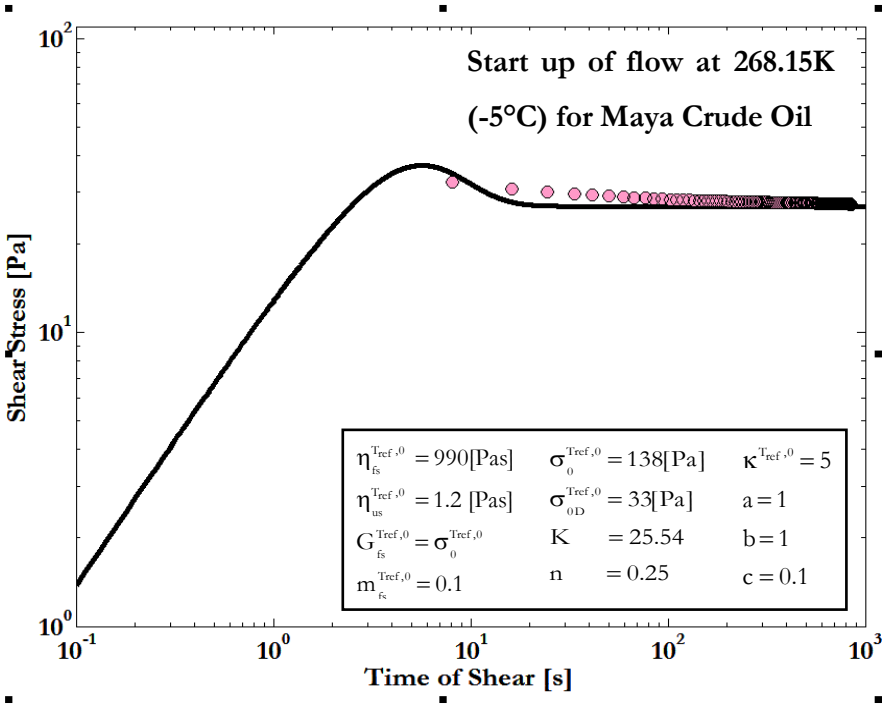

Figure IV.2 : Prediction of a Start-up of steady shear rate for a sample of Maya Crude oil initially at rest. A shear stress overshoot can be observed (Symbols are data; lines are simulated).

IV.2.2. **Start-up of flow**

After a shear flow condition has been imposed on a fluid for a long period of time, the shear stress often (but not always) comes to a steady state. That fact depends on the imposed shear rate and temperature. During Start-up, the complex fluid is initially a rest and thus fully structured (λ=1). For the example shown in **Figure IV.2**, at t=0, a shear rate of $\dot{\gamma} = \mathbf{10^{-3}}\,[1/s]$ is applied and kept constant for a period of time. The shear stress response is observed. The model predicts a stress overshoot, partially observable on the experimental curve.

At the early time of inception of flow, the stress increases linearly to reach a maximum. It then falls down progressively to finally level off as steady state is approached. The brief linear behaviour at early times is related to the elastic deformation of the virgin structure present in the fluid, while the stress overshoot indicates a dramatic breakup of the microstructure. The experimental data evolve toward an asymptotic value of 27Pa, for shear stress as predicted by the model. The shape and the behaviour of this curve is typical to real materials (elastic-thixotropic) as describe in **Figure 1** of [27] . Thus, parameters identified at lower temperature (**263.15K**) are capable of computing transient flow at higher temperature (**268.15K**).

IV.2.3. **Shear rate ramp-up experiment**

This type of flow is characterized by a step increase in shear rate followed by a holding time to allow steady state to de reached. At steady state the shear rate and the shear stress are constant.

A sample of Maya Crude Oil was sheared isothermally at 265.15K (-8°C). The experimental and predicted rheological curves are shown below on **Figure IV.3** .

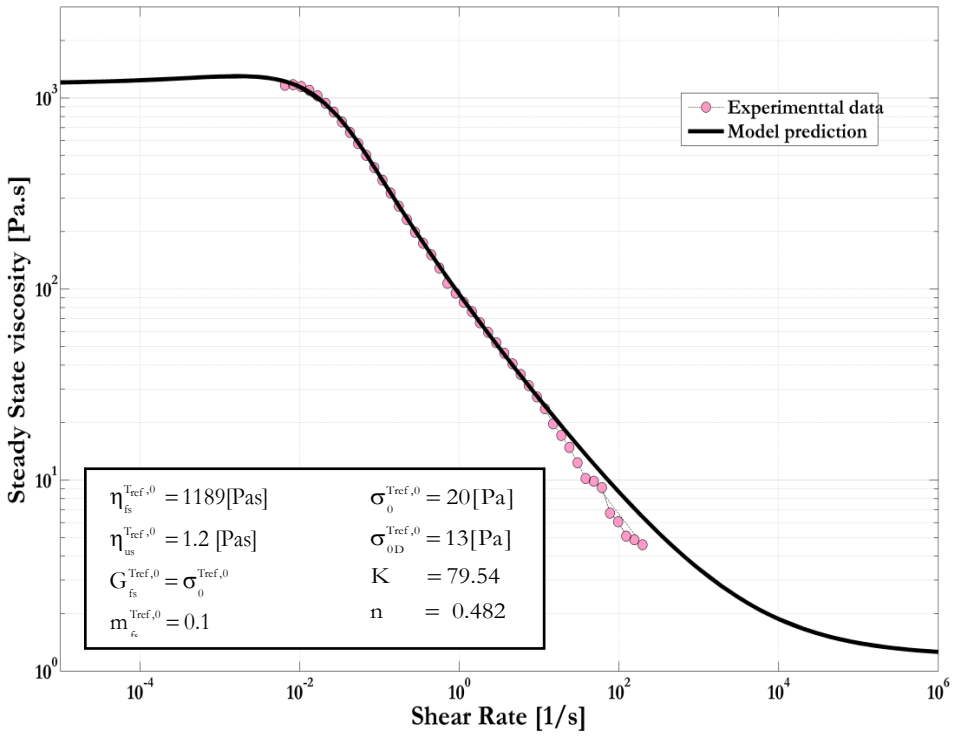

Figure IV.3 : Simulation of experimental flow curves for Maya crude oil at 265.15K(-8°C). Symbols are data; line is calculated.

On application of shear rate, the sample, initially acts as an elastic solid. The steady state viscosity appears to be constant as a higher shear rate is applied. The sample is effectively absorbing energy and as result, resists flow. When the yield stress is reached, the sample starts to flow and the measured viscosity starts to decrease. A strong decline of the viscosity curve happens at $\dot{\gamma}_0 = \mathbf{10}^{-2}[1/s]$ which corresponds to the transition from static to dynamic yield stress $\sigma_{0D} = \dot{\gamma}_{0D} \times \eta_{fs} = \mathbf{10}^{-2} \times 1189 = 11.89[Pa]$. This value is lower than the dynamic yield stress (20Pa) reported in **Table III-3** for a lower temperature 273.15K (-10°C), corroborating the decrease of yield stress as temperature increases.

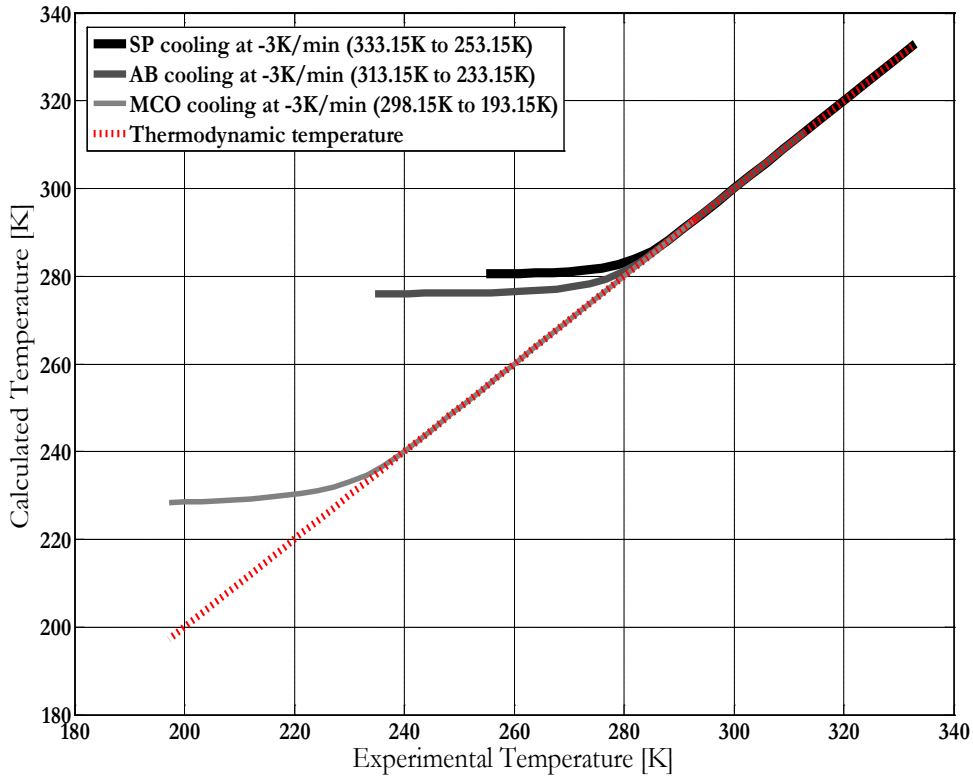

Figure IV.4 : Evolution of fictive temperature $\mathbf{T}_{\mathbf{eff}}$ when cooling at -3K/min.

IV.2.4. **Tracking thermal history**

Samples of Athabasca Bitumen Maya Crude Oil and Safaniya Oil, initially at constant temperature, are cooled slowly (q=-3K/min) to low temperatures. Rheological measurements were performed at constant shear rate $\dot{\gamma} = \text{cte}[1/\text{s}]$ and constant shear stress $\sigma = \text{cte}[\text{Pa}]$. While cooling, the fictive temperature remains identical to the thermodynamic temperature as long as the fluid structure is able to relax toward equilibrium (**Figure IV.4**). The transition to the limiting value of $\mathbf{T}_{\mathbf{eff}}$ occurs almost at the same value of temperature (**T=280K**) for Athabasca Bitumen and Safaniya Heavy Oil (**Figure IV.5)** while lower temperature (**T=220K**) is needed for Maya Crude Oil.

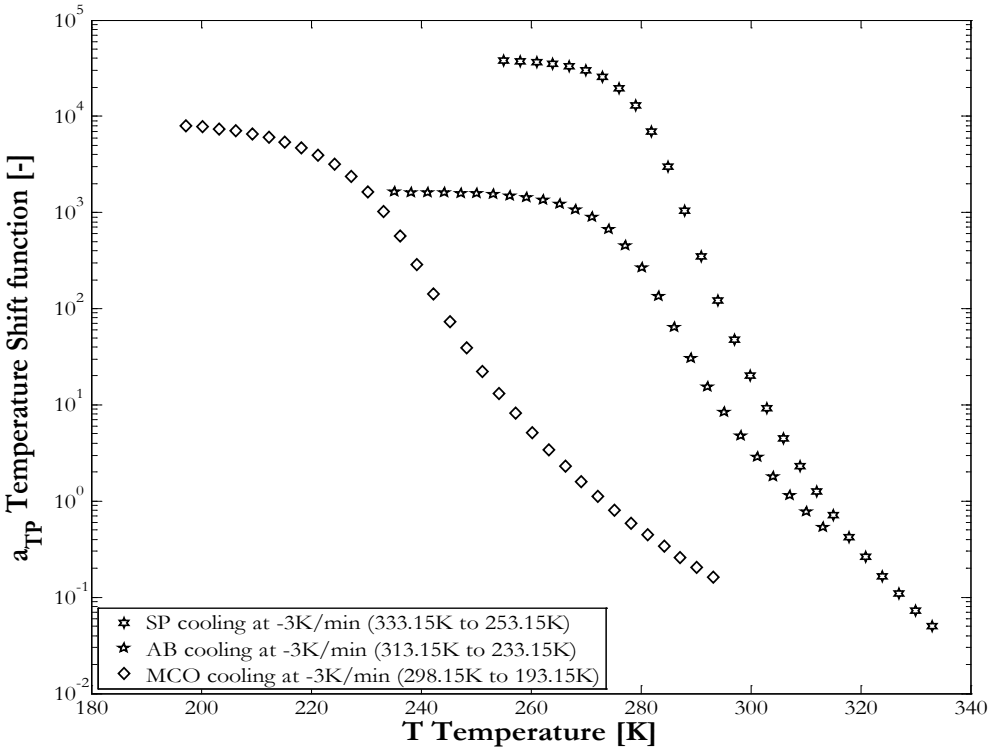

Figure IV.5 :Plot of simulated temperature shift functions for the hydrocarbon materials when cooling at -3K/min.

When the time scale of the relaxation process becomes longer than the time scale of the experiment, a transition to a constant value of T_{eff} occurs and a **β**-transition [6], i.e.: a transition from viscoelastic flow to elastic glassy behaviour, takes place.. This transition is attributed to the glass transition of the Newtonian liquid phase and leads to a constant value of the temperature shift factor ($\mathbf{a_{TP}}$) as shown in **Figure IV.5**. In the original WLF equation, $\mathbf{a_{TP}}$ increases toward infinity, causing a significant deviation from test data [86, 100]. Therefore the validity of the classic WLF model is being extended, here, to low temperatures region using the $\mathbf{T_{eff}}$ instead of **T**.

When samples are kept at constant temperature for a sufficiently long time (annealing or ageing) to allow the structured phase to relax, the fictive temperature approaches the thermodynamic temperature promoting viscosity.

IV. 3. COMPUTING THE FLOW RESPONSES OF FEEDSTOCKS

IV.3.1. **Simulation Algorithm**

The simulation procedure for a *temperature sweep* processes (**Figure IV.6**) is similar as the one on **Figure IV.1** :

Step 1 Specification of thermal conditions as input to the TNM model (Heating or cooling rate; Initial and final temperatures; Annealing Time after each temperature step).

Step 2 Base on these data the TNM model will generate a Table of fictive temperature $\mathbf{T_{fic}}$.

Step 3 The WLF parameters ($C_1^{Tref\,0}$ and $C_2^{Tref\,0}$) and the pressure dependency parameters (A1; A2; B1; B2) are specified to the WLF equation.

Step 5 Using the table of fictive temperatures (instead of the thermodynamic temperature), the WLF Model computes a set values for the shift function $\mathbf{a_{TP}}$ as function of Temperature **T**.

Step 6 The shift function values are used to calculate the flow curve parameters at each temperature during the cooling/heating process.

Step 7 In the case of constant shear stress procedure, [Eq. II.14] is integrated until steady state is reached.

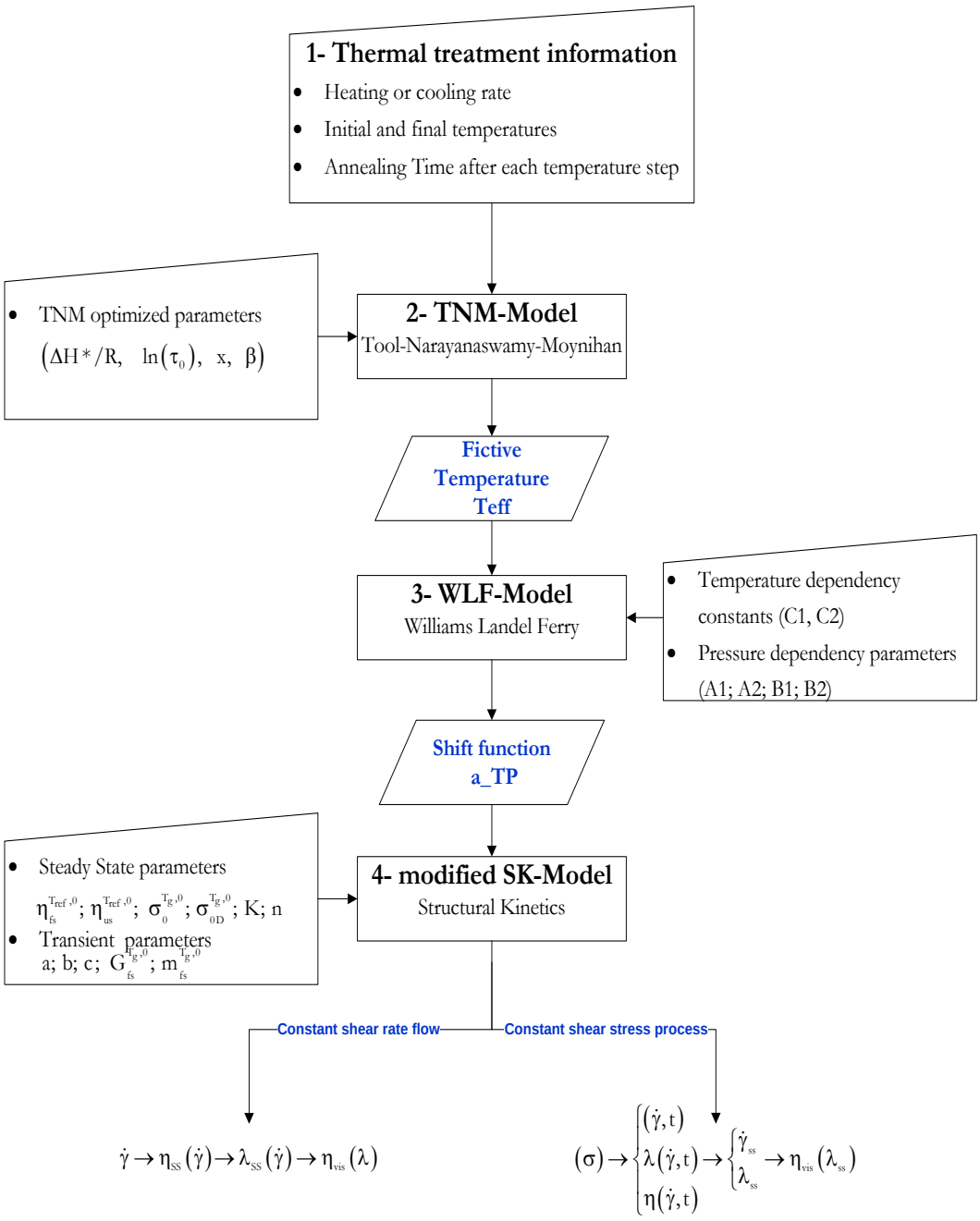

Figure IV.6 : Diagram of steps for the calculation of rheological properties for complex fluids during a temperature sweep procedure, using the modified SK-Model.

IV.3.2. **Flow behaviours of Maya Crude Oil, Athabasca Bitumen and Safaniya Heavy Oil with temperature**

The thermal susceptibility of the three feedstocks is evaluated through a temperature sweep test, at cooling rate of q=-3°K/min under a controlled stress mode for different values of shear stresses. The model calculations were done using the flow curve parameters $(n, K, \sigma_0, \sigma_{0D}, \eta_{fs}, \eta_{us})$ of:

- Maya Crude Oil (MCO) at $T_{ref} = 273.15[K]$
- Athabasca Bitumen (AB) at $T_{ref} = 308.15[K]$
- And Safaniya Heavy Oil (SP) at $T_{ref} = 313.15[K]$

The temperature shift function $\mathbf{a_{TP}}$ is computed using the effective temperatures $\mathbf{T_{eff}}$ into [Eq. II.20]. For every temperature step, [Eq. II.14] is integrated until steady stated is reached. The corresponding value of shear rate and $\dot{\gamma}$ are respectively used in [Eq. II.11] and [Eq. II.10a] to calculate, in two different ways, the steady state viscosity. Both value of steady state shear viscosity should agree, when the calculation is performed accurately.

For Maya Crude Oil (**Figure IV.7**), the model is able to predict a shear stress dependence of **b**-transition. Indeed the transition from viscoelastic to plastic region occurs around 240K for 50Pa and 220K for 500Pa. In the region of 350K, the **a**-transition from Newtonian to Viscoelastic behaviour occurs. In between these two transitions, the rheology of MCO is calculated to be strongly shear dependant. Indeed, it is appears on **Figure IV.7** that increasing the shear stress by one decade, results in about ten times reduction in resistance to flow.

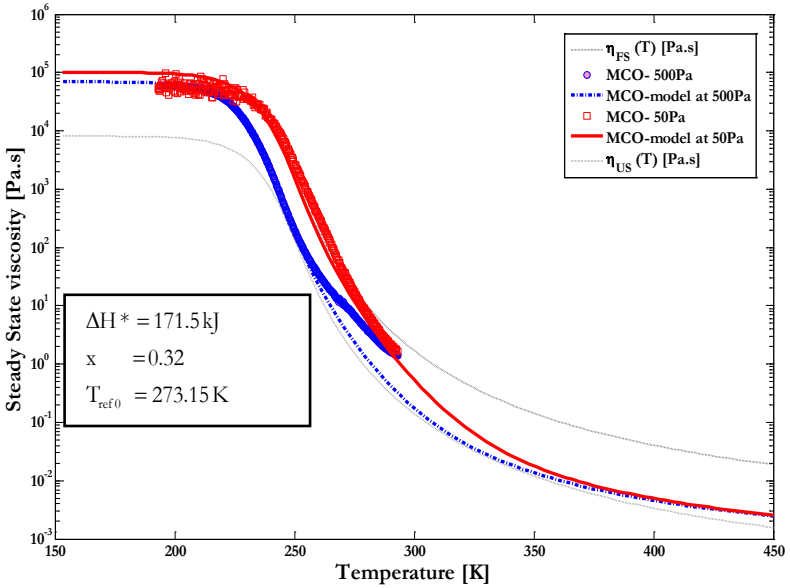

Figure IV.7: Simulated viscosity curve for Maya Crude Oil (MCO). Temperature sweep is done at constant shear stress. Symbols are data; lines are simulated. (Refer to **Appendix 1** for the extrapolation** data set)

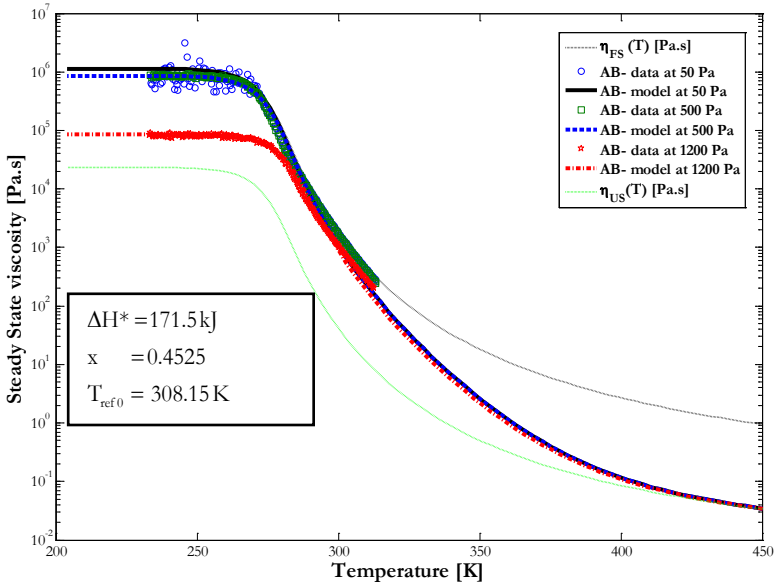

Figure IV.8 : Apparent viscosity calculated for Athabasca Bitumen (AB) using the Modified SKM model. Symbols are data; lines are simulated. (See **Appendix 2** for the extrapolation** data set)

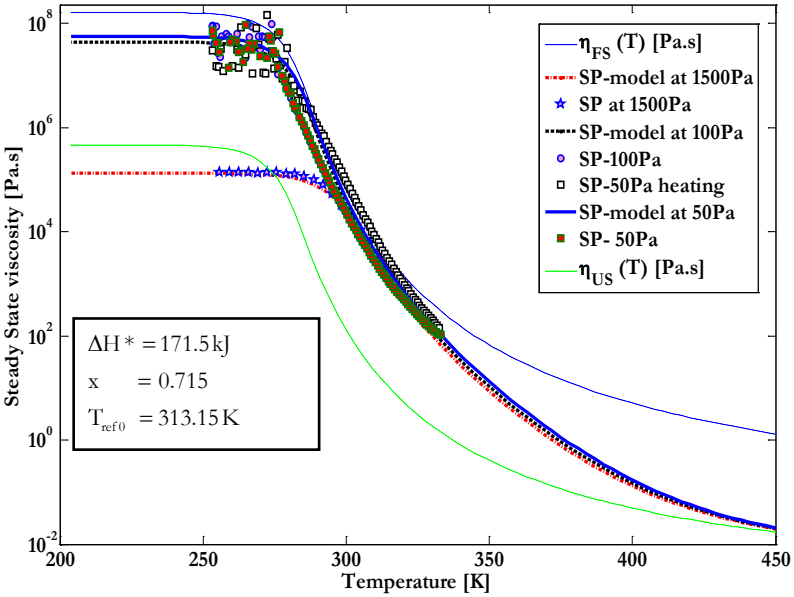

Figure IV.9 : Apparent shear viscosity calculation during a temperature sweep process on Safaniya Heavy Oil (SP) at different shear conditions. The shear stress is kept constant as temperature varies. Symbols represent data; lines are simulated. (Consult **Appendix 3** for the extrapolation** data set)

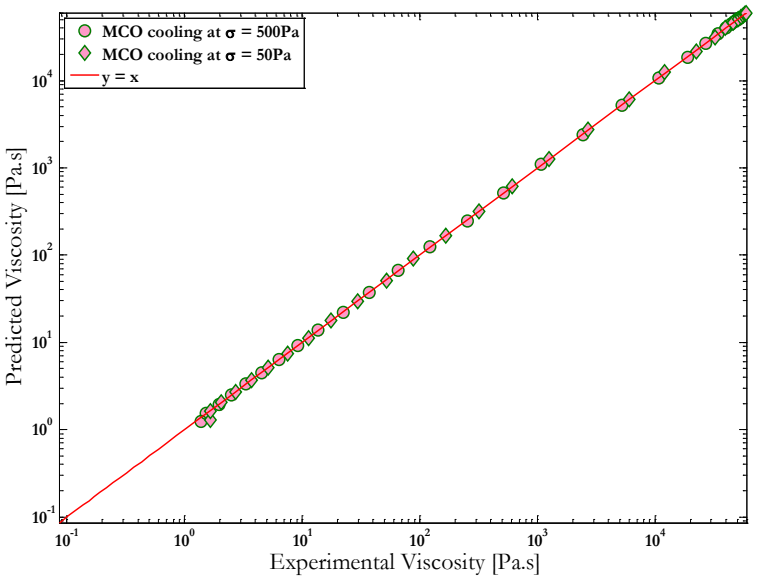

Figure IV.10 : Dispersion diagram of viscosity data for Maya Crude Oil. (See **Appendix 1** for the extrapolation** data set)

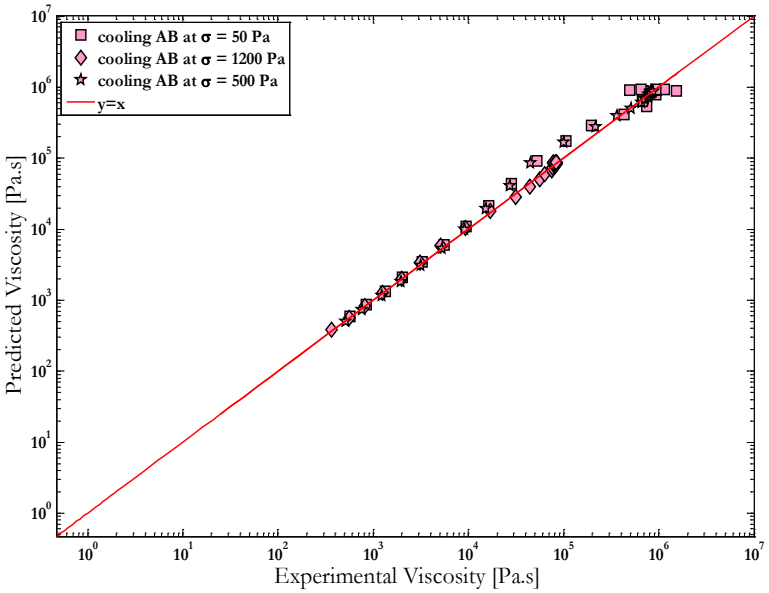

Figure IV.11 : Scattered plot of calculated viscosity data for Athabasca Bitumen. (Refer to **Appendix 2** for the extrapolation** data set)

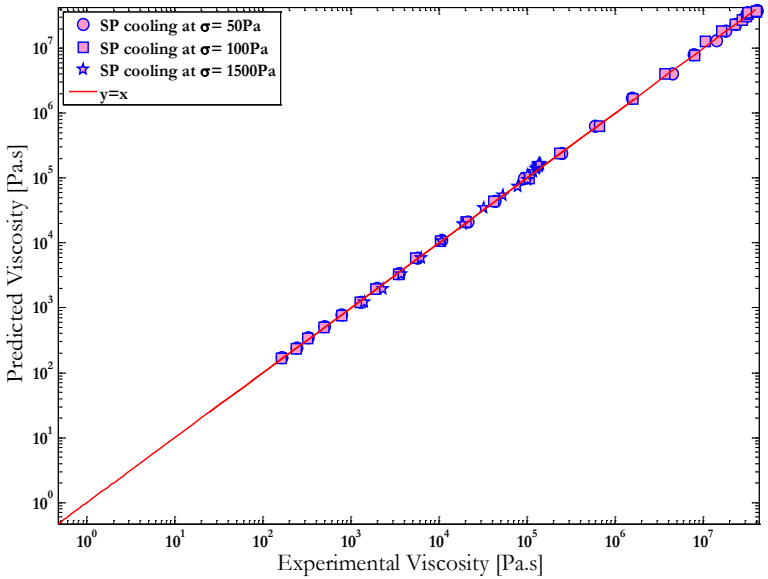

Figure IV.12 : Scattered diagram of calculated viscosity curve for Safaniya Petroleum using the Modified SK-Model. (consult **Appendix 3** for the extrapolation** data set)

When the calculated values are compared to experimental data, even if some differences are observable, the trends and transitions are similar and in acceptable agreement as illustrated using scatter plots - **Figure IV.10**. The flow response of Athabasca Bitumen (AB) was computed under various shear stress conditions ($\sigma = 50\,\text{Pa}$, $\sigma = 500\,\text{Pa}$ and $\sigma = 1200\,\text{Pa}$). The model is able to predict that the **b**-transition depends not only on the level of shear stress but also on the amount of heavy component present in the material. Indeed the transition from viscoelastic to plastic region occurs around 270K if AB is sheared below 500Pa and approximately 280K when the stress level is 1200Pa.

Athabasca Bitumen (**Figure IV.8**) has a shear thinning behaviour more pronounced at lower temperatures and merely noticeable at high temperatures where less structure is present. At high temperature the consistency of the material is so high that no major reduction of viscosity is observed when it is sheared below 500Pa. Comparisons of calculated and measured values are illustrated on the dispersion plots on **Figure IV.11**. The presence of a structured network adds more complexity to the flow behaviour of Athabasca Bitumen causing some random variations in flow measurement at low temperatures. But in general, the overall rheological trend and transition are well observed by the model.Safanyia Heavy Oil samples were simulated under similar shear conditions and thermal history as for Athabasca Bitumen. The model values (**Figure IV.9**) show similar behaviour to AB. Indeed, the transition from the viscoelastic to the plastic region occurs around 270K if SP is sheared below 500Pa and approximately 300K if the stress level is 1500Pa. Agreement between the model and experimental measurements are illustrated on the scattered plots in **Figure IV.11**. A good accuracy is observed through the whole range of temperature.

IV.3.3. **Model quality**

On **Table IV-1**, the %AAD between predicted values of viscosity and the experimental one are below 10% and the regression coefficients ($\mathbf{R^2}$) are close to **unity**. That reveals a strong flexibility, a high fitting capability, and more importantly, a decent prediction ability of the Modified SK-Model for the native feedstock. The reason for elevated values of RMSE observed in Athabasca Bitumen and Safaniya Heavy Oil can be better understood by looking at the scatter plots -**Figure IV.10** and **Figure IV.11**. For Maya Crude Oil little divergence is observed over the range of temperatures covered and

Materials	Process	Data points	% AAD	R^2	RMSE[Pa.s]
MCO	Cooling from 450K to 150K at Shear stress of 500 [Pa]	26	1%	1.000	15.6
	Cooling from 450K to 150K at Shear stress of 50 [Pa]	30	2%	1.000	40.8
AB	Cooling from 450K to 200K at Shear Stress of 50 [Pa]	26	9%	0.987	3584
	Cooling from 450K to 200K at Shear Stress of 1200 [Pa]	26	6%	0.988	746
	Cooling from 450K to 200K at Shear Stress of 500 [Pa]	26	9%	0.994	5629
SP	Cooling from 450K to 200K at Shear Stress of 50 [Pa]	27	4%	0.993	22558
	Cooling from 450K to 200K at Shear Stress of 1500 [Pa]	22	10%	0.932	3090
	Cooling from 450K to 200K at Shear Stress of 100 [Pa]	27	3%	0.998	1528

Table IV-1: Statistical results of flow predictions for Maya Crude Oil (MCO), Athabasca Bitumen (AB) and Safaniya Heavy Oil (SP) during cooling processes.

this makes the sum of squared residuals $\sum_{i}^{n}\left(y_i^{exp} - y_i^{pred}\right)^2$ very small and the RMSE low. For the two other feedstocks, deviations between calculation and measurements occur for low temperature viscosities. The high value of viscosities in this range of temperature (values up to 1MPa.s are expected) amplifies $\sum_{i}^{n}\left(y_i^{exp} - y_i^{pred}\right)^2$ leading to elevated RMSE but the average absolute percentage error remains less than 10%.

IV. 4. CALCULATING THE FLOW BEHAVIOUR OF NANO-FILTERED FEEDSTOCKS

IV.4.1. **Simulation Algorithm**

This second evaluation involves computing the flow response of hydrocarbon fractions with different concentrations of structured and unstructured phases using parameters fit to the native feedstocks. The computation procedure follows the same method as in **IV.3.1.** The Sudduth equation[89] (with the coefficients from [37]) and the Chateau-Ovarlez-Trung model[101] are used to calculate the flow curve parameters $\left(\eta_{fs}^{T_{ref},0};\ \eta_{us}^{T_{ref},0};\ \sigma_0^{T_g,0};\ \sigma_{0D}^{T_g,0};\ K;\ n\right)$ of nano-filtered samples. The algorithm is illustrated in **Figure IV.13**. The statistical assessments are summarized on **Table IV-2**. The model parameters are shown in the plots.

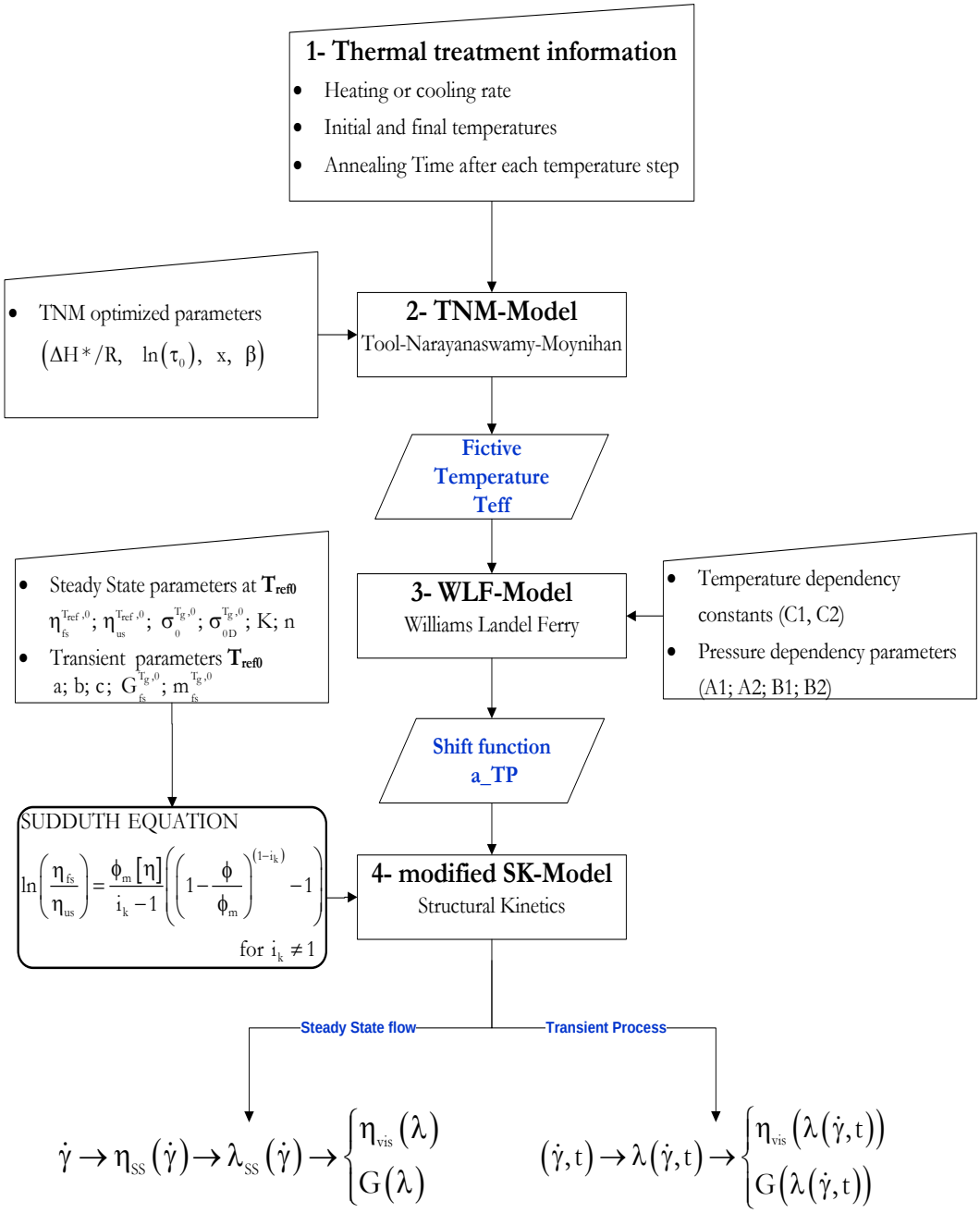

Figure IV.13 : Simplified diagram of steps for the calculation of rheological properties for nano-filtered permeated using the Modified SK-Model.

IV.4.2. **Flow responses of nano-filtered permeates with temperature**

Nano-filtered permeates from Safanyia Heavy Oil (SP P) and Athabasca Bitumen (AB P), are subjected to temperature variation while keeping the shear rate constant. The model shows, in accordance with experimental data, that the **b**-transition occurs around 250K independent of the shear rate and the source of the permeate. In **Figure IV.15**, samples of 10nm, 20nm and 50nm permeates from Safaniya Heavy Oil show a marked shear thinning behaviour, noticeable at low temperatures where the presence of a network of structure dictated flow responses. In this area the model prediction are in good agreement with experimental data. As temperature increases a transition from the elastic plateau to viscoelastic behaviour occurs. This transition is well predicted for 10nm and 20nm permeate samples from Athabasca Bitumen on **Figure IV.14** as well.

Increasing temperature causes the viscosity curves to converge toward a shear independent region, characteristic of Newtonian behaviour, possibly due to the disappearance the network of structures. The model predictions diverge slightly form experimental values as ahown in the parity plots - **Figure IV.18** and **Figure IV.19**. AB-P10 and SP-P10 seem to behave similarly to flow. In fact, for the same shear rate and a similar thermal history, both materials share a low temperature limiting viscosity of about **1MPa.s** with **b**-transition occurring at 260K and almost no hysteresis upon cooling annealing and reheating.

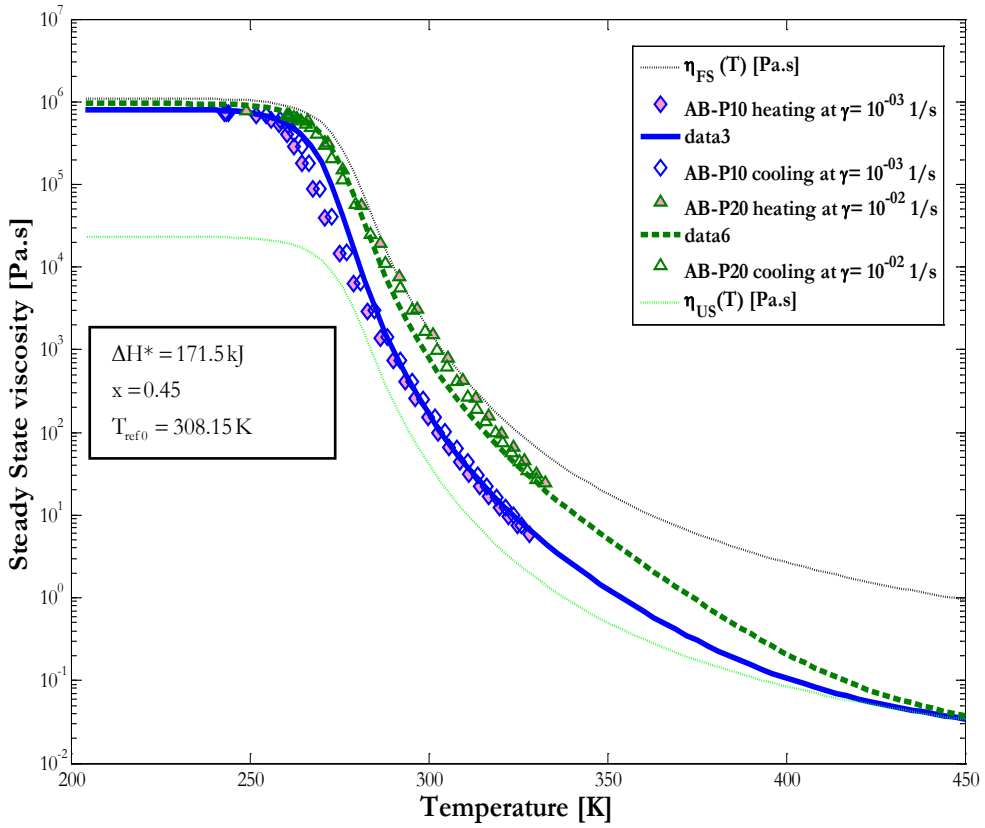

Figure IV.14 : Shear viscosity of Athabasca Bitumen permeates (AB-P10 and AB-P20).at constant shear rate for a temperature sweep. Symbols are experimental; lines are calculated. (Refer to **Appendix 2** for the prediction*** data set)

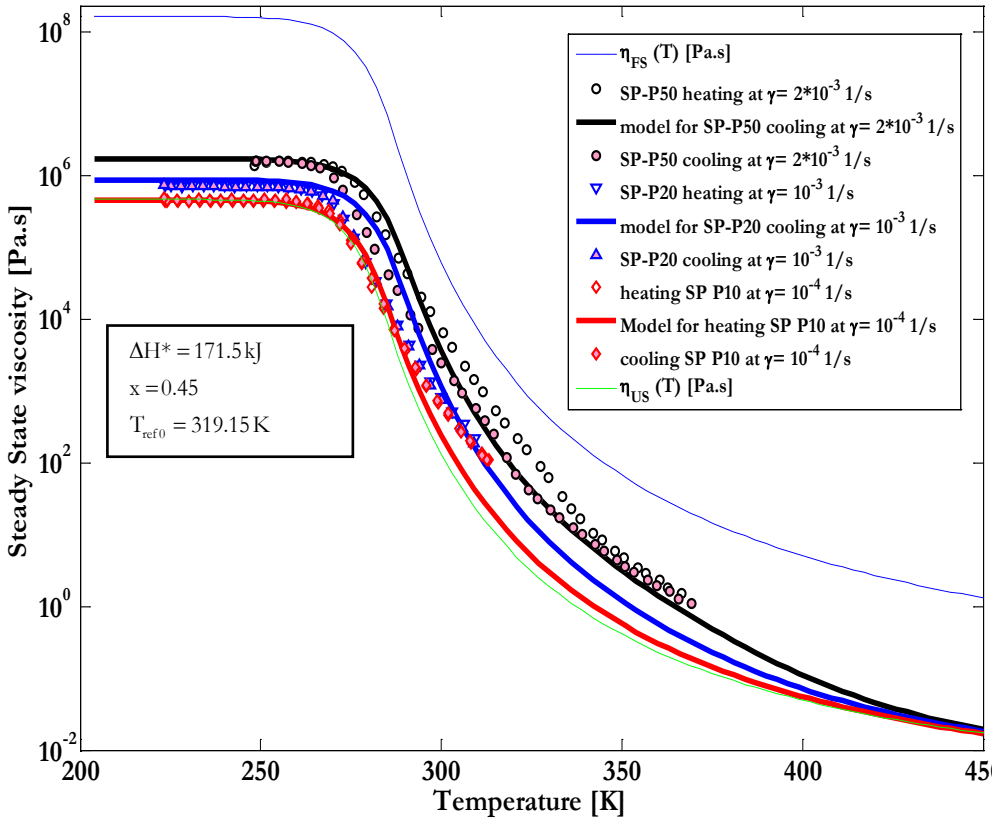

Figure IV.15 : Apparent shear viscosity calculation during a temperature sweep process on Safaniya Heavy Oil permeates. The rate of shear is kept constant as temperature decreases. Symbols represent data; lines are simulated. (see **Appendix 3** for the prediction*** data set)

IV.4.3. **Flow responses of nano-filtered retentates with temperature**

Nano-filtered retentate from Safanyia Heavy Oil (SP-R20) and Maya Crude Oil (MCO-R5) were subjected to temperature sweep under constant shear stress. Both retentates are so viscous that flow measurements were performed at high temperatures. Despite that, the main evolution of the flow resistance, previously observed in native samples and their permeate samples at low temperatures are still apparent for those thick materials. Their reference temperatures are set at higher values and the simulated plots can be seen on **Figure IV.16** and **Figure IV.17**, respectively for Maya Crude 5nm retentate and Safaniya 20nm retentate.

On **Figure IV.16** the apparent viscosity has a constant value of below 370K. As temperature increases a dramatic decline in viscosity occurs around 400K leading to a viscoelastic region. The model predictions follow fairly well those transitions and have a good agreement with experimental data. However the scatter plot, **Figure IV.20**, reveals over prediction of experimental viscosity data at low temperatures.

The Safaniya Heavy Oil 20nm retentate sample was measured using two consecutive cooling procedures to cover the temperature range from 270K to 470K. The measurements are well aligned on a single curve characterized by a low temperature plateau and a decreasing viscosity above 340K. The model is able to predict with reasonable accuracy these transitions (**Figure IV.17**). Substantial deviations, during the shift to high viscosity plateau, are noticeable in **Figure IV.21**.

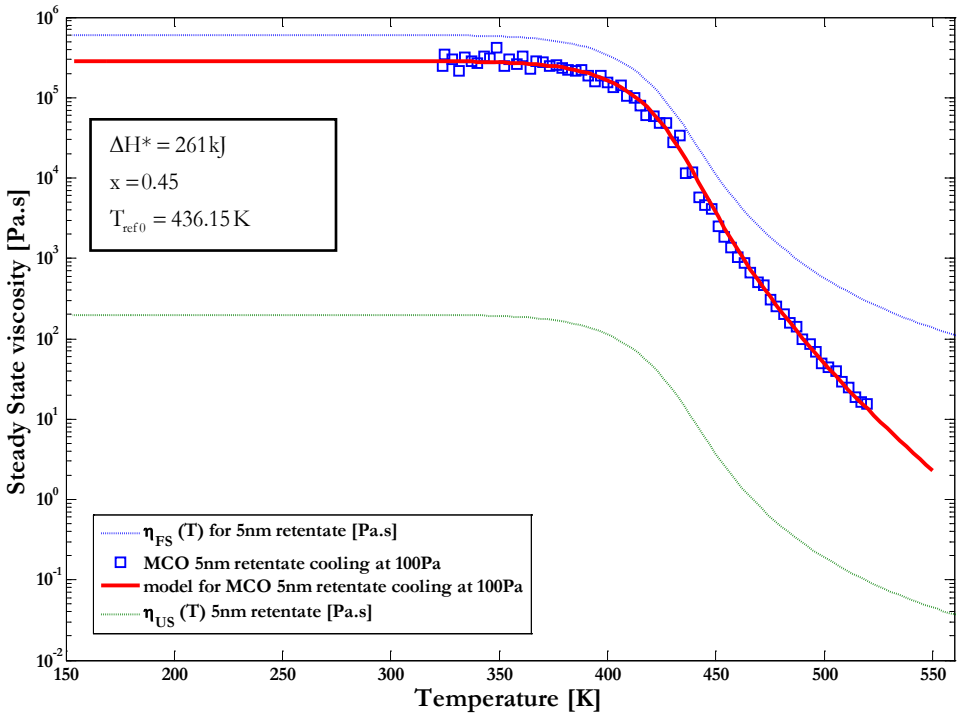

Figure IV.16 : Shear viscosity of Maya Crude Oil retentate (MCO-R5).at constant shear stress during a temperature sweep. Symbols are experimental; lines are calculated. (Refer Refer to **Appendix 1** for the prediction*** data set)

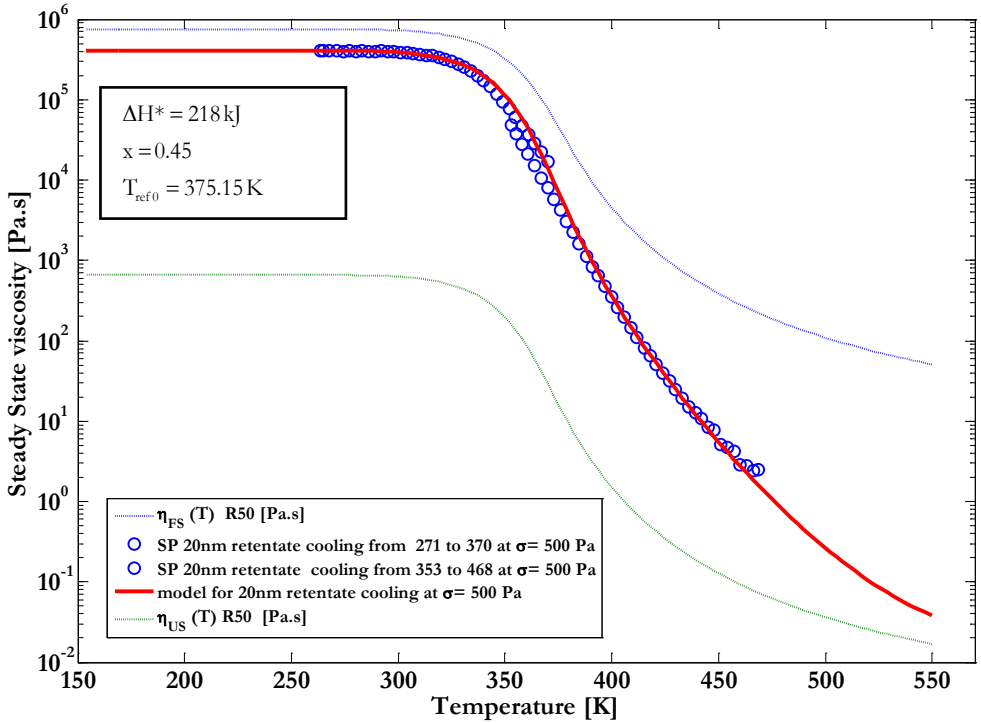

Figure IV.17 : Apparent shear viscosity calculation during a temperature sweep process on Safaniya Heavy Oil 50nm retentate (SP R50). The shear rate or stress is kept constant as temperature decreases. Symbols represent data; lines are simulated. (see Refer to **Appendix 3** for the prediction*** data set)

IV.4.4. **Prediction quality**

Table IV-2 shows that the maximum %AAD is 15% for the prediction data set compared to 10% for the extrapolation data, while regression coefficients remain above 0.98. Retentate samples have **% AAD** of 12% for the 5nm MCO retentate and 6% for the SP 20nm retentate. Results for the permeates are also variable. % AAD values vary from 1 to 15 %. The variability of prediction outcomes may reflect uncertainty related to structured phase volume fraction. However, the results clearly show that it is possible to use the Modified SK-Model to predict the rheological responses of samples with different volume fractions of structured and unstructured phases where individual phase composition is invariant within experimental error. This is a stringent test of the model, and one typically not performed.

Materials	Process	Data points	% AAD	R^2	RMSE [Pa.s]
MCO	Cooling R5 from 450K to 200K under shear stress of 100 [Pa]	67	12%	0.985	2270
AB	Cooling P10 from 450K to 200K under shear rate of 10^{-3} [1/s]	30	1%	1.000	332
	Cooling P20 from 450K to 200K under shear rate of 10^{-2} [1/s]	30	15%	0.987	6571
SP	Cooling P10 from 450K to 200K under shear rate of 10^{-4} [1/s]	30	2%	0.999	1284
	Cooling P20 from 450K to 200K under shear rate of 10^{-3} [1/s]	30	14%	0.992	5394
	Cooling P50 from 450K to 200K under shear rate of $2*10^{-3}$ [1/s]	42	12%	0.989	3596
	Cooling R20 from 450K to 200K under shear stress of 500 [Pa]	37	6%	0.993	192

Table IV-2 : Statistical results of rheological predictions for nano-filtered samples of Maya Crude Oil (MCO), Athabasca Bitumen (AB) and Safaniya Heavy Oil (SP).

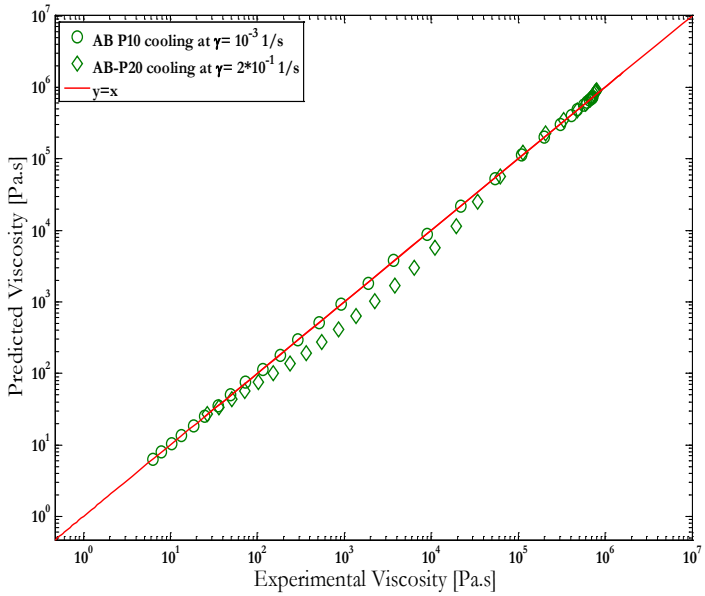

Figure IV.18 : Scattered diagram of calculated viscosity curve for Athabasca Bitumen 10nm and 20nm permeates using the Modified SK-Model. (Consult **Appendix 2** for data)

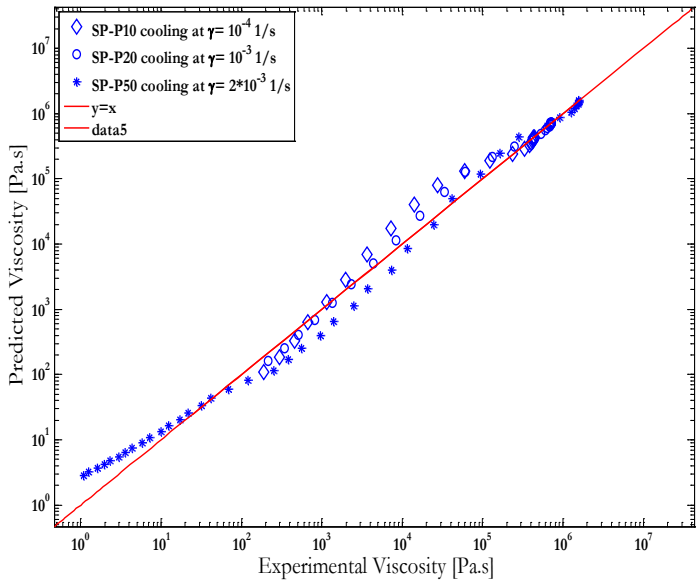

Figure IV.19 : Scattered plot of calculated viscosity curve for Safanyia permeates using the Modified SK-Model. (Refer to **Appendix 3** for data)

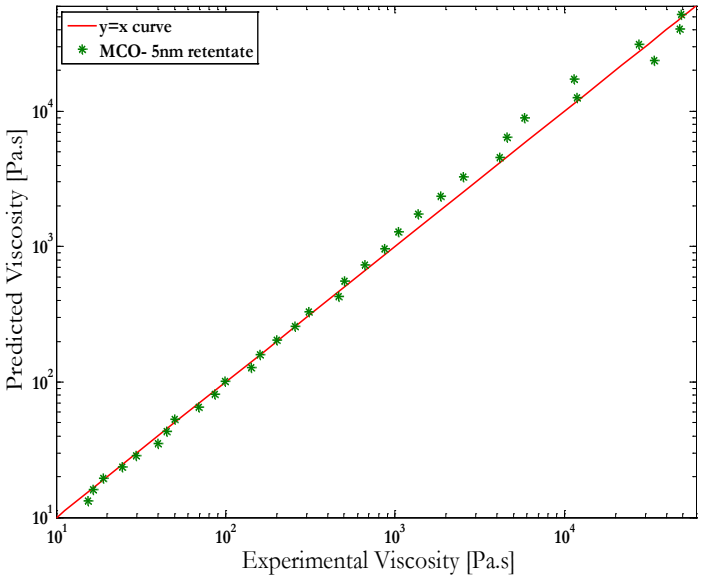

Figure IV.20 : Scattered diagram of calculated viscosity curve for Maya Crude permeates using the Modified SK-Model. (Refer to **Appendix 1** for data)

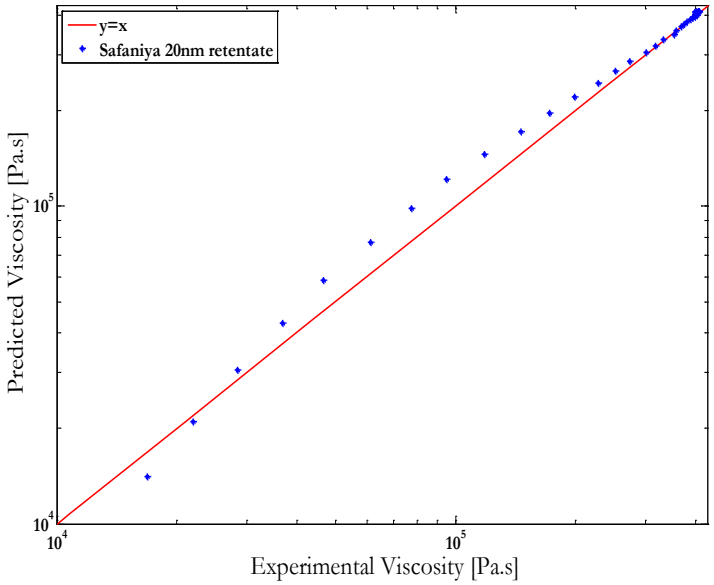

Figure IV.21 : Scattered plot of calculated viscosity curve for Safanyia permeates using the Modified SK-Model. (See **Appendix 3** for data)

IV. 5. SUMMARY

The goal of this chapter was to assess how well the proposed model simulates the effects of shear, temperature and structured phase volume fraction on the flow behaviour "bitumen", "heavy oils" and their nano-filtered fractions. The flexibility and the prediction quality of the model were not adversely affected by the simplification procedure described in **Chapter III**. The proposed model followed the influences of composition and stress level on the low temperature limiting viscosity as well as the **a** and **b** transitions. %AAD less than **15%** and regression coefficients ($\mathbf{R^2}$) close to **1,** for specific fluids within the data sets, were obtained vis-a-vis experimental viscosity measurements. Thus the practicality of the modeling approach and the model, containing only 3 feedstocks specific parameters, has been demonstrated. The one remaining topic, the physical meaning of the parameters appearing in the model and their variation with feedstock is needed to generalize the results. This important topic is addressed in the next chapter.

Chapter V:
MODEL ANALYSIS AND DISCUSSION

V. 1. PARAMETER VARIATIONS

The quality of a model relies on its ability to accurately capture the physics of the system being simulated. The model should be based on a small number of parameters that are easily accessible through experimentation or routine usage in the literature (see **Table III-9**). The complex flow behaviour of petroleum material, with temperature, is expressed by the mean of 5 equations depending on 13 parameters. This under constrained system (more variable that equations) required further simplification which was made possible after a fitting procedure and literature review. Indeed, out of these 13 parameters, 4 $\left(\tau_0; \beta; C_1^{Tref0}; C_2^{Tref0}\right)$ were found to be almost similar among feedstocks and 6 $\left(\mathbf{G_{fs}}, \mathbf{m}, \mathbf{a}, \mathbf{b}, \mathbf{c} \text{ a } d \iota\right)$ are adopted from literature [17, 22, 92]. The remaining 3 parameters $\left(\Delta H_{fs}^{*}; x; T_{ref0}\right)$ are fluid dependent variables and summarised in **Table V-1**.

Materials	T_{ref0} [K]	ΔH^* [kJ]	x [-]
MCO	273.15	167	0.32
AB	308.15	168	0.45
SP	313.15	164	0.72

Table V-1: List of fluids specific variables as they change among feedstock

V. 2. PHYSICAL MEANING OF MODEL PARAMETERS

V.2.1. **Individual meaning**

The proposed model, **Table III-10**, is based on the idea that some material properties can be considered akin for the three feedstocks covered in this study, and by extension to other hydrocarbon resources. **Table III-7** shows that, even if acceptable numerically, this approach hides some fundamental details related to the intrinsic nature of each material.

The model captures the four fundamental aspects of the relaxation phenomena[64] apparent in the experimental curves. τ_0 determines the temperature at which the structural relaxation is noticeable on a given "experimental time scale", **DH*** determines how that temperature changes with a change in time scale, β accounts for the non-exponential character of the relaxation (the memory effect), and **x** accounts for the nonlinear character.

The non-linearity parameter **x** increases with the fraction of structured constituents. In **[Eq. II.17']**, **x**, partitions the activation energy ΔH^* of the structural relaxation process into two parts that characterize the relative contribution of **temperature** and **fluid structure** to the relaxation time [67]. Thus, the structure present in Safaniya Heavy Oil (x=0.715) has the higher temperature susceptibility (changes easily with temperature) than the one present in Athabasca Bitumen (x=0.45) and Maya Crude Oil (x= 0.32) as shown in **Figure III.22**.

DH* is the activation enthalpy for the relaxation process and expresses the temperature dependence of the relaxation time **t**. The fact that **DH*** are almost similar among feedstocks (168.kJ for Athabasca bitumen, 167kJ for Maya crude oil and 164kJ for Safaniya vacuum residue) in the spectrum implied by

[Eq.II.17'] signifies "thermorheological simplicity" or a "temperature independent spectrum of relaxation times." This parameter will be a good candidate for further simplification of the model.

The reference temperature **Tref** defines the area where the flow response of hydrocarbon fluids is equally dominated by the viscous Newtonian matrix and the non-Newtonian structured phase. This transition region is located at higher temperature as the concentration of heavier constituent increases. Indeed **Tref** is 273.15K for Maya Crude Oil is 308.15K for Athabasca Bitumen and 313.15K for Safaniya Heavy Oil.

V.2.2. **Collective meaning**

The dissimilarity of model parameters, among hydrocarbons, supports the idea of a structure present in those fluids and that disorganized in a different way, upon shear and thermal perturbations. This relaxation mechanism is "non-linear" (since $\mathbf{x \neq 1}$) and has "temperature independent spectrum of relaxation times" (**DH*** are almost constant among feedstocks). The phenomenology of these observations is apparent through the disparities in temperature susceptibility and extends of hysteresis behaviours observed in the viscosity-temperature curve (**Figure V.1**). Indeed, the resistance to flow increase by 3 orders of magnitude for Maya Crude Oil and by 6 orders magnitude for Safaniya Heavy Oil from 260K to 340K and a more pronounced hysteresis is obvious for Safaniya Heavy Oil.

These rheological and thermodynamics evidences concur to the networked structural nature of hydrocarbon material. When break-up occurs, at high temperatures where the Newtonian matrix is very fluid, the rebuild process is quick and no hysteresis is observables. At low temperature the viscous matrix hinders this process, making the relaxation behaviour perceptible.

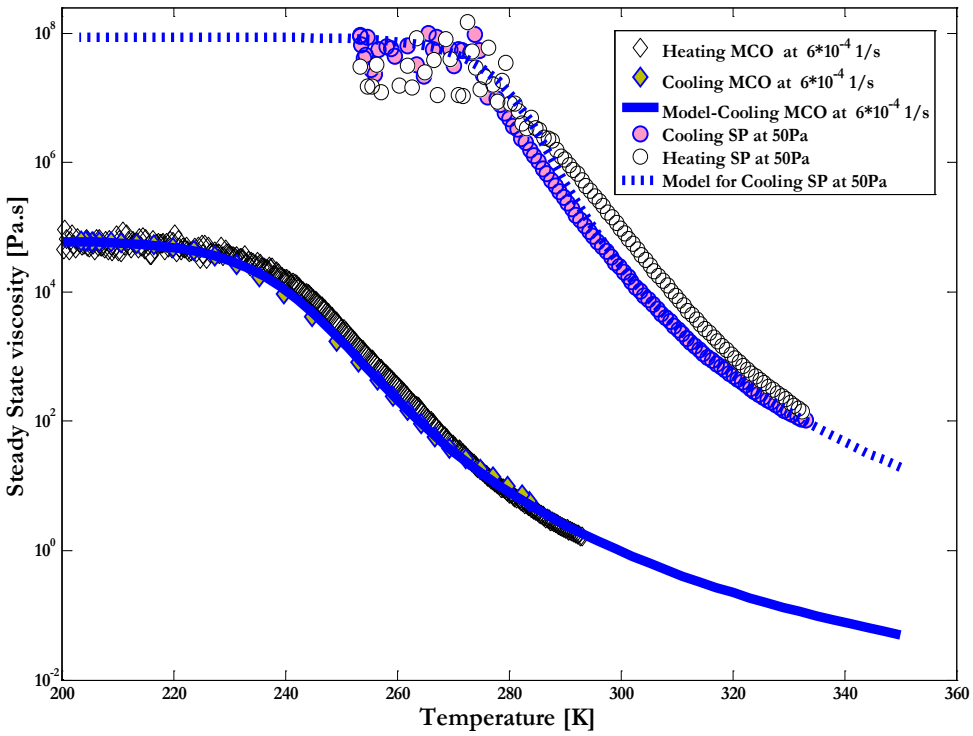

Figure V.1 : Illustration of hysteresis behaviour showing how thermal annealing affects differently the structure present is Maya Crude Oil (MCO) and Safaniya Heavy Oil (SP)

V. 3. RHEOLOGICAL EFFECTS CAUSED BY STRUCTURE

The level of shear (stress or rate) and temperature alters the structure present in feedstocks at low temperatures. This explains why the viscoelasticity decreases upon heating or increasing the level of shear stress or shear rate. For nano-filtered permeates, where part of the structured material has been removed at 473.15K, there are similarities in flow behaviours. In fact, for the same shear rate and a similar thermal history, AB-P10 and SP-P10 have similar low temperature limiting viscosities (**Figure V.2**) and their apparent shear viscosities are of a similar magnitude. From this perspective, it can be hypothesized that the Newtonian matrices are rheologically similar for the feedstocks covered in this study.

Since at high temperatures the flow behaviours of feedstocks and that of their permeate converge (**Figure V.2**), it can be inferred that part of the liquid matrix contributes to the arrangement of the network of structural found at low temperatures.

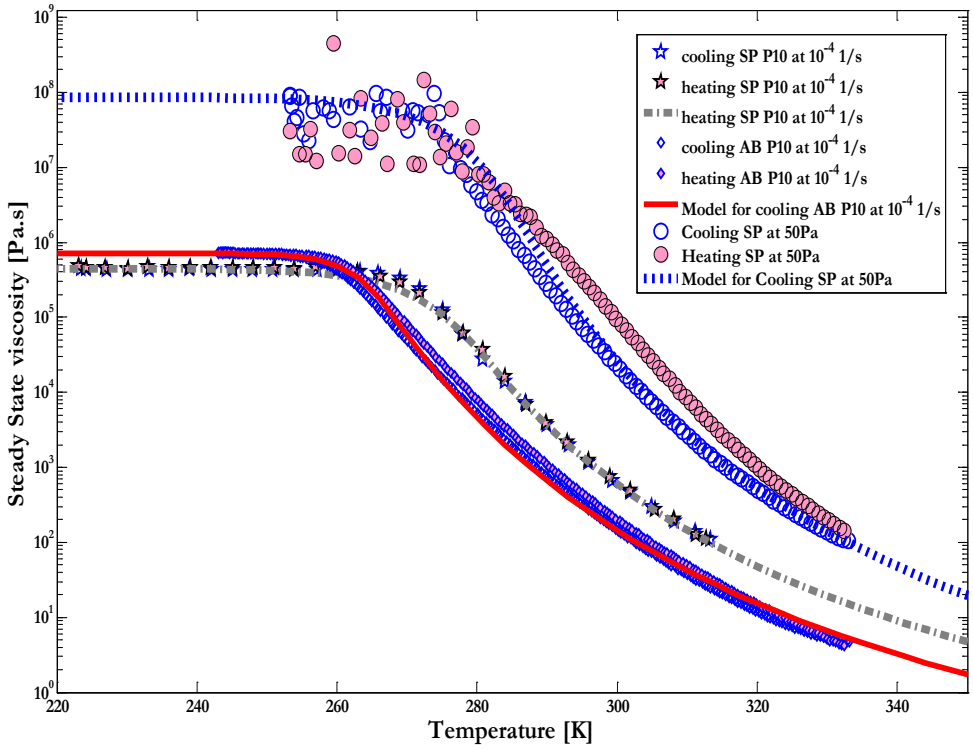

Figure V.2 : Rheology of nano-filtered samples compared to that of native heavy Oil. Lines are model predictions and symbols are experimental data

V. 4. SUMMARY

In order to simplify the proposed model, some parameters were kept constant due to their similarities between feedstocks. Analysis based on the variations of the non-linearity parameter **x** reveals that samples with more physical-asphaltenes are less sensitive to physical alteration but more susceptible to temperature. The collective meaning of the parameters observed in this study suggests a networked structure of petroleum material at low temperatures. Structure present in these materials is the main source of their shear and temperature susceptibility. It breaks down then rebuilds-up at time scale dependent on temperature. Low temperature relaxations are slower while at high temperature equilibrium is reach in shorter time scale. The viscous liquid matrix contributes to the arrangement of the network of structural found at low temperatures.

Chapter VI: CONCLUSIONS

VI. 1. WORK ACCOMPLISHED

Heavy oils and bitumen are complex fluids at low temperature. Their flow behaviour is strongly related to the temperature, shear and time dependence of their structured phases.

From a practical perspective, steady state properties govern the flow in most fields, transport and process applications as they involve steady shear flow environments. When flow occurs, steady state is reached in a matter of minutes. As a result, an accurate predictive tool for steady state flow properties was the main goal of this work. To accomplish this challenging task a Maxwell Mechanical representation was used to define these fluids as a structured phase within a Newtonian fluid matrix. A modified Structural Kinetics model was adopted to describe the rheological behaviour upon deformation. The effects of intensive thermodynamic variables (temperature and pressure) are accounted for using a free-volume based theory.

The parameters for the modified Structural Kinetics model were identified on the basis of laboratory measurements and literature data, and then optimized using a Levenberg-Marquardt fitting algorithm coded in MATLAB. The similarities in these parameters allowed a generalization of the model which reduced the adjustable parameters from 10 to 3 for each feedstock.

The simplification procedure lumped properties of feedstocks without affecting the flexibility and the prediction quality of the model. The maximum value of %AAD, between the predicted viscosity and the experimental ones, is 4% for the training data set; 10% for the extrapolation data set (temperature and rheological conditions for the feedstocks were varied); and <15% for the prediction data set (volume fraction of the structured phases in the feedstocks was varied). The structure present in Safaniya Heavy Oil (x=0.715) has the highest temperature susceptibility. Its properties change more easily with temperature than the ones present in Athabasca Bitumen (x=0.45) and Maya Crude Oil (x= 0.32).

VI. 2. PERSPECTIVES GAINED

Simulating the flow properties of complex materials such as heavy oils and bitumen at low temperatures is a very complex task. This work contributed in suggesting a new approach that consists in tracking the *mechanical history* of the fluid through a structural parameter λ and accounting for the *thermal history* by using the fictive temperature introduced Tool [65] in 1946.

VI. 3. RECOMMENDATIONS

Transient flow phenomena can be well calculated by the Modified SK-Model. Therefore, a qualitative behaviour of this model needs to be further assessed for experiments such as, Creep and Recovery, Cessation of flow[27], Flow bifurcations [28] and even Oscillatory Flows. That will shed a light in how well the model discriminates between thixotropy and viscoelasticity.By the time this work was completed, no clear consensus about the structure and shape, of the heavy fractions in bitumen and heavy oils, existed. However, integrating structural probing data from SAXS techniques can bring further physical meaning to the proposed model.

REFERENCES

1. Yasutomi, S., S. Bair, and W.O. Winer, *An Application of a Free Volume Model to Lubricant Rheology I---Dependence of Viscosity on Temperature and Pressure*. Journal of Tribology, 1984. **106**(2): p. 291-302.

2. Ferry, J.D., *Introduction to polymer viscoelasticity, John J. Aklonis and William J. MacKnight, Wiley-Interscience, New York, 1983, 295 pp. Price: $39.95*. Journal of Polymer Science: Polymer Letters Edition, 1983. **21**(11): p. 958-959.

3. Wendt, C.J. and A. Cyphers, *How the Olmec used bitumen in ancient Mesoamerica*. Journal of Anthropological Archaeology, 2008. **27**(2): p. 175-191.

4. Connan, J., *Use and trade of bitumen in antiquity and prehistory: molecular archaeology reveals secrets of past civilizations*. Philos. Trans. R. Soc. London, Ser. B, 1999. **354**(1379): p. 33-50.

5. Boeda, E., et al., *Bitumen as a hafting material on Middle Palaeolithic artifacts*. Nature (London), 1996. **380**(6572): p. 336-8.

6. Lesueur, D., *The colloidal structure of bitumen: Consequences on the rheology and on the mechanisms of bitumen modification*. Adv. Colloid Interface Sci., 2009. **145**(1-2): p. 42-82.

7. Yarranton, H.W. and M.A. Satyro, *Expanded Fluid-Based Viscosity Correlation for Hydrocarbons*. Ind. Eng. Chem. Res., 2009. **48**(7): p. 3640-3648.

8. Quinones-Cisneros, S.E., C.K. Zeberg-Mikkelsen, and E.H. Stenby, *The friction theory (f-theory) for viscosity modeling*. Fluid Phase Equilib., 2000. **169**(2): p. 249-276.

9. Aasberg-Petersen, K., K. Knudsen, and A. Fredenslund, *Prediction of viscosities of hydrocarbon mixtures*. Fluid Phase Equilib., 1991. **70**(2-3): p. 293-308.

10. Tomkins, R.P.T., *Viscosity and diffusivity: A predictive treatment (Hildebrand, Joel H.)*. Journal of Chemical Education, 1978. **55**(11): p. A420.

11. Eduljee, G.H., *Correlating the fluidity of some n-alcohols using a modified free volume equation*. Chem. Eng. J. (Lausanne), 1987. **35**(1): p. 1-7.

12. Luo, P. and Y. Gu, *Effects of asphaltene content on the heavy oil viscosity at different temperatures*. Fuel, 2007. **86**(7-8): p. 1069-1078.

13. Fulem, M., et al., *Phase behaviour of Maya crude oil based on calorimetry and rheometry*. Fluid Phase Equilib., 2008. **272**(1-2): p. 32-41.

14. Sonntag, R.C. and W.B. Russel, *Structure and breakup of flocs subjected to fluid stresses : I. Shear experiments*. Journal of Colloid and Interface Science, 1986. **113**(2): p. 399-413.

15. Storm, D.A., R.J. Barresi, and S.J. DeCanio, *Colloidal nature of vacuum residue*. Fuel, 1991. **70**(6): p. 779-782.

16. Bazyleva, A.B., et al., *Bitumen and Heavy Oil Rheological Properties: Reconciliation with Viscosity Measurements*. J. Chem. Eng. Data: p. ACS ASAP.

17. de Souza Mendes, P.R., *Modeling the thixotropic behavior of structured fluids*. Journal of Non-Newtonian Fluid Mechanics, 2009. **164**(1-3): p. 66-75.

18. Larson, R.G., *The structure and rheology of complex fluids*. 1999, New York: Oxford University Press.

19. Barnes, H.A., *Thixotropy--a review*. Journal of Non-Newtonian Fluid Mechanics, 1997. **70**(1-2): p. 1-33.

20. Martínez-Boza, F., et al., *Rheology and microstructure of asphalt binders*. Rheol. Acta, 2001. **40**(2): p. 135-141.

21. Říha, P., *The unified description of viscoelastic and thixotropic properties of human blood*. Rheol. Acta, 1982. **21**(4): p. 650-652.

22. Dullaert, K. and J. Mewis, *A structural kinetics model for thixotropy*. Journal of Non-Newtonian Fluid Mechanics, 2006. **139**(1-2): p. 21-30.

23. Cragg, L.H., *The terminology of intrinsic viscosity and related functions*. Journal of Colloid Science, 1946. **1**(3): p. 261-269.

24. Dealy, J.M., *Official nomenclature for material functions describing the response of a viscoelastic fluid to various shearing and extensional deformations*. Journal of Rheology, 1995. **39**(1): p. 253-265.

25. Hackley, et al., *Guide to rheological nomenclature, measurements in ceramic particulate systems*. 2001, Gaithersburg, MD, ETATS-UNIS: National Institute of Standards and Technology. IV, 31 p.

26. Dealy, J.M., *Official Nomenclature for Material Functions Describing the Response of a Viscoelastic Fluid to Various Shearing and Extensional Deformations*. Journal of Rheology, 1984. **28**(3): p. 181-195.

27. Mewis, J. and N.J. Wagner, *Thixotropy*. Adv. Colloid Interface Sci., 2009. **147-148**: p. 214-227.

28. COUSSOT, et al., *Viscosity bifurcation in thixotropic, yielding fluids*. Vol. 46. 2002, Melville, NY, ETATS-UNIS: Society of Rheology. 17.

29. Chanda, D., et al., *Combined effect of asphaltenes and flow improvers on the rheological behaviour of Indian waxy crude oil*. Fuel, 1998. **77**(11): p. 1163-1167.

30. Trouton, F.T., *On the Coefficient of Viscous Traction and Its Relation to that of Viscosity*. Proceedings of the Royal Society of London. Series A, Containing Papers of a Mathematical and Physical Character, 1906. **77**(519): p. 426-440.

31. Barnes, H.A., *A HANDBOOK OF ELEMENTARY RHEOLOGY*. 2000, Aberystwyth: University of Wales. 210.

32. Boger, D.V., D.U. Hur, and R.J. Binnington, *Further observations of elastic effects in tubular entry flows*. Journal of Non-Newtonian Fluid Mechanics, 1986. **20**: p. 31-49.

33. De Kee, D., *Nonlinear effects (discontinuties) in rheology*. Journal of Central South University of Technology, 2007. **14**(0): p. 242-245.

34. Davenport, P. and S. Roath, *Blood thixotropy*. Journal of Clinical Pathology, 1981. **34**(1): p. 106-107.

35. Boger, D.V. and H. Nguyen, *A model viscoelastic fluid*. Polymer Engineering & Science, 1978. **18**(13): p. 1037-1043.

36. James, D.F., *Boger Fluids*. Annual Review of Fluid Mechanics, 2009. **41**(1): p. 129-142.

37. Hasan, M.A., et al., *Rheological Properties of Nanofiltered Athabasca Bitumen and Maya Crude Oil*. Energy Fuels, 2009. **23**(10): p. 5012-5021.

38. Evdokimov, I.N., N.Y. Eliseev, and D.Y. Eliseev, *Rheological evidence of structural phase transitions in asphaltene-containing petroleum fluids*. Journal of Petroleum Science and Engineering, 2001. **30**(3-4): p. 199-211.

39. De Kee, D., E. Chornet, and W. Zhang, *Viscous and yield stress properties of athabasca topped heavy oil*. The Canadian Journal of Chemical Engineering, 1998. **76**(4): p. 816-821.

40. Kanti, M., et al., *Viscosity of liquid hydrocarbons, mixtures and petroleum cuts, as a function of pressure and temperature*. J. Phys. Chem., 1989. **93**(9): p. 3860-4.

41. Lesueur, D., et al., *A structure-related model to describe asphalt linear viscoelasticity*. Journal of Rheology, 1996. **40**(5): p. 813-836.

42. Macosko, C.W., *Rheology - Principles, Measurements and Applications*, John Wiley & Sons.

43. Larson, R.G., *The Structure and Rheology of Complex Fluids*. 1999, New York: Oxford University Press. 692.

44. Riande, E., et al., *Polymer Viscoelasticity: Stress and Strain in Practice*. 1999: CRC.

45. Mavridis, H. and R.N. Shroff, *Temperature dependence of polyolefin melt rheology*. Polymer Engineering & Science, 1992. **32**(23): p. 1778-1791.

46. Lesueur, D., *Letter to the Editor: On the thermorheological complexity and relaxation modes of asphalt cements*. Journal of Rheology, 1999. **43**(6): p. 1701-1704.

47. Masson, J.F., G. Polomark, and P. Collins, *Time-dependent microstructure of bitumen and its fractions by modulated differential scanning calorimetry*. Energy Fuels, 2002. **16**: p. 470.

48. Masson, J.F. and G. Polomark, *Bitumen microstructure by modulated differential scanning calorimetry*. Thermochim. Acta, 2001. **374**: p. 105.

49. Quinones-Cisneros, S.E., C.K. Zeberg-Mikkelsen, and E.H. Stenby, *Friction theory prediction of crude oil viscosity at reservoir conditions based on dead oil properties*. Fluid Phase Equilib., 2003. **212**(1-2): p. 233-243.

50. Saber, N. and J.M. Shaw, *Toward multiphase equilibrium prediction for ill-defined asymmetric hydrocarbon mixtures*. Fluid Phase Equilib., 2009. **285**(1-2): p. 73-82.

51. Sadighian, A., et al., *Forced and Diffusive Mass Transfer between Pentane and Athabasca Bitumen Fractions*. Energy & Fuels, 2011. **25**(2): p. 782-790.

52. Argillier, J.-F., C. Coustet, and I. Henaut, *Heavy Oil Rheology as a Function of Asphaltene and Resin Content and Temperature*, in *SPE International Thermal Operations and Heavy Oil Symposium and International Horizontal Well Technology Conference*. 2002, Copyright 2002,SPE/PS-CIM/CHOA International Thermal Operations and Heavy Oil Symposium and International Horizontal Well Technology Conference: Calgary, Alberta, Canada.

53. Ter Haar, D., *A phenomenological theory of visco-elastic behaviour. I.* Physica, 1950. **16**(9): p. 719-737.

54. Ter Haar, D., *A phenomenological theory of visco-elastic behaviour. II.* Physica, 1950. **16**(9): p. 738-752.

55. Edgeworth, R., B.J. Dalton, and T. Parnell, *The pitch drop experiment*. European Journal of Physics, 1984. **5**(4): p. 198-200.

56. Denny, D.A. and R.S. Brodkey, *Kinetic Interpretation of Non-Newtonian Flow*. Journal of Applied Physics, 1962. **33**(7): p. 2269-2274.

57. Mujumdar, A., A.N. Beris, and A.B. Metzner, *Transient phenomena in thixotropic systems*. Journal of Non-Newtonian Fluid Mechanics, 2002. **102**(2): p. 157-178.

58. Ruckenstein, E. and J. Mewis, *Kinetics of structural changes in thixotropic fluids*. Journal of Colloid and Interface Science, 1973. **44**(3): p. 532-541.

59. Sonntag, R.C. and W.B. Russel, *Structure and breakup of flocs subjected to fluid stresses : III. Converging flow*. Journal of Colloid and Interface Science, 1987. **115**(2): p. 390-395.

60. Sonntag, R.C. and W.B. Russel, *Structure and breakup of flocs subjected to fluid stresses : II. Theory*. Journal of Colloid and Interface Science, 1987. **115**(2): p. 378-389.

61. Williams, M.L., R.F. Landel, and J.D. Ferry, *The Temperature Dependence of Relaxation Mechanisms in Amorphous Polymers and Other Glass-forming Liquids*. Journal of the American Chemical Society, 1955. **77**(14): p. 3701-3707.

62. Doolittle, A.K. and D.B. Doolittle, *Studies in Newtonian Flow. V. Further Verification of the Free-Space Viscosity Equation*. Journal of Applied Physics, 1957. **28**(8): p. 901-905.

63. Eyring, H., *Viscosity, plasticity and diffusion as examples of absolute reaction rates*. J. Chem. Phys., 1936. **4**: p. 283-91.

64. Moynihan, C.T., et al., *STRUCTURAL RELAXATION IN VITREOUS MATERIALS**. Annals of the New York Academy of Sciences, 1976. **279**(1): p. 15-35.

65. Tool, A.Q., *RELATION BETWEEN INELASTIC DEFORMABILITY AND THERMAL EXPANSION OF GLASS IN ITS ANNEALING RANGE**. Journal of the American Ceramic Society, 1946. **29**(9): p. 240-253.

66. Narayanaswamy, O.S., *A Model of Structural Relaxation in Glass*. Journal of the American Ceramic Society, 1971. **54**(10): p. 491-498.

67. Hodge, I.M. and A.R. Berens, *Effects of annealing and prior history on enthalpy relaxation in glassy polymers. 2. Mathematical modeling*. Macromolecules, 1982. **15**(3): p. 762-770.

68. Petrellis, N.C. and R.W. Flumerfelt, *Rheological behavior of shear degradable oils: Kinetic and equilibrium properties*. The Canadian Journal of Chemical Engineering, 1973. **51**(3): p. 291-301.

69. Ferroir, T., et al., *Motion of a solid object through a pasty (thixotropic) fluid*. Physics of Fluids, 2004. **16**(3): p. 594-601.

70. Souza Mendes, P.R. and E.S.S. Dutra, *Viscosity function for yield-stress liquids*. Applied Rheology, 2004. **14**(6): p. 296-302.

71. Coussot, P., et al., *Avalanche Behavior in Yield Stress Fluids*. Physical Review Letters, 2002. **88**(17): p. 175501.

72. Papanastasiou, T.C., *Flows of materials with yield*. Journal of Rheology, 1987. **31**(5): p. 385-404.

73. Mitsoulis, E., *Professor T. C. Papanastasiou's contributions to rheology and computational fluid mechanics*. Rheologica Acta, 1996. **35**(6): p. 525-530.

74. Turian, R.M., *Viscous heating in the cone-and-plate viscometer--III : Non-Newtonian fluids with temperature-dependent viscosity and thermal conductivity*. Chemical Engineering Science, 1965. **20**(8): p. 771-781.

75. Mallik, S., et al., *Modeling the Structural Breakdown of Solder Paste Using the Structural Kinetic Model*. Journal of Materials Engineering and Performance, 2010. **19**(1): p. 40-45.

76. Elimelech, M., et al., *Particle Deposition and Aggregation - Measurement, Modelling and Simulation*. 1998, Elsevier. p. 113-150.

77. Loria, H., P. Pereira-Almao, and M. Satyro, *Prediction of Density and Viscosity of Bitumen Using the Peng-Robinson Equation of State*. Ind. Eng. Chem. Res., 2009. **48**(22): p. 10129-10135.

78. Partington, J.R., *An Advanced Treatise on Physical Chemistry. Volume I*. Journal of Chemical Education, 1952. **29**(4): p. 208-null.

79. Buchmann, M., R. Theriault, and T.A. Osswald, *Polymer flow length simulation during injection mold filling*. Polymer Engineering & Science, 1997. **37**(3): p. 667-671.

80. Rusch, K.C. and R.H. Beck, *Yielding of ABS and an ABS-polycarbonate blend*. Journal of Polymer Science Part C: Polymer Symposia, 1970. **30**(1): p. 447-452.

81. Doolittle, A.K., *Mechanism of Solvent Action*. Industrial & Engineering Chemistry, 1944. **36**(3): p. 239-244.

82. Rehage, G. and H. Breuer, *Über die Druckabhängigkeit der Glasigen Erstarrung von Hochpolymeren*. Journal of Polymer Science Part C: Polymer Symposia, 1967. **16**(4): p. 2299-2312.

83. Miadonye, A. and V.R. Puttagunta, *MODELING THE VISCOSITY-TEMPERATURE RELATIONSHIP OF NIGERIAN NIGER-DELTA CRUDE PETROLEUM.* Petroleum Science and Technology, 1998. **16**(5): p. 627 - 638.

84. Mehrotra, A.K., *Generalized one-parameter viscosity equation for light and medium liquid hydrocarbons.* Industrial & Engineering Chemistry Research, 1991. **30**(6): p. 1367-1372.

85. Tschoegl, N.W., W.G. Knauss, and I. Emri, *The Effect of Temperature and Pressure on the Mechanical Properties of Thermo- and/or Piezorheologically Simple Polymeric Materials in Thermodynamic Equilibrium – A Critical Review.* Mechanics of Time-Dependent Materials, 2002. **6**(1): p. 53-99.

86. Martín-Alfonso, M.J., et al., *Pressure-temperature-viscosity relationship for heavy petroleum fractions.* Fuel, 2007. **86**(1-2): p. 227-233.

87. Yen, T.F., *THE COLLOIDAL ASPECT OF A MACROSTRUCTURE OF PETROLEUM ASPHALT.* Fuel Science and Technology International, 1992. **10**(4): p. 723-733.

88. Sirota, E.B., *Physical Structure of Asphaltenes†.* Energy Fuels, 2005. **19**(4): p. 1290-1296.

89. Sudduth, R.D., *A generalized model to predict the viscosity of solutions with suspended particles. I.* J. Appl. Polym. Sci., 1993. **48**(1): p. 25-36.

90. Mahaut, F., et al., *Suspensions of Noncolloidal Particles in Yield Stress Fluids: Experimental and Micromechanical Approaches.* AIP Conference Proceedings, 2008. **1027**(1): p. 671-673.

91. Mahaut, F., et al., *Yield stress and elastic modulus of suspensions of noncolloidal particles in yield stress fluids.* Journal of Rheology, 2008. **52**(1): p. 287-313.

92. Cheng, D.C.H. and F. Evans, *Phenomenological characterization of the rheological behaviour of inelastic reversible thixotropic and antithixotropic fluids.* British Journal of Applied Physics, 1965. **16**(11): p. 1599.

93. Marquardt, D., *An Algorithm for Least-Squares Estimation of Nonlinear Parameters.* SIAM Journal on Applied Mathematics, 1963. **11**(2): p. 431-441.

94. Kopsch, H., *On the thermal behavior of petroleum asphaltenes*. Thermochimica Acta, 1994. **235**(2): p. 271-275.

95. Zhang, Y., et al., *Observation of Glass Transition in Asphaltenes*. Energy & Fuels, 2003. **18**(1): p. 283-284.

96. Richardson, M.J. and N.G. Savill, *Derivation of accurate glass transition temperatures by differential scanning calorimetry*. Polymer, 1975. **16**(10): p. 753-757.

97. Han, Y., A. D'Amore, and L. Nicolais, *The effect of structural parameters on the enthalpy relaxation of an inorganic glass (Li2O · 2SiO2)*. Materials Chemistry and Physics, 1997. **51**(1): p. 64-69.

98. RICHARDS, F.J., *A Flexible Growth Function for Empirical Use*. Journal of Experimental Botany, 1959. **10**(2): p. 290-301.

99. Rasmussen, R.O., R.L. Lytton, and G.K. Chang, *Method to Predict Temperature Susceptibility of an Asphalt Binder*. Journal of Materials in Civil Engineering, 2002. **14**(3): p. 246-252.

100. Kazmer, B.f.F.a.D., *Effect of Low Temperature Shift Factor Modeling on Predicted Part Quality*. Society of Plastics Engineers Annual Technical Conference: Applied Rheology Special Interest Group, 2003.

101. Chateau, X., G. Ovarlez, and K.L. Trung, *Homogenization approach to the behavior of suspensions of noncolloidal particles in yield stress fluids*. Journal of Rheology, 2008. **52**(2): p. 489-506.

APPENDICES

VI. 4. APPENDIX 1: TRAINING*, VALIDATION** AND PREDICTION*** DATA SETS FOR MAYA CRUDE OIL

*Maya Crude Oil **s**=2 [Pa]				
Temperature [K]	**Shear Stress [Pa]**	**Shear rate[1/s]**	**Apparent Shear Viscosity [Pa.s]**	
			Experimental	Simulated
293.15	2	0.6905	1.381	1.423258152
290.15	2	0.8105	1.621	1.764797213
287.15	2	0.9945	1.989	2.2164634
284.15	2	1.3215	2.643	2.820418237
281.15	2	1.7555	3.511	3.640477848
278.15	2	2.43	4.86	4.776174773
275.15	2	3.367	6.734	6.383238091
272.15	2	4.5615	9.123	8.711780604
269.15	2	5.92	11.84	12.20430213
266.15	2	8.25	16.5	17.70620398
263.15	2	11.645	23.29	23.81008387
260.15	2	17.175	34.35	35.27440857
257.15	2	26.72	53.44	56.38327161
254.15	2	43.975	87.95	88.820317

251.15	2	78	156	160.299016
248.15	2	149.95	299.9	381.663142
245.15	2	306.35	612.7	628.508059
242.15	2	646.5	1293	1386.637705
239.15	2	1283	2566	3112.117106
236.15	2	2375.5	4751	5200.720997
233.15	2	4114.5	8229	8491.77583
230.15	2	6600	13200	13748.01784
227.15	2	9750	19500	20584.72499
224.15	2	13500	27000	28605.14817
221.15	2	16950	33900	34473.83672
218.15	2	20200	40400	39947.53275
215.15	2	23350	46700	46872.8076
212.15	2	25350	50700	49173.93087
209.15	2	26650	53300	52836.47569
206.15	2	27700	55400	55888.30074
203.15	2	29250	58500	58383.92739
200.15	2	29800	59600	60389.8465
197.15	2	30400	61000	61978.28919

**Maya Crude Oil s=500 [Pa]				
Temperature [K]	**Shear Stress [Pa]**	**Shear rate[1/s]**	**Apparent Shear Viscosity [Pa.s]**	
			Experimental	Simulated
293.15	500	406.186909	1.381	1.230960401
291.25	500	325.225873	1.523	1.53739306
287.45	500	256.264139	1.951	1.951111857
284.55	500	198.190784	2.512	2.522821641
281.75	500	149.940882	3.333	3.334647574
278.95	500	110.507602	4.495	4.524575607
275.65	500	78.9434991	6.379	6.333643752
272.15	500	54.346352	9.123	9.200249547
267.65	500	35.8294691	13.69	13.95499327
263.35	500	22.4862145	22.43	22.23584588
259.65	500	13.3700527	36.92	37.39701049
255.95	500	7.51390238	65.08	66.5433186
252.35	500	3.99474218	122.3	125.164523
248.85	500	2.01743766	253.3	247.8391321
245.95	500	0.97419705	517	513.2431892
242.85	500	0.4532168	1080	1103.224771
239.35	500	0.20876975	2442	2394.982995
235.65	500	0.09621109	5270	5196.906111
231.45	500	0.04691583	10800	10657.38465
227.45	500	0.02700079	18900	18517.97848
224.15	500	0.01856234	27000	26936.25853
220.95	500	0.01457178	34100	34312.89775
218.85	500	0.01248619	40000	40044.25486
215.65	500	0.01131581	44100	44185.98392
212.55	500	0.00980812	51000	50978.16276
210.85	500	0.00960314	52000	52066.2866

Maya Crude Oil **s=50 [Pa]

Temperature [K]	Shear Stress [Pa]	Shear rate[1/s]	Apparent Shear Viscosity [Pa.s]	
			Experimental	Simulated
293.05	50	38.7022157	1.647	1.291915697
290.65	50	24.0581996	2.054	2.078293506
288.05	50	18.3639419	2.705	2.722726975
285.35	50	13.6347521	3.703	3.667100037
283.05	50	9.79198059	5.135	5.106219272
280.35	50	6.76219431	7.466	7.394049577
277.35	50	4.46841664	11.31	11.18964591
274.75	50	2.81878155	17.53	17.73816067
271.95	50	1.70013231	29.8	29.40947573
268.75	50	0.98517223	52.23	50.75254687
266.45	50	0.55156955	88.18	90.65039944
263.65	50	0.29956515	165.9	166.9086001
260.45	50	0.15805266	316.5	316.3502666
257.25	50	0.08093176	607.4	617.8043962
253.85	50	0.04414318	1251	1266.634764
249.95	50	0.02515944	2682	2744.627863
246.45	50	0.01298026	6001	6063.585715
242.15	50	0.00658732	12000	12515.08114
236.65	50	0.00375268	22500	21710.04557
225.75	50	0.00251113	32300	31442.10552
227.85	50	0.00192046	39600	39884.92636
207.55	50	0.0016126	46500	46396.38
211.15	50	0.00144059	51100	51077.91917
224.95	50	0.00133999	54300	54295.66698
195.75	50	0.00127957	56300	56438.11871
218.05	50	0.0012428	58000	57829.85717
199.25	50	0.00122035	58500	58715.38915
213.25	50	0.00120668	59500	59268.49047

198.25	50	0.00119842	59700	59608.00958
194.15	50	0.00119348	59900	59812.9389

Maya Crude Oil **s=6.10-3 [Pa]

Temperature [K]	Shear Stress [Pa]	Shear rate[1/s]	Apparent Shear Viscosity [Pa.s]	
			Experimental	Simulated
287.05	0.01493418	0.006	2.373	2.489030104
285.65	0.02062125	0.006	3.478	3.436875266
284.35	0.02906834	0.006	4.947	4.844723949
282.05	0.04191752	0.006	7.139	6.986253095
279.35	0.06198231	0.006	10.12	10.3303849
275.85	0.09423461	0.006	15.96	15.70576786
272.65	0.14775202	0.006	24.85	24.62533626
268.95	0.2396493	0.006	39.9	39.94154934
265.75	0.40309711	0.006	67.5	67.18285116
262.85	0.70357208	0.006	118	117.2620127
259.85	1.27088359	0.006	215.1	211.8139324
256.85	2.35873105	0.006	391.7	393.1218409
253.55	4.44427258	0.006	753.5	740.7120969
250.25	8.36460862	0.006	1387	1394.101436
247.05	15.4339543	0.006	2573	2572.32571
243.85	27.3928751	0.006	4608	4565.479188
240.95	45.995408	0.006	7625	7665.901338
237.95	72.2180366	0.006	12000	12036.33944
234.95	105.485694	0.006	17800	17580.94897
232.15	143.524292	0.006	24000	23920.71538
229.45	183.048137	0.006	30700	30508.02286
226.75	220.830396	0.006	36900	36805.06596
224.05	254.515681	0.006	42300	42419.28012
221.05	282.889447	0.006	47200	47148.24113
218.25	305.720013	0.006	51000	50953.33557
215.35	323.425085	0.006	54000	53904.18084
212.65	336.749053	0.006	56100	56124.84222
210.25	346.529248	0.006	57700	57754.87463

208.15	353.557692	0.006	58900	58926.28203
205.85	358.515812	0.006	59800	59752.63535
205.25	361.955395	0.006	60300	60325.89915
203.35	364.30466	0.006	60700	60717.44328
202.85	365.885505	0.006	61000	60980.91754
202.05	366.933863	0.006	61200	61155.64381

***Maya Crude Oil s=100 [Pa]

Temperature [K]	Shear Stress [Pa]	Shear rate[1/s]	Apparent Shear Viscosity [Pa.s]	
			Experimental	Simulated
518.95	100	6.2215496	15.08	16.07316598
516.35	100	5.1515496	17.61	19.41163505
512.85	100	4.2528075	20.25	23.51387874
509.95	100	3.4998582	27.25	28.57258578
507.15	100	2.8707468	32.81	34.83414185
504.05	100	2.3465816	38.4	42.61518123
501.15	100	1.9111401	46.28	52.32478794
497.75	100	1.5505202	54.97	64.49448253
495.05	100	1.2528341	69.9	79.81902552
492.25	100	1.0079388	87.74	99.21237708
488.75	100	0.8071997	109.1	123.8850869
486.05	100	0.6432842	135.5	155.4522782
482.85	100	0.5099809	175.1	196.0857571
480.15	100	0.4020416	219.7	248.7304581
476.85	100	0.3150442	291	317.4157843
474.15	100	0.2452732	342.6	407.7086479
470.85	100	0.1896163	551	527.3809003
468.15	100	0.1454745	570.5	687.405662
464.95	100	0.110685	712.4	903.4650474
462.25	100	0.0834546	882.1	1198.256429
459.25	100	0.0623051	1209	1605.004784
456.05	100	0.046028	1614	2172.589498
453.25	100	0.0336441	2117	2972.289765
449.95	100	0.0243598	2892	4105.118127
447.05	100	0.0175216	6421	5707.234658
444.25	100	0.012579	6710	7949.745435
440.95	100	0.0090667	6640	11029.35997
438.05	100	0.0066012	15000	15148.67729

434.85	100	0.0048807	13300	20488.77645
432.05	100	0.0036791	31400	27180.33951
428.75	100	0.0028344	35500	35280.64492
425.85	100	0.002234	63400	44761.85794
422.95	100	0.0018014	60400	55512.33373
420.05	100	0.0014848	64100	67349.06024
417.25	100	0.0012494	66000	80037.23637
413.95	100	0.0010717	88000	93312.56425
411.15	100	0.0009354	103000	106902.6205
407.85	100	0.0008296	132000	120544.9462
405.05	100	0.0007463	130000	134000.7285
401.75	100	0.00068	151000	147063.8797
398.95	100	0.0006267	158000	159565.9148
395.75	100	0.0005835	189000	171377.3372
392.85	100	0.0005482	205000	182406.3518
390.15	100	0.0005192	223000	192595.7087
386.85	100	0.0004952	221000	201918.3909
383.95	100	0.0004753	234000	210372.7377
381.25	100	0.0004588	241000	217977.4606
377.95	100	0.0004449	239000	224766.8793
375.15	100	0.0004333	227000	230786.5938
371.95	100	0.0004236	255000	236089.7133
369.05	100	0.0004154	250000	240733.6896
365.85	100	0.0004085	252000	244777.7514
363.05	100	0.0004028	224000	248280.8997
359.85	100	0.0003979	301000	251300.4036
357.05	100	0.0003939	235000	253890.7262
354.25	100	0.0003905	277000	256102.8094
350.95	100	0.0003876	270000	257983.6465
348.15	100	0.0003852	344000	259576.0832
344.85	100	0.0003833	314000	260918.7893
342.15	100	0.0003816	274000	262046.3573
338.85	100	0.0003802	272000	262989.4893
336.15	100	0.0003791	263000	263775.2419
332.85	100	0.0003782	247000	264427.3056
330.25	100	0.0003774	316000	264966.3006

327.15	100	0.0003768	283000	265410.0752
324.05	100	0.0003763	243000	265773.9982
323.65	100	0.0003758	245000	266071.2377

VI. 5. APPENDIX 2: TRAINING*, VALIDATION** AND PREDICTION*** DATA SETS FOR ATHABASCA BITUMEN

*Athabasca Bitumen s=2 [Pa]				
Temperature [K]	**Shear Stress[Pa]**	**Shear rate[1/s]**	**Apparent Shear Viscosity [Pa.s]**	
			Experimental	Simulated
313.15	2	145.8316408	261.3	291.6632815
310.15	2	211.841014	406.1	423.682028
307.15	2	316.7898852	612.8	633.5797705
304.15	2	489.4002703	965.3	978.8005405
301.15	2	784.2870498	1532	1568.5741
298.15	2	1310.099956	2335	2620.199912
295.15	2	2294.243933	3752	4188.487866
292.15	2	4240.797814	6442	8481.595628
289.15	2	8341.322436	11100	16682.64487
286.15	2	17489.58528	18800	18979.17056
283.15	2	37280.41369	33700	34560.82739
280.15	2	73162.3793	61600	146324.7586
277.15	2	124229.4622	137000	148458.9243
274.15	2	182818.934	240000	245637.8681
271.15	2	240143.6407	566000	580287.2815
268.15	2	290387.5598	894000	580775.1195
265.15	2	331225.5003	666000	662451.0005
262.15	2	362709.1506	502000	725418.3012
259.15	2	386067.0608	812000	772134.1217
256.15	2	402900.3356	463000	805800.6712
253.15	2	414756.5003	886000	829513.0006
250.15	2	422950.8852	764000	845901.7704
247.15	2	428523.3368	765000	857046.6737
244.15	2	432258.3405	733000	864516.681

241.15	2	434728.5028	1080000	869457.0057
238.15	2	436341.4659	1120000	872682.9317
235.15	2	437381.6698	523000	874763.3396

Athabasca Bitumen **s=1200 [Pa]

Temperature [K]	Shear Stress[Pa]	Shear rate[1/s]	Apparent Shear Viscosity [Pa.s]	
			Experimental	Simulated
308	1200	0.321321759	363.9	385.5861104
305	1200	0.463199126	556.2	555.8389512
302	1200	0.687575802	821.1	825.0909621
299	1200	1.054837969	1247	1265.805563
296	1200	1.679543953	1974	2015.452744
293	1200	2.788935813	3096	3346.722976
290	1200	4.85014152	5099	5820.169824
287	1200	8.696935176	9314	10436.32221
284	1200	15.08281152	16900	18099.37383
281	1200	23.69613291	31300	28435.35949
278	1200	33.18946175	43900	39827.35411
275	1200	42.18657137	55900	50623.88564
272	1200	49.88670842	63400	59864.0501
269	1200	56.04530839	75100	67254.37006
266	1200	60.74880148	76200	72898.56177
263	1200	64.22449725	79900	77069.3967
260	1200	66.72981402	80000	80075.77682
257	1200	68.50025508	82000	82200.3061
254	1200	69.73080126	84100	83676.96151
251	1200	70.57376929	83100	84688.52314
248	1200	71.14366193	78000	85372.39432
245	1200	71.52419576	77200	85829.03491
242	1200	71.77527154	84700	86130.32585
239	1200	71.93899393	78200	86326.79271
236	1200	72.04450562	82300	86453.40674
233	1200	72.1116977	83300	86534.03724

Athabasca Bitumen **s=500 [Pa]

Temperature [K]	Shear Stress[Pa]	Shear rate[1/s]	Apparent Shear Viscosity [Pa.s]	
			Experimental	Simulated
308	500	0.020613333	515	495.8344406
305	500	0.012804878	757.8	738.7768603
302	500	0.007947561	1221	1138.739682
299	500	0.004057	1962	1823.570374
296	500	0.003427397	3181	3048.538075
293	500	0.001834146	5291	5349.018511
290	500	0.001070488	9066	9911.049542
287	500	0.000691067	15400	19524.95185
284	500	0.000321667	27500	40833.06781
281	500	0.000195778	45200	85850.6956
278	500	8.47312E-05	101000	164308.1817
275	500	3.95376E-05	216000	271290.2611
272	500	2.82597E-05	366000	389575.1202
269	500	0.00002088	508000	502027.5379
266	500	1.32444E-05	667000	598497.5462
263	500	1.20217E-05	720000	675668.7271
260	500	1.27125E-05	783000	734454.1168
257	500	0.000012725	782000	777665.3822
254	500	1.21513E-05	819000	808576.8958
251	500	1.04778E-05	844000	830215.5644
248	500	8.79455E-06	823000	845091.9664
245	500	1.16488E-05	854000	855160.1834
242	500	0.00001054	839000	861878.4603
239	500	1.16963E-05	851000	866302.5249
236	500	1.19475E-05	833000	869179.0545
233	500	0.00000835	866000	871026.1722

Athabasca Bitumen **s=50 [Pa]				
Temperature [K]	**Shear Stress[Pa]**	**Shear rate[1/s]**	**Apparent Shear Viscosity [Pa.s]**	
			Experimental	Simulated
308	50	11.65578578	566.5	582.7892888
305	50	17.2650439	843.6	863.2521952
302	50	26.41349693	1342	1320.674846
299	50	41.9087341	2009	2095.436705
296	50	69.29269753	3289	3464.634877
293	50	120.0639242	5566	6003.196211
290	50	219.4563189	9470	10972.81594
287	50	426.3969882	16500	21319.84941
284	50	880.4258611	28300	44021.29305
281	50	1833.061849	52000	91653.09243
278	50	3488.158499	105000	174407.9249
275	50	5744.213044	197000	287210.6522
272	50	8241.006536	428000	412050.3268
269	50	10617.72024	746000	530886.012
266	50	12659.02767	679000	632951.3833
263	50	14293.5037	689000	714675.1848
260	50	15539.44968	926000	776972.484
257	50	16455.77375	748000	822788.6874
254	50	17111.51101	831000	855575.5505
251	50	17570.65588	1530000	878532.7939
248	50	17886.36875	682000	894318.4374
245	50	18100.06546	954000	905003.273
242	50	18242.67127	495000	912133.5635
239	50	18336.58374	1150000	916829.1871
236	50	18397.64776	940000	919882.388
233	50	18436.85991	648000	921842.9953

***Athabasca Bitumen P10 $\dot{\gamma}=10^{-3}$ [1/s]

Temperature [K]	Shear Stress[Pa]	Shear rate[1/s]	Apparent Shear Viscosity [Pa.s]	
			Experimental	Simulated
325.85	0.007144471	0.001	7.083	7.144470733
322.65	0.009103971	0.001	9.188	9.103971239
320.25	0.011747441	0.001	11.69	11.74744106
317.65	0.015365335	0.001	15.23	15.36533508
315.05	0.02039433	0.001	20.5	20.39432994
312.55	0.027503119	0.001	27.33	27.50311876
310.05	0.037736186	0.001	37.15	37.73618587
307.35	0.052760306	0.001	52.28	52.76030644
304.45	0.075297704	0.001	77.23	75.29770412
301.95	0.109907759	0.001	110.4	109.9077587
299.35	0.164439082	0.001	162.4	164.4390816
296.35	0.25281294	0.001	255.2	252.8129398
293.45	0.400544736	0.001	413.2	400.5447356
290.85	0.656115679	0.001	640.6	656.1156791
287.95	1.115378394	0.001	1084	1115.378394
284.65	1.976370552	0.001	2034	1976.370552
281.65	3.668775563	0.001	3696	3668.775563
278.65	7.177283849	0.001	6996	7177.283849
275.25	14.9013673	0.001	14700	14901.3673
271.75	33.10476138	0.001	32600	33104.76138
267.95	78.5517231	0.001	79800	78551.7231
264.65	180.1614519	0.001	179000	180161.4519
261.55	335.982003	0.001	334000	335982.003
259.05	488.8587529	0.001	480000	488858.7529
256.55	594.9166867	0.001	592000	594916.6867
253.95	654.1447251	0.001	653000	654144.7251
251.75	683.3765827	0.001	682000	683376.5827

***Athabasca Bitumen P20 $\dot{\gamma}$=0.2 [1/s]

Temperature [K]	Shear Stress[Pa]	Shear rate[1/s]	Apparent Shear Viscosity [Pa.s]	
			Experimental	Simulated
330.05	5.337791483	0.2	26.63	26.68895742
327.05	6.754940481	0.2	36.33	33.7747024
324.05	8.665496063	0.2	50.93	43.32748031
321.15	11.27837136	0.2	71.53	56.39185679
318.25	14.90709352	0.2	103.1	74.5354676
315.15	20.03495775	0.2	152.4	100.1747888
311.85	27.43511675	0.2	239.6	137.1755838
308.95	38.4001598	0.2	361.8	192.000799
306.05	55.18399481	0.2	550.5	275.9199741
303.15	81.85616594	0.2	861.5	409.2808297
300.15	126.0056902	0.2	1372	630.0284509
297.15	202.3276051	0.2	2234	1011.638026
294.05	340.6208345	0.2	3822	1703.104172
291.15	604.6757697	0.2	6418	3023.378849
288.05	1139.760818	0.2	11100	5698.80409
285.15	2300.835619	0.2	19400	11504.1781
282.15	5014.005115	0.2	34200	25070.02557
279.15	11450.3053	0.2	62700	57251.52652
276.05	24586.67805	0.2	114000	122933.3902
272.95	45206.72681	0.2	205000	226033.634
269.95	70358.65351	0.2	336000	351793.2676
267.05	95748.12091	0.2	481000	478740.6046
263.95	118264.0916	0.2	601000	591320.458
260.95	136564.4687	0.2	677000	682822.3435
257.85	150573.4584	0.2	721000	752867.2921
254.85	160848.8052	0.2	749000	804244.0258
251.85	168149.5423	0.2	766000	840747.7115
248.95	173209.7778	0.2	775000	866048.8892

	245.95	176646.9351	0.2	785000	883234.6753
	243.25	178941.7708	0.2	794000	894708.8539

VI. 6. APPENDIX 3: TRAINING*, VALIDATION** AND PREDICTION*** DATA SETS FOR SAFANIYA HEAVY OIL

*Safaniya Heavy Oil P20 **s=2 [Pa]**				
Temperature [K]	**Shear Stress[Pa]**	**Shear rate[1/s]**	**Apparent Shear Viscosity [Pa.s]**	
			Experimental	Simulated
333.05	2	34.88859445	105	109.7718889
330.05	2	50.58918097	136.7	131.1783619
327.05	2	75.15214408	195.7	150.3042882
324.05	2	114.6557576	291.4	229.3115153
321.05	2	180.1483106	444.9	360.2966213
318.05	2	292.4340565	692.8	584.8681123
315.05	2	492.243388	1120	994.4867759
312.05	2	862.8260534	1927	1925.652107
309.05	2	1582.63071	3452	3465.261421
306.05	2	3054.449528	6360	6408.899055
303.05	2	6236.724524	11900	11473.44905
300.05	2	13520.03228	24300	24040.06456
297.05	2	31057.41579	41700	62114.83158
294.05	2	74748.7272	86700	89497.46544
291.05	2	184208.0841	192000	268416.1683
288.05	2	449613.6439	440000	499227.2879
285.05	2	1046370.385	1040000	1092740.771
282.05	2	2242336.923	2320000	2484673.845
279.05	2	4317631.875	5770000	5635263.749
276.05	2	7392607.731	10500000	10785215.46
273.05	2	11288727.73	49900000	22577455.46
270.05	2	15567281.78	31300000	31134563.56
267.05	2	19723758.8	87100000	39447517.63
264.05	2	23377867.01	32400000	46755734.02

261.05	2	26348290.23	63800000	52696580.45
258.05	2	28622726.97	62100000	57245453.94
255.05	2	30287692.91	27700000	60575385.82

Safaniya Heavy Oil **s=1500 [Pa]

Temperature [K]	Shear Stress[Pa]	Shear rate[1/s]	Apparent Shear Viscosity [Pa.s]	
			Experimental	Simulated
317	1500	1.248244255	1411	1201.68789
314	1500	0.769231213	2293	1949.99888
311	1500	0.456159768	3724	3288.32156
308	1500	0.259103544	6259	5789.19136
305	1500	0.141051539	10720	10634.4107
302	1500	0.07618272	18900	19689.5044
299	1500	0.043816117	32440	34233.9785
296	1500	0.028148156	53110	53289.4582
293	1500	0.020240088	78980	74110.3484
290	1500	0.015957295	101700	94000.8941
287	1500	0.01347466	101700	111320.06
284	1500	0.011954771	117700	125472.92
281	1500	0.010986153	128400	136535.507
278	1500	0.010351445	130500	144907.311
275	1500	0.009927939	137300	151088.768
272	1500	0.00964231	138200	155564.39
269	1500	0.009448664	135700	158752.595
266	1500	0.009317235	138100	160991.974
263	1500	0.009228203	141300	162545.196
260	1500	0.009168143	139800	163610.017
257	1500	0.009127865	136800	164331.971
254	1500	0.009101046	136800	164816.22

Safaniya Heavy Oil **s=100 [Pa]

Temperature [K]	Shear Stress[Pa]	Shear rate[1/s]	Apparent Shear Viscosity [Pa.s]	
			Experimental	Simulated
325.45	100	0.424147705	238	235.7669248
323.15	100	0.309504735	323	323.0968342
320.85	100	0.220717435	444.9	453.06797
318.65	100	0.153419113	618.6	651.8092678
315.45	100	0.103625904	985.8	965.0096753
313.25	100	0.067773323	1463	1475.506816
310.95	100	0.042741208	2224	2339.662469
307.95	100	0.025865275	3988	3866.187358
305.65	100	0.014934126	6360	6696.073126
302.65	100	0.008171297	11900	12237.95864
299.65	100	0.004202913	24300	23793.01992
296.65	100	0.002012631	50200	49686.21485
293.55	100	0.000886857	105000	112757.7222
289.75	100	0.000354788	288000	281858.535
285.95	100	0.000129672	806000	771177.058
282.95	100	4.73944E-05	2080000	2109951.699
279.95	100	1.98094E-05	4740000	5048110.505
277.65	100	1.00798E-05	9750000	9920796.866
276.85	100	6.16154E-06	16100000	16229705.88
255.95	100	4.34707E-06	23000000	23003992.07
255.25	100	3.40487E-06	27700000	29369739.26
263.35	100	2.87232E-06	32400000	34815012.52
253.95	100	2.55291E-06	40500000	39170994.68
259.55	100	2.35353E-06	43400000	42489349.9
254.25	100	2.22587E-06	45600000	44926237.93
254.25	100	2.1429E-06	45600000	46665743.4
273.05	100	2.08857E-06	49900000	47879551.36

Safaniya Heavy Oil **s=50 [Pa]

Temperature [K]	Shear Stress[Pa]	Shear rate[1/s]	Apparent Shear Viscosity [Pa.s]	
			Experimental	Simulated
329	50	0.001779297	165.2	170.1234048
326	50	0.000862318	241.8	239.8186354
323	50	0.000440965	327.8	345.8323389
320	50	0.000194364	503.1	511.3608221
317	50	8.15184E-05	789.1	777.3709496
314	50	3.1673E-05	1295	1218.705333
311	50	1.28256E-05	1972	1977.296779
308	50	4.24457E-06	3533	3333.670483
305	50	1.5023E-06	5671	5868.349252
302	50	4.26704E-07	10800	10845.91796
299	50	1.10459E-07	21400	21184.27529
296	50	2.6187E-08	43300	44067.60324
293	50	5.48026E-09	92600	98535.47949
290	50	8.41682E-10	248000	239401.4643
287	50	1.33713E-10	592000	631950.7764
284	50	1.88118E-11	1570000	1690427.057
281	50	2.7337E-12	4530000	4023849.732
278	50	8.08393E-13	7810000	7916936.817
275	50	2.70811E-13	14300000	12961070.34
272	50	1.51422E-13	18000000	18359231.68
269	50	9.05687E-14	23500000	23407646.78
266	50	6.38841E-14	28300000	27706445.1
263	50	5.23563E-14	30800000	31132858.66
260	50	4.59444E-14	32300000	33736421.82
257	50	4.34839E-14	32300000	35645344.52
254	50	3.32371E-14	40700000	37006847.09
251	50	3.24054E-14	40700000	37956646.88

***Safaniya Heavy Oil P10 $\dot{g}=10^{-4}$ [1/s]

Temperature [K]	Shear Stress[Pa]	Shear rate[1/s]	Apparent Shear Viscosity [Pa.s]	
			Experimental	Simulated
308	0.010936705	0.0001	190.5	109.367048
305	0.018595323	0.0001	297.7	185.953234
302	0.033286151	0.0001	459.6	332.86151
299	0.063243614	0.0001	668.6	632.436138
296	0.128844301	0.0001	1146	1288.44301
293	0.285018996	0.0001	1977	2850.18996
290	0.689225643	0.0001	3675	6892.25643
287	1.732083375	0.0001	7245	17320.8338
284	4.016481537	0.0001	14100	40164.8154
281	7.896856432	0.0001	27400	78968.5643
278	13.05834062	0.0001	59500	130583.406
275	18.72573845	0.0001	124000	187257.385
272	24.14406806	0.0001	237000	241440.681
269	28.84229869	0.0001	332000	288422.987
266	32.64318059	0.0001	381000	326431.806
263	35.56724638	0.0001	404000	355672.464
260	37.73391049	0.0001	418000	377339.105
257	39.29362909	0.0001	426000	392936.291
254	40.39086649	0.0001	430000	403908.665
251	41.1482051	0.0001	429000	411482.051
248	41.66246884	0.0001	433000	416624.688
245	42.00662951	0.0001	432000	420066.295
242	42.23388023	0.0001	437000	422338.802
239	42.38203067	0.0001	438000	423820.307
236	42.47741817	0.0001	435000	424774.182
233	42.53807796	0.0001	436000	425380.78
230	42.57617426	0.0001	437000	425761.743
227	42.59979703	0.0001	430000	425997.97

	224	42.61425459	0.0001	440000	426142.546
	221	42.62298411	0.0001	443000	426229.841

***Safaniya Heavy Oil P20 $\dot{\gamma}=10^{-3}$ [1/s]

Temperature [K]	Shear Stress[Pa]	Shear rate[1/s]	Apparent Shear Viscosity [Pa.s]	
			Experimental	Simulated
309.25	0.161926129	0.001	213.4	161.9261291
306.25	0.251746086	0.001	344.9	251.7460862
303.05	0.40842093	0.001	507.7	408.4209299
299.95	0.695718195	0.001	824	695.718195
296.85	1.253560078	0.001	1353	1253.560078
294.15	2.410476255	0.001	2328	2410.476255
291.05	5.000042643	0.001	4381	5000.042643
287.85	11.30556318	0.001	8406	11305.56318
284.95	27.23191466	0.001	16600	27231.91466
281.85	63.10322347	0.001	33800	63103.22347
278.95	126.6400873	0.001	61100	126640.0873
275.75	213.8346922	0.001	132000	213834.6922
273.05	311.2200623	0.001	249000	311220.0623
270.15	404.9953559	0.001	411000	404995.3559
266.85	486.4513199	0.001	529000	486451.3199
264.15	552.2960795	0.001	604000	552296.0795
261.25	602.8556981	0.001	636000	602855.6981
257.75	640.2341963	0.001	686000	640234.1963
254.95	667.0781983	0.001	699000	667078.1983
251.95	685.9176813	0.001	708000	685917.6813
249.05	698.8902586	0.001	707000	698890.2586
245.95	707.6780753	0.001	719000	707678.0753
242.85	713.5447717	0.001	704000	713544.7717
240.05	717.4088052	0.001	721000	717408.8052
237.05	719.9212506	0.001	713000	719921.2506
234.15	721.5344517	0.001	712000	721534.4517
231.15	722.5573633	0.001	722000	722557.3633
228.15	723.1978195	0.001	701000	723197.8195

	225.15	723.593668	0.001	711000	723593.668
	223.45	723.8351029	0.001	718000	723835.1029

***Safaniya Heavy Oil P50 $\dot{g}=10^{-3}$ [1/s]

Temperature [K]	Shear Stress[Pa]	Shear rate[1/s]	Apparent Shear Viscosity [Pa.s]	
			Experimental	Simulated
369.35	0.005734235	0.002	1.082	2.86711735
365.75	0.006450263	0.002	1.266	3.22513126
363.25	0.007301189	0.002	1.616	3.65059459
359.65	0.008320157	0.002	1.957	4.16007856
357.25	0.009550364	0.002	2.335	4.77518201
353.45	0.011048713	0.002	2.972	5.52435627
350.95	0.012891012	0.002	3.569	6.44550613
348.55	0.015179496	0.002	4.351	7.58974807
344.95	0.018053842	0.002	5.838	9.02692087
342.55	0.021707587	0.002	7.175	10.8537936
338.95	0.026412999	0.002	9.939	13.2064993
336.45	0.032559431	0.002	12.31	16.2797155
332.75	0.040713678	0.002	17.2	20.3568391
330.35	0.051716951	0.002	21.87	25.8584754
326.65	0.066844346	0.002	31.98	33.422173
324.25	0.088073738	0.002	41.45	44.036869
320.65	0.118551736	0.002	69.01	59.275868
318.25	0.1634257	0.002	119.6	81.7128499
314.45	0.231379116	0.002	251.8	115.689558
311.95	0.337569708	0.002	382.1	168.784854
309.55	0.509482651	0.002	560.5	254.741326
305.85	0.799124954	0.002	952.7	399.562477
303.55	1.309734932	0.002	1402	654.867466
299.85	2.25767112	0.002	2487	1128.83556
297.45	4.12524127	0.002	3729	2062.62063
293.75	8.066467931	0.002	7367	4033.23397
291.35	17.07758638	0.002	11600	8538.79319

	287.75	39.61716844	0.002	24900	19808.5842
	285.35	98.66531373	0.002	41600	49332.6569
	281.65	237.9523819	0.002	93300	118976.191
	279.25	496.8975414	0.002	163000	248448.771
	276.65	867.9511666	0.002	283000	433975.583
	272.75	1297.092524	0.002	631000	648546.262
	270.25	1721.476477	0.002	915000	860738.239
	266.45	2097.425071	0.002	1260000	1048712.54
	263.95	2405.673571	0.002	1390000	1202836.79
	261.55	2644.779079	0.002	1470000	1322389.54
	257.65	2822.820009	0.002	1540000	1411410
	255.15	2951.326643	0.002	1560000	1475663.32
	251.45	3041.829998	0.002	1570000	1520915
	248.75	3104.300248	0.002	1580000	1552150.12
	248.55	3146.689426	0.002	1580000	1573344.71

***Safaniya Heavy Oil R20 s=500 [Pa]

Temperature [K]	Shear Stress[Pa]	Shear rate[1/s]	Apparent Shear Viscosity [Pa.s]	
			Experimental	Simulated
370.15	500	0.03541971	16900	14116.43387
367.05	500	0.02383204	22000	20980.15969
364.05	500	0.01641091	28400	30467.53579
360.95	500	0.011642579	36800	42945.81306
358.15	500	0.008539276	46700	58552.97661
354.75	500	0.006480294	61200	77156.98738
351.95	500	0.005082751	77600	98371.91741
349.15	500	0.00411123	95100	121618.1008
346.15	500	0.003419886	118000	146203.6857
342.85	500	0.002917044	146000	171406.4224
339.85	500	0.002543989	172000	196541.7147
337.05	500	0.002262334	199000	221010.7212
333.85	500	0.002046429	228000	244328.0521
330.85	500	0.001878768	252000	266131.9152
328.05	500	0.001747146	274000	286180.9583
324.85	500	0.001642887	301000	304342.2208
321.95	500	0.001559702	318000	320574.0985
319.25	500	0.00149295	332000	334907.4155
315.85	500	0.001439152	353000	347426.8237
313.25	500	0.001395658	358000	358253.9481
309.95	500	0.001360422	369000	367533.0365
306.95	500	0.001331844	375000	375419.3796
304.05	500	0.001308659	381000	382070.4312
300.85	500	0.001289859	388000	387639.3595
297.85	500	0.00127463	393000	392270.6607
295.05	500	0.001262316	398000	396097.4387
291.95	500	0.00125238	404000	399239.9749
289.15	500	0.001244384	398000	401805.2543

	285.95	500	0.00123797	401000	403887.1679
	283.15	500	0.001232841	404000	405567.167
	280.15	500	0.001228757	401000	406915.1961
	277.05	500	0.001225518	409000	407990.7744
	274.25	500	0.00122296	399000	408844.1309
	271.05	500	0.00122095	402000	409517.3319
	267.75	500	0.001219377	404000	410045.3543
	264.95	500	0.001218154	408000	410457.0818
	263.45	500	0.001217208	406000	410776.2094